Analytical and experimental investigation of fixed connections of RC cladding walls to precast buildings

by

Ioannis M. Kalyviotis

A thesis

Presented to the Faculty of Civil Engineering

of the National Technical University of Athens

in Partial Fulfilment of the Requirements

for the Degree of

Master of Science

in Civil Engineering

National Technical University of Athens

December 2013

Supervisor:

Ioannis N. Psycharis

Program Authorised to Offer Degree:

Design and Analysis of Structures

Abstract

Analytical and experimental investigation of fixed connections of RC

cladding walls to precast buildings

by

Ioannis M. Kalyviotis

Master of Science in Civil Engineering

National Technical University of Athens, December 2013

Supervisor: Ioannis N. Psycharis

Scope of the present thesis is to study the response of fully fixed connections of R.C. cladding walls to the precast buildings. In common design practice cladding panels are not designed to contribute to the structure's stiffness but to resist only their self-weight and wind and local seismic loads. Based on this view, the fastenings are dimensioned with a local calculation while the frame behaves similarly to cast-in-situ structures due to the comparable energy dissipation capacity. However, damages even in recent earthquake events indicate that panels come to be integral part of the resisting system conditioning its seismic response.

Ensuring that connections are fully fixed the designer is able to determine a priori the increase in stiffness of the system providing an upper limit of the induced forces. The present work is an attempt to quantify the impact of these integrated connections in the modal characteristics of the building and the magnitude of forces. Additionally, the detrimental effect of the roof diaphragm in the transmission of forces is also examined. The investigation of the influence of the connections is composed mainly by two parts: an analytical and an experimental. The sequence of these two studies is not straightforward as they are not independent; the analyses are supplemented by the experimental results and vice versa.

As far as the analytical part is concerned, firstly a simplified theoretical study is conducted. Vertical panels with four or three connections are taken into consideration and the resultant forces are estimated. It is interesting to note that according to this procedure, the forces are independent of the width of the panels and their major component is in the vertical direction.

Subsequently, two single-storey industrial buildings of precast concrete are examined. In the first building Modal and Response Spectrum analyses are performed while in the second Modal, Static Pushover and Nonlinear Response History analyses. Vertical and horizontal panels are used, whereas three alternative roof diaphragm configurations are also investigated. The role of the roof diaphragm is proved to be significant, affecting tremendously the response of the structure. Moreover, in the columns which are not connected to the panels aligned in the loading direction much larger forces are induced compared with the corresponding forces induced to the outer (façade) columns. The main conclusions are summarised in a separate section.

As far as the experimental part is concerned, it is described in four sections. In the first, additional analytical investigation is carried out for the estimation of the magnitude of the expected forces to be induced to the connections under seismic action. Although they are not as detailed as the analyses in previous sections, they are important for selecting representative tests to be performed. In the second section, the design of the specimens and the experimental setup is taken place. The connections tested are materialized using vertical reinforcement bars that are stressed mainly in tension during the loading and they are called "rebar connections". Finally, in the third and the fourth sections the results of the test, the figures of the damages and the conclusions are presented. Basic problem of this type of connection is the permanent opening of the joint caused by the plastic axial strains of the bars. For this reason, full contact of the panel with the beam cannot be re-established during the reverse loading and the friction force at the joint cannot be fully developed resulting in pinching effect. It also worth mentioning that the ultimate displacement that corresponds to breaking of the rebars is independent of their cross section and is mainly determined by the strains induced to the rebars.

The card files of the conducted experiments and additional information about the material used are reported in Appendices A and B respectively.

Περίληψη

Αναλυτική και πειραματική διερεύνηση σταθερών συνδέσεων τοίχων

πλαγιοκάλυψης από Ω.Σ. με προκατασκευασμένα κτήρια

του

Ιωάννη Μ. Καλυβιώτη

Μεταπτυχιακό Δίπλωμα Ειδίκευσης

Εθνικό Μετσόβιο Πολυτεχνείο, Δεκέμβριος 2013

Επιβλέπων: Ιωάννης Ν. Ψυχάρης

Στόχος της παρούσας διπλωματικής εργασίας είναι να μελετήσει την απόκριση σταθερών συνδέσεων τοίχων πλαγιοκάλυψης από Ω.Σ. με προκατασκευασμένα κτήρια. Στο συνήθη σχεδιασμό οι τοίχοι πλαγιοκάλυψης (cladding panels) δεν σχεδιάζονται κατά τρόπο που να συμβάλλουν στη συνολική δυσκαμψία του κτηρίου, παρά μόνο για να ανθίστανται στις εντάσεις που προκαλούν το ίδιον βάρος, οι δράσεις ανεμοπίεσης και σεισμικά φορτία ευθέως ανάλογα του ιδίου βάρους των τοίχων. Σύμφωνα με αυτή τη λογική, οι συνδέσεις διαστασιολογούνται βάσει τοπικών ελέγχων ενώ ο πλαισιωτός φορέας συμπεριφέρεται ως επιτόπου έγχυτος λόγω της συγκρίσιμης ικανότητας απόσβεσης ενέργειας. Οι συνδέσεις διακρίνονται σε δύο κατηγορίες ανάλογα με τη λειτουργία τους. Στη πρώτη περιλαμβάνονται οι συνδέσεις οι οποίες καλούνται να παραλάβουν φορτία εντός του επιπέδου του τοίχου μέσω απλής έδρασης, μεταλλικών στοιχείων κτλ. Στη δεύτερη περίπτωση εντάσσονται “επικουρικού” τύπου συνδέσεις και οι οποίες καλούνται να εξασφαλίσουν την κατασκευή έναντι εκτός επιπέδου ανατροπή και έναντι μεγάλων μετακινήσεων. Ενδεικτικώς αναφέρονται τα μεταλλικά ελάσματα και οι ράγες ολίσθησης.

Παρά ταύτα πλήθος ζημιών σε συστήματα πλαγιοκάλυψης εξαιτίας σεισμικών γεγονότων μαρτυρούν πως η συμπεριφορά των στοιχείων αυτών δεν είναι πλήρως κατανοητή καθώς υπάρχουν μηχανισμοί που καθιστούν τους τοίχους μέρος του ανθιστεκόμενου φορέα και επηρεάζουν τη σεισμική απόκριση της κατασκευής. Επιπλέον, η χρήση του συντελεστή συμπεριφοράς για την απομείωση των σεισμικών δράσεων προϋποθέτει την κατανάλωση ενέργειας διαμέσου των πλαστικών αρθρώσεων στην βάση των υποστυλωμάτων και κατ’ επέκταση μεγάλων μετακινήσεων ικανών να οδηγήσουν στην ανάπτυξη αυτών. Η παραδοχή όμως αυτή δεν είναι ορθή καθώς η αντοχή των συνδέσεων τοίχου – πλαισίου έχει εξαντληθεί προτού αναπτυχθούν μεγάλες μετακινήσεις.

Η πραγματική συμπεριφορά των στοιχείων πλαγιοκάλυψης είναι δύσκολο να καθοριστεί καθώς η απόκρισή τους βρίσκεται μεταξύ πλήρους ελευθερίας και πλήρους πάκτωσης με τα όρια να μην είναι πάντα ξεκάθαρα. Παρόλο που στην πρώτη υπάρχει σχετική εμπειρία σχεδιασμού, η δεύτερη χρειάζεται αναθεώρηση δεδομένης και της ανάπτυξης βελτιωμένων υλικών. Εξασφαλίζοντας ότι παρέχεται πλήρης σύνδεση, ο σχεδιαστής μπορεί να καθορίσει εκ των προτέρων την αύξηση της δυσκαμψίας του συστήματος παρέχοντας ένα άνω όριο στις αναπτυσσόμενες δυνάμεις.

Η παρούσα εργασία αποτελεί μια προσπάθεια να ποσοτικοποιηθεί η επίδραση αυτών των συνδέσεων όσον αφορά στα ιδιομορφικά χαρακτηριστικά της κατασκευής και στη τιμή των δυνάμεων. Επίσης εξετάζεται ο καθοριστικός ρόλος του διαφράγματος στη μεταφορά των

αδρανειακών δυνάμεων μεταξύ των ανθιστάμενων τοίχων. Οι υπό εξέταση τοίχοι έχουν κατακόρυφο και οριζόντιο προσανατολισμό και διαθέτουν τρεις ή τέσσερις συνδέσεις ανά στοιχείο.

Η διερεύνηση περιλαμβάνει ένα αναλυτικό και ένα πειραματικό τμήμα. Η σειρά διαδοχής των δύο φάσεων δεν είναι μονοσήμαντα ορισμένη καθώς οι δύο διαδικασίες δεν είναι ανεξάρτητες. Αντιθέτως, οι αναλύσεις τροφοδοτούν τα πειράματα με τα αναγκαία δεδομένα και αντίστροφα.

Όσον αφορά στο αναλυτικό μέρος, αρχικά πραγματοποιείται μια απλοποιημένη θεωρητική ανάλυση. Κατακόρυφοι τοίχοι πλαγιοκάλυψης λαμβάνονται υπ' όψιν και εκτιμώνται οι προκύπτουσες δυνάμεις στις αντίστοιχες θέσεις. Ενδιαφέρον είναι να σημειωθεί ότι βάσει της παραπάνω διαδικασίας οι υπολογιζόμενες δυνάμεις είναι ανεξάρτητες του πλάτους των τοίχων, εξαρτώνται ωστόσο από το ποσοστό της καλυπτόμενης πλαϊνής όψης. Επίσης οι δυνάμεις είναι ευθέως ανάλογες του ύψους των τοίχων ενώ τέλος η βασική τους συνιστώσα βρίσκεται στον κατακόρυφο άξονα. Το τελευταίο μάλιστα χαρακτηριστικό είναι ιδιαιτέρως χρήσιμο για το σχεδιασμό των πειραματικών διατάξεων.

Στη συνέχεια εξετάζονται δύο μονώροφα βιομηχανικά κτήρια από προκατασκευασμένο σκυρόδεμα. Στο πρώτο κτήριο χρησιμοποιούνται τοίχοι κατακόρυφου και οριζόντιου προσανατολισμού ενώ εξετάζεται ένα εύρος δυσκαμψιών συνδέσεων (εύκαμπτες έως "άκαμπτες"). Από τις Ιδιομορφικές αναλύσεις και Ιδομορφικές αναλύσεις Φάσματος Απόκρισης που πραγματοποιούνται προκύπτει ότι τα ιδιομορφικά χαρακτηριστικά επηρεάζονται εντόνως από τη μεταβολή της δυσκαμψίας των συνδέσεων. Η επιρροή αυτή αποτυπώνεται και στην ένταση των αναπτυσσόμενων δυνάμεων. Ενδιαφέρον στοιχείο είναι ότι στην περίπτωση οριζόντιας διάταξης των πλαγιοκαλύψεων οι δυνάμεις είναι μεγαλύτερες έως και 50% των αντίστοιχων στην κατακόρυφη διάταξη. Επίσης τα αποτελέσματα συγκρίνονται με τα συμπεράσματα που εξήχθησαν από τη θεωρητική διερεύνηση ελέγχοντας την ακρίβειά τους, η οποία κρίνεται ως πολύ ικανοποιητική.

Στο δεύτερο υπό εξέταση κτήριο μόνο κατακόρυφοι τοίχοι εξετάζονται. Η σύνδεση των στοιχείων αυτών με την κατασκευή δεν λαμβάνεται ως θεωρητική πάκτωση αλλά μέσω της πραγματικής συμπεριφοράς τους, όπως αυτή προκύπτει από ένα ακριβές αριθμητικό μοντέλο που σχεδιάστηκε γι' αυτό το σκοπό. Επίσης, ο ρόλος του διαφράγματος ελέγχεται θεωρώντας τρεις εναλλακτικές διατάξεις ("ασθενές", "παραμορφώσιμο", "άκαμπτο"). Πέραν των Ιδιομορφικών πραγματοποιούνται και Ανελαστικές Στατικές και Δυναμικές αναλύσεις οι οποίες αποκαλύπτουν την καθοριστική επίδραση του διαφράγματος στην απόκριση. Πιο συγκεκριμένα, προκύπτει ότι στα υποστυλώματα τα οποία δεν είναι συνδεδεμένα με τοίχους επένδυσης κατά τη διεύθυνση της φόρτισης αναπτύσσονται πολύ μεγαλύτερες δυνάμεις σε σχέση με τα υποστυλώματα των εξωτερικών όψεων. Τα πρώτα συμπεριφέρονται εντόνως ανελαστικά, αφήνοντας τα δεύτερα και τους τοίχους πρακτικώς ελαστικά.

Όσον αφορά στο πειραματικό μέρος, αρχικά πραγματοποιείται μια πρόσθετη αναλυτική διερεύνηση ούτως ώστε το μέγεθος των δυνάμεων για τις οποίες θα γίνουν τα πειράματα να επιλεχθεί με γνώμονα την αντιπροσωπευτικότητα μεγάλου πλήθους πραγματικών περιπτώσεων. Δεδομένου ότι ιδιαίτερη ακρίβεια δεν ήταν το ζητούμενο, χρησιμοποιούνται οι προσεγγιστικές θεωρητικές σχέσεις που αναπτύχθηκαν προηγουμένως.

Στη συνέχεια ακολουθεί ο καθορισμός κατάλληλων πειραματικών διατάξεων και ο σχεδιασμός των δοκιμίων και του καταγραφικού δικτύου. Όπως αναφέρθηκε προηγουμένως, η κυριαρχία της κατακόρυφης συνιστώσας στις αναπτυσσόμενες δυνάμεις υπαγορεύει την επιλογή κατάλληλων διατάξεων που να εκμεταλλεύονται αυτό το χαρακτηριστικό. Κατά συνέπεια επιλέγονται δύο εναλλακτικοί τύποι σύνδεσης: ο τύπος που βασίζεται σε σιδηροπλισμό και αυτός που βασίζεται σε μεταλλική πλάκα. Επίσης εξετάζεται και η περίπτωση βιομηχανικού τύπου σύνδεσης.

Τέλος πραγματοποιείται εκτενής περιγραφή των πέντε πειραμάτων βασιζόμενων σε σιδηροπλισμό που εκτελέστηκαν και γίνεται σύγκριση των αποτελεσμάτων. Βασικό πρόβλημα αυτό του τύπου σύνδεσης είναι ότι λόγω των ανελαστικών παραμορφώσεων των ράβδων προκαλείται μόνιμο άνοιγμα του αρμού μεταξύ τοίχου και δοκού. Το άνοιγμα αυτό καθυστερεί ή και εμποδίζει τη πλήρη επαφή των επιφανειών και την ανάπτυξη τριβής με συνέπεια την εμφάνιση pinching. Επιπλέον αξίζει να τονιστεί ότι η μετακίνηση αστοχίας είναι ανεξάρτητη της διατομής της ράβδου. Πρόσθετοι πίνακες αποτελεσμάτων και δεδομένα σχετικά με τα χρησιμοποιούμενα υλικά παρατίθενται στα Παραρτήματα Α και Β.

Acknowledgement

I would like to express my deepest appreciation and gratitude to Associate Professor I. Psycharis for his constant guidance and encouragement throughout the course of this study. I would also like to thank Assistant Professor C. Mouzakis for his contribution in the design of the specimens and the experimental setup and for various discussions that have been very helpful.

Furthermore, I wish to express my gratitude to my family and close friends for their patience and support throughout my postgraduate studies.

Finally, I am deeply grateful to Onassis Foundation for the scholarship that offered me, without which this thesis would not have been possible.

The research presented herein was conducted in the framework of the FP7 project “SAFECLADDING: Improved fastening systems of cladding wall panels of precast buildings in seismic zones”, Research for SME Associations, Grant Agreement number 314122. The financial support provided by the Commission of the European Communities through this project is greatly appreciated.

Table of Contents

List of Figures

List of Tables

1 Precast Cladding Systems

1.1 Introduction

For over one century precast concrete is widely used as an alternative of the common cast in situ practice. The growth has been based on enhanced features that enabled the designers to create economically competitive structures. Basic assets of precast concrete structures are the following:

- Construction speed
- Higher quality control
- Fire resistance and durability
- In combination with prestressing: larger spans covered
- Construction less affected by weather conditions
- Thermal and acoustical control
- Architectural advantages (smoother surfaces, finishes etc.)

Moreover a vast variety of shapes and sizes of columns, beams and slabs as well as special roof and pile elements can be manufactured. Hollow core sections and elements with variable sections are some of main reasons that precast concrete structures satisfy the design criteria (strength, deformability etc.) with the minimum required weight.

However, been an industrially manufactured product, maximum economy is achieved with the maximum repetition of standard section. Therefore, precast concrete technology is mostly applicable in structures like the following:

- Large buildings
  - Residential
  - Office premises
  - Warehouses and Industrial Buildings
  - Public (i.e., hospitals, airports, shopping malls etc.)
- Parking Structures
- Stadiums
- Bridges
- Tunnels
- Railway track systems

The exterior facade of precast buildings is often covered by precast panels offering protection from the weather condition and freedom of architectural expression. In common practice the panels are not designed to contribute to the structure's stiffness but to resist only their self-weight and wind and local seismic loads. In this case, the panels are termed ***cladding panels***. Based on this view, the current design practice of precast buildings is based on a bare frame model where the cladding panels enter only as masses. The panels are then connected to the structure with fastenings dimensioned with a local calculation while the frame behaves similarly to cast-in-situ structures due to the comparable energy dissipation capacity.

Industry-specific terms that are encountered in cladding system design are defined below:

Non-load-bearing precast concrete panels (cladding) refer to precast concrete panels that are not designed to participate in the gravity or lateral resistance of the building structure.

Load-bearing precast concrete panels refer to precast concrete panels that are designed to participate in the gravity and/or lateral resistance of the building structure.

Cladding system is a collective term that refers to the cladding panels, caulking between the panels, connections between the panels and the structure and the window glazing system.

Spandrel panels are cladding panels that cover the beam and floor slab of the building. The vertical dimension of the spandrel panels may be small and only cover the beam or they may span the full height of the story. The horizontal dimension often extends the full-bay width of the structure. Spandrel panels can either be solid panels or include openings for windows.

Column cover panels and mullions are panels that cover the columns of the building structure. Both column cover panels and mullions have the same panel design; however, column cover panels cover the columns of the building structure and mullions are spaced between the column cover panels and do not cover any columns. In most cases, these two types of panels are both called column cover panels. Column cover panels are often used in conjunction with spandrel panels.

Cladding connections or connectors are the connections that attach the panels to the building structure or attach a panel to other panels in the cladding system. There are several types of connectors in a cladding system, each designed to resist specific types of forces.

Caulking or sealant refers to the material used to seal the joints between the edges of adjacent cladding panels and the edges between the cladding panels and the window framing. Caulking is usually made of polysulfides, polyurethanes, or silicones.

1.2 Configurations

A typical cladding system with spandrel panels, column covers and mullions is shown in Fig.1.1. However, there is a large number of different configurations. The most characteristic facade configurations according to Arnold (1989) and PCI (2007) are listed below:

- The structural frame is covered with panels horizontally (spandrel panels) and vertically (column covers) while the openings are filled with glass (Fig. 1.2(a)).
- The structural frame is covered only with horizontal panels (spandrel panels). The intermediate bands are filled with glass (Fig. 1.2(b)).
- The structural frame is covered by full-bay panels with window openings punched in the panels (Fig. 1.2(c)).

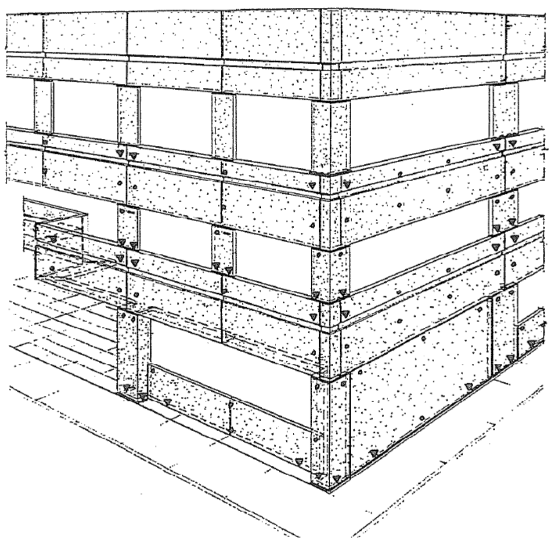

Figure 1.1. Typical cladding system (Hegle 1989).

(a) (b) (c)

Figure 1.2. Panel configurations: (a) spandrel beams and column covers; (b) spandrel panels and glazing; (c) punched window openings (PCI 1989).

1.3 Cladding connections

In the cladding systems there is a variety of connection types depending on the shape and direction of the longitudinal axis of the panel, the support conditions and the force and displacement direction. As mentioned above, the cladding panels are not designed so as to be integral part of the resisting system but only to resist their self-weight, wind and local seismic loads. For the in-plane forces ***Bearing connections*** are used while for out-of-plane forces ***Push-pull (tie-back) connections***.

Bearing connections are intended to transfer the loads from the cladding panel to the building structure. Bearing can be either directly in the plane of the panel along the bottom edge (Fig. 1.3(a)), or eccentric using concrete corbels, haunches, cast-in steel shapes, or attached panel brackets. Eccentric bearing connections (Fig. 1.4) are usually used for cladding panels when movements of the support system are possible. The most common types of eccentric bearing connections involve welding an angle or tube steel section to an embedment in the panel and using a levelling bolt to adjust the panel to the correct position. Besides mechanical devices eccentric connections can be created through cast-in-situ concrete (Fig. 1.3(b)).

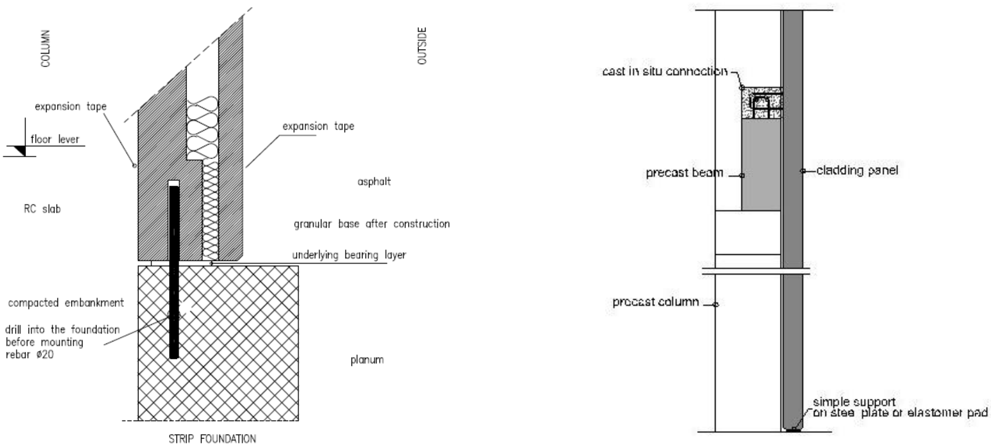

(a) (b)

Figure 1.3. (a) Direct Connection along the bottom edge of the panel; (b) Eccentric Connection cast-in-situ (Fischinger et al. 2013).

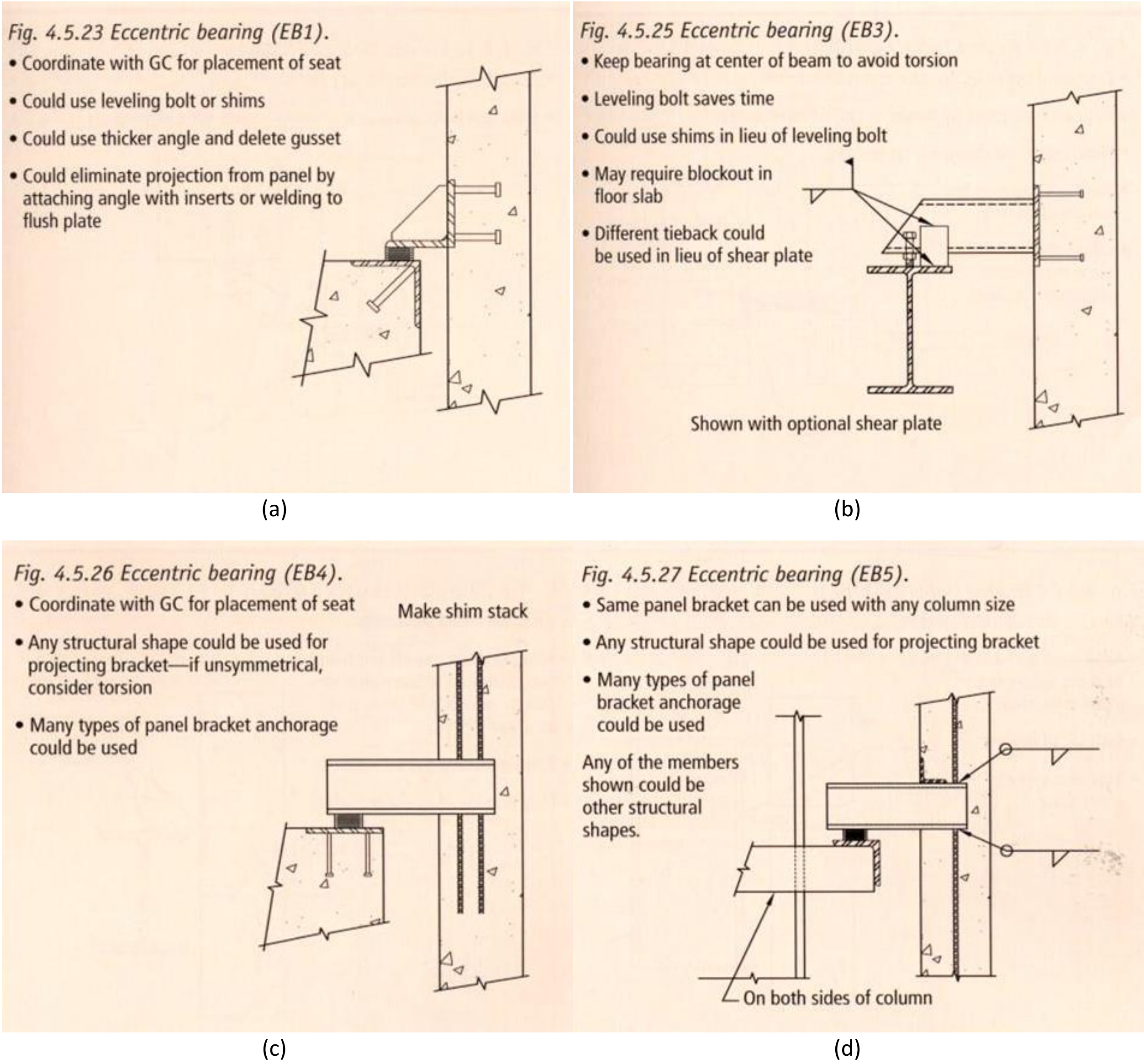

Figure 1.4. Eccentric Bearing Connections: (a) with steel angle; (b) with cast-in steel shape; (c)-(d) with projecting brackets (PCI 2007).

Push-pull (tie-back) connections are primarily intended to keep the precast concrete panel in a vertical position and to resist wind and seismic loads perpendicular to the panel. Tiebacks may be designed to withstand forces in the plane of the panel, or isolate them to allow frame distortions independent of the panel and allow movement vertically and/or horizontally. Common push-pull connections are made of threaded coil rods bolted or welded to angle or tube steel sections attached to the beam or column of the building structure (Fig. 1.5). Additionally, when the movement is not restrained, connections with slots that allow the sliding are widely used (Fig.1.6).

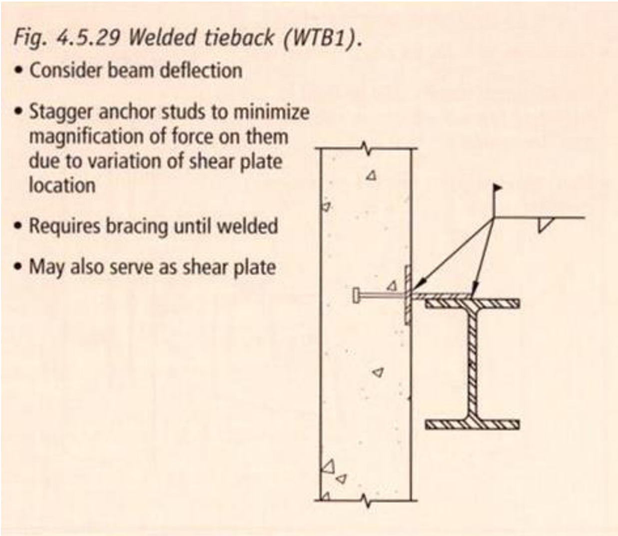

(a)

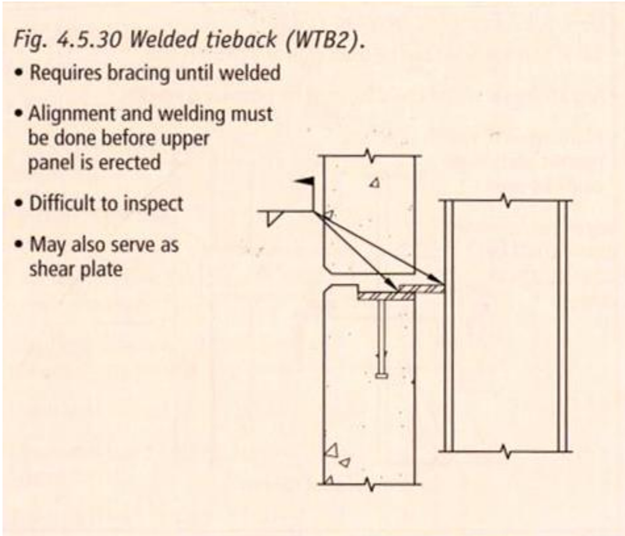

(b)

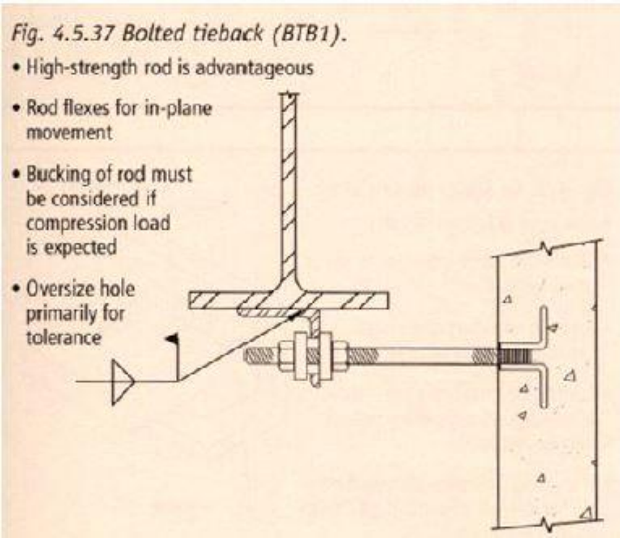

(c)

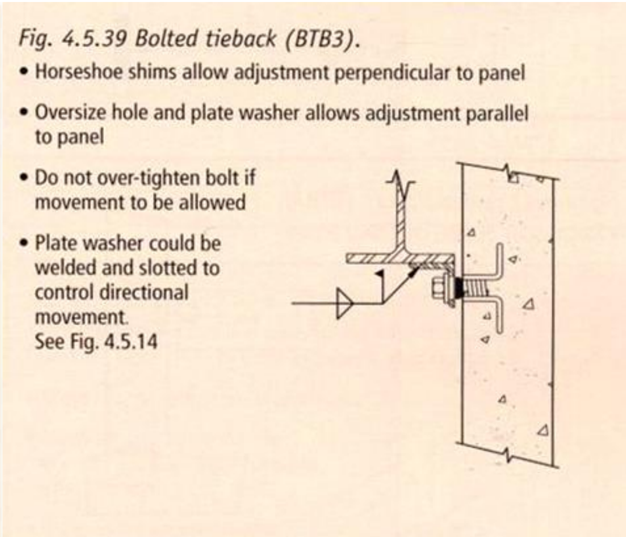

(d)

Figure 1.5. Push-pull (tie-back) Connections: (a) - (b) with welded steel plate; (c) with high-strength rod; (d) with steel bolt (PCI 2007).

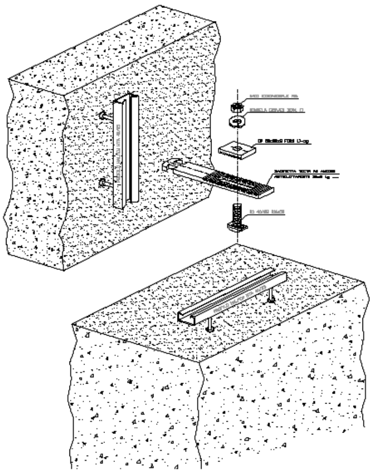

(a)

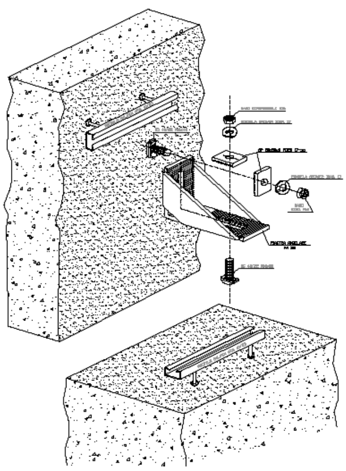

(b)

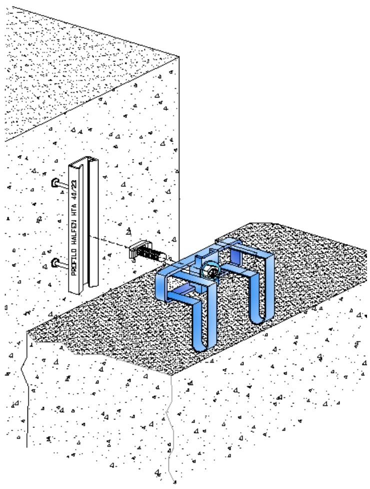

(c)

Figure 1.6. Sliding Bearing Connections: (a) sliding in both directions; (b) sliding in one direction with steel angle; (c) sliding in one direction with special box embedment (courtesy of Halfen).

When the cladding connections are achieved through mechanical devices, they consist of three parts: the body, the fasteners, and the anchorage. The body is the main part of the connector and usually consists of a threaded rod (for a push-pull connector) and angle or tube (for a bearing connection). The fastener is the portion of the cladding connection that attaches the body of the connection to the building structure and usually consists of bolts and nuts or welds. Finally, the anchorage attaches the precast panel to the body of the connection and usually consists of an embedment in the panel or expansion anchors.

1.4 Panel's Degrees-of-Freedom

The behaviour of the panels is governed by the connections' configuration within each element. Usually bearing connections are provided at one level of the structure and at no more than points per panel. On the contrary, no less than four tie-back connections should be provided. The reason for this is to avoid the development of an indeterminate distribution of gravity loads and to secure from out-of-plane collapse.

According to McCann (1991), the position of the bearing connections lie at the panel's bottom, top, or center (Fig. 1.7(a)). The exact configuration, according to the recommendations of PCI 2007, also depends on the type of the panel (spandrel of column cover) and on the shape. In Fig. 1.7(b) different panel sizes and the location of the bearing and tieback connections are illustrated. For square-shaped panels, the bearing connections are placed at the bottom and the tieback connections are placed at the corners. For the slender column cover panels, the bearing connections could be placed at the bottom or center of the panel. In the spandrel panel, the self-weight is supported at the floor level and restrained at a column or vertical member rather than at the underside of the floor member.

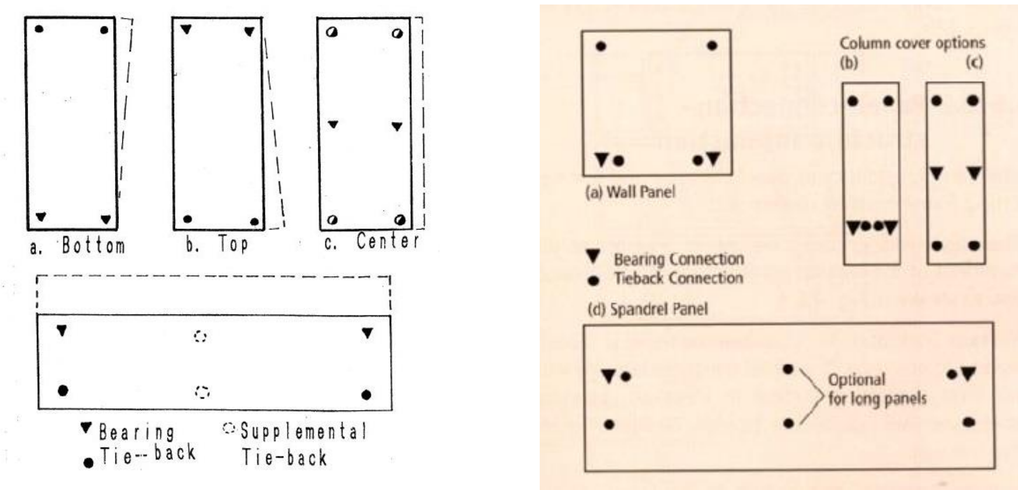

(a) (b)

Figure 1.7. Connections' configuration: (a) according to McCann (McCann 1991); (b) according to PCI (PCI 2007).

The potential movements of the cladding panels when the building undergoes interstorey drift are in-plane translation, in-plane rotation, out-of-plane rotation and out-of-plane translation.

In-plane translation (Fig. 1.8(a)) occurs when the panel is fixed to one level and is subjected to in-plane motion, such as a spandrel panel fixed to a beam. The panel translates laterally with that level, remaining vertical in elevation. In-plane rotation (Fig. 1.8(b)), also known as "rocking" occurs when the panel is supported at two levels and is subjected to in-plane motion, such as a column cover panel. This type of movement requires connections with slotted holes or gaps. Out-of-plane rotation occurs when the panel is attached to two different levels and is subjected to out-of-plane motion (i.e., interstorey drift perpendicular to the plane of the panel). This type of movement creates tension and compression forces in the push-pull connections. Out-of-plane translation is the movement that occurs when a panel is attached to one level of framing, such as a short spandrel panel, and is subjected to out-of-plane motion. The movements that cause the most significant potential for structural interaction are the in-plane translation and in-plane rotation.

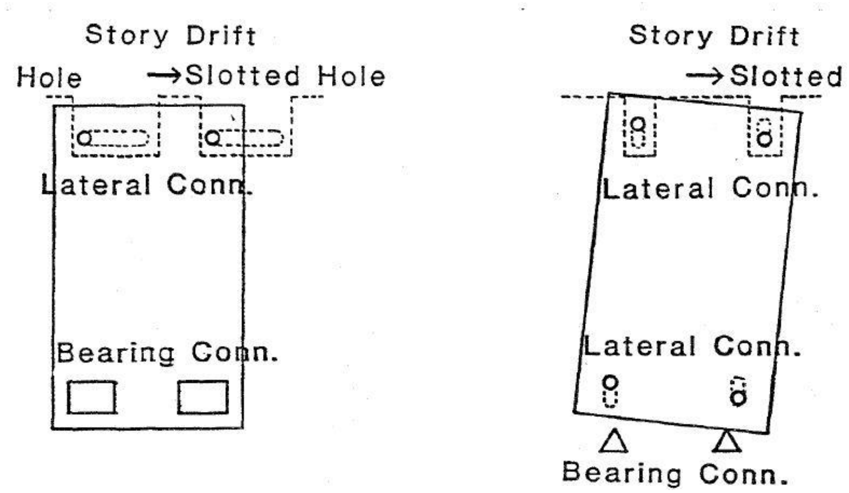

(a) (b)

Figure 1.8. In-plane movements: (a) translation; (b) rotation or "rocking" (Wang 1987).

2 Seismic Behaviour of Precast Cladding Systems

2.1 Observed Damages

Considerable damage to cladding systems has been reported since the 1964 Anchorage earthquake. However, damages even in recent earthquake events, like L'Aquila in 2009 and Grenada in 2010, verify that the design approach is still incorrect since there is a lack of knowledge about how cladding systems and their components truly behave in earthquakes.

The panels, connected to the structure in the way described above, come to be integral part of the resisting system conditioning its seismic response. As a result, the overall stiffness is increased leading to forces much higher than those calculated from the frame model. Furthermore, the seismic force reduction in the type of precast structures of concern relies on energy dissipation in plastic hinges formed in the columns. Very large drifts of the columns are needed to activate this energy dissipation foreseen in design. However, typically the capacity of the connections between cladding and structure is exhausted well before such large drifts can develop. Therefore the design of these connections cannot rely on the seismic reduction factor used for design of the bare structure.

The unforeseen intensity of the forces and the lower energy dissipation drove many fastenings to failure, leaving the frame of columns and beams practically undamaged. As shown in Fig. 2.1(a) even though the building frame kept its integrity, many cladding panels have collapsed. The cause of the collapse is the failure of the fastenings (Fig. 2.1(b)) of the panels under forces for which they were not designed.

(a) (b)

Figure 2.1. (a) Out-of-plane collapse; (b) Failure of sliding connection (Fischinger et al. 2013).

Failures though did not regard only channel bars but also other types of fastenings, as shown in Fig. 2.2. It is vital to say that it is mainly a matter of inadequate design of the connection and not a matter of product inadequacy.

(a) (b)

Figure 2.2. (a) Failure of steel angle; (b) Failure of other types of connections (Fischinger et al. 2013).

2.2 Connections under Investigation

Determining the actual behaviour of the existing cladding panels is a difficult task. This is because the response lies between that of total independence and total fixation. As it seems, the solution to the problem of the cladding panels would be to design the claddings towards one of these two directions.

The current design practice is shifted over the former by providing connections that can sustain large displacements. However, the specific type of connection still needs to be investigated as it is affected by numerous parameters. As far as the total fixation is concerned, load-bearing precast concrete panels are used only in wall systems. Even in these cases the design philosophy is completely different than in claddings since the bearing walls are relatively few in each structure, heavily reinforced and with large dimensions.

From what mentioned above it becomes evident that investigating the behaviour of precast cladding panels connected to the structure in a way that make them part of the overall resisting mechanism is of vital importance. With respect to the present production, new products with improved capacities are needed. Of course it is not only the steel connectors to be renewed, but also the nearby concrete part of the panel that shall resist without early failures. Furthermore, it is also important to verify the roof diaphragm through which the inertia forces shall be transmitted to the resisting lateral walls.

These connections - hereinafter referred as “integrated” - are based on a hyperstatic arrangement of the fixed supports of each panel. Several arrangements can be used, as the ones shown in Figures 2.3 and 2.4. In Fig. 2.3 vertical panels connected to the beams are shown, while in Fig. 2.4 horizontal panels connected to the columns. In both cases, connections at all four corners of each panel are provided forcing the panel elements to act as beams clamped at both ends.

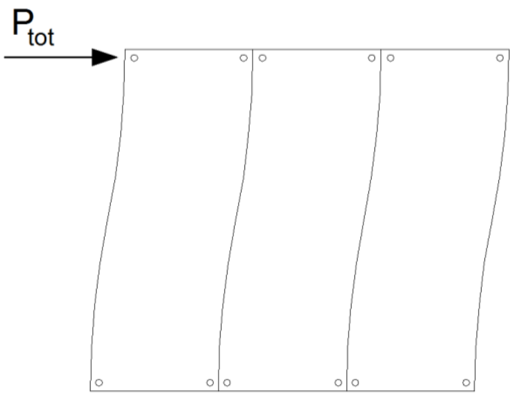

Figure 2.3. Vertical panel arrangement with four connections.

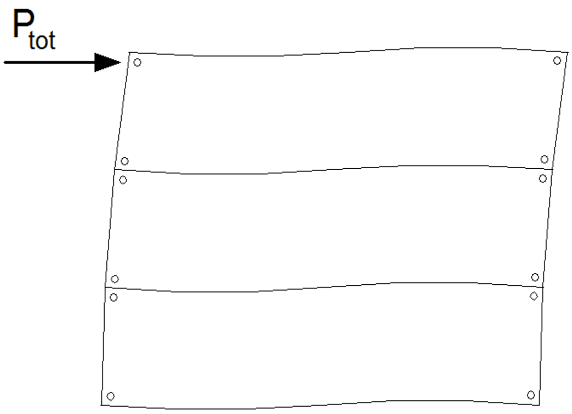

Figure 2.4. Horizontal panel arrangement with four connections.

It is noted that reduced number of connections at one end of the panels can also be used; however, such arrangements would lead to increased forces induced to the connections. For example, if three connections are used at the vertical panel arrangement, one at the top and two at the bottom (Fig. 2.5(a)), the forces induced to the bottom connectors for the same total horizontal force are double the ones for panels with four connections. However, it must be taken under consideration that the four-connection type might have significant problems in its materialization. In case of three-connection type, placing dissipative devices (Fig. 2.5(b)) along the panels' height so that both energy is consumed but also panels interact would alleviate the forces.

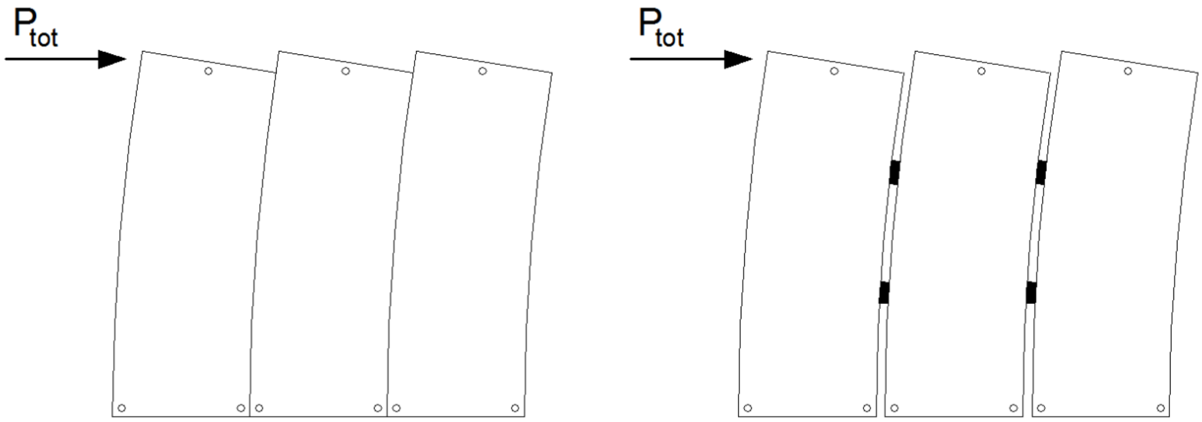

(a) (b)

Figure 2.5. Vertical panel arrangement with three connections: (a) without dissipative devices; (b) with dissipative devices.

In case of horizontal panels, it is recognized that the fixed connections to the columns affect significantly the deformation of the columns during earthquakes. Moreover, any damage during strong seismic excitation may have disastrous consequences to the overall strength of the columns and the stability of the whole building. Therefore, horizontal panel arrangement in integrated systems is not examined.

It is also noted that for long panels (either in the vertical direction for vertical panels or in the horizontal direction for horizontal panels), thermal fluctuations might induce significant axial forces to the panels which can lead even to out-of-plane buckling. In such cases, thermal forces must be considered in the design of the panels. If these forces are significant, the application of the "integrated system" might not be feasible. Using sliding connections at one end of the panels, instead of fixed ones, could be a solution to this problem, provided that the channel bars can bear the large earthquake loads in the transverse direction of the channels.

ANALYTICAL PART

3 Simplified theoretical analysis

3.1 Panels with four connections

For a symmetrical building and the cladding wall panels placed at the ***two** outer sides* along the direction of the seismic action, and accounting for the large stiffness of the panels compared with the stiffness of the precast frame, it can be assumed that the total base shear due to the earthquake load P_{base} is undertaken solely by the panels.

Let us assume that there are n vertical panels at each side of the building and that each panel is fixed to the top and the bottom beam by two connectors at each end. Then, the horizontal force, $P_{i,h}$, that is induced to each connection is (Fig. 3.1):

$$P_{i,h} \cong \frac{P_{base}/2}{2n} \tag{3.1}$$

where P_{base} is the total shear at the level of the base of the panels due to the earthquake load. For fully clamped conditions, the moment that develops at the panel's ends is:

$$M = 2P_{i,h}\frac{H}{2} \tag{3.2}$$

which produces vertical forces

$$P_{i,v} = P_{i,h}\frac{H}{L} \tag{3.3}$$

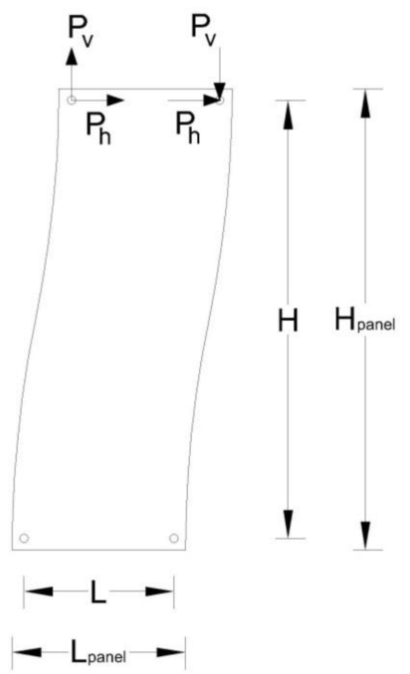

Figure 3.1. Distribution of forces at the connections.

In the above equations, H is the vertical distance between the connections of the panel and L is the corresponding horizontal distance (Fig. 3.1). These distances are smaller than the actual dimensions of the panel due to the insertion of the connections from the panel's edges. Taking also under consideration that the total length L_{total} of the building's sides on which the panels are placed is not necessarily fully covered with panels, one can write:

$$L = C_1 L_{panel} \tag{3.4}$$

$$n \cdot L_{panel} = C_2 L_{total} \tag{3.5}$$

where C_1 and C_2 are coefficients generally smaller than unity. Note that C_2 = 1 for sides fully covered with panels, but it can be significantly smaller than unity for sides with long openings. Combining (3.4) and (3.5), one gets:

$$L_{total} = \frac{nL}{C_1 C_2} \tag{3.6}$$

The total force developed in one connection is:

$$P_i = \sqrt{P_{i,h}^2 + P_{i,v}^2} \tag{3.7}$$

Using the above relations, the force induced to ***each*** connection can be normalized with respect to the total seismic load:

$$\frac{P_i}{P_{base}} = \frac{1}{4}\sqrt{\frac{1}{n^2} + \left(\frac{H}{C_1 C_2 L_{total}}\right)^2} \tag{3.8}$$

The plot of Eq. (8) for C_1 = 0.87, C_2 = 0.90 and three values of H/L_{total} is shown in Fig. 3.2. It is seen that, for values of n larger than about 4, the normalized force is independent of the number of panels, i.e., the term $1/n^2$ can be neglected. Then, using Eq. (3.6) one can write:

$$P_i \cong \frac{P_{base}}{nL} \cdot \frac{H}{4} \tag{3.9}$$

Denoting with P^* the base shear per unit length, i.e.

$$P^* = \frac{P_{base}}{L_{total}} = \frac{C_1 C_2 P_{base}}{nL} \tag{3.10}$$

equation (3.9) becomes:

$$P_i = \frac{P^*}{C_1 C_2} \cdot \frac{H}{4} \tag{3.11}$$

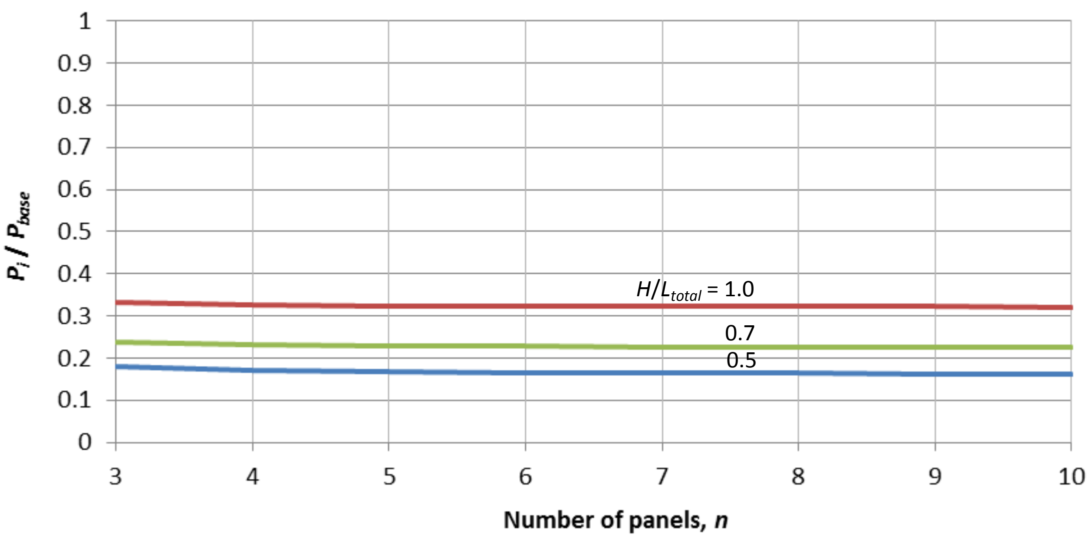

Figure 3.2. Normalized force at the panel connections (C_1 = 0.87, C_2 = 0.90).

In case of panels covering the full length of the external sides, one can assume, as a first approximation, that $C_1 C_2 \cong 1$, thus,

$$P_i \cong P^* \cdot \frac{H}{4} \tag{3.12}$$

Remarks

1. Eq. (3.11) implies that the force induced to each connection is independent of the width of the panels. This practically means that the connection forces cannot be reduced by using more panels of smaller length or less panels of larger length. However, the connection forces greatly depend on the "*coverage*" of the external sides by panels (coefficient C_2) and increase significantly in case of sides with long openings, i.e., sides partially covered with panels.
2. The force induced to each connection is linearly increasing with the vertical distance H of the connections, i.e., with the height of the storey.
3. As evident from Eq. (3.8), the major component of P_i is in the vertical direction.

3.2 Panels with three connections

For the same assumptions with the above analysis, but considering panels with three connections (one at the top and two at the bottom), it can easily be proven that:

$$P_i = \frac{P^*}{C_1 C_2} \cdot \frac{H}{2} \tag{3.13}$$

In this case, therefore, larger forces are induced to the bottom connectors, which are double the ones for panels with four connections [compare with Eq. (3.11)].

4 Numerical Analyses

The analytical investigation is performed on two structural assemblies representing the most common typologies of precast buildings. Both buildings selected are industrial facilities as this category of structures represents that largest portion of precast concrete application.

4.1 Industrial single-storey building – case A

4.1.1 Description

As a first part of the numerical analyses, a single-storey industrial building was analysed. The building considered (Fig. 4.1 and 4.2) is a single-storey industrial building with external axial dimensions of 42.0 m × 100.0 m while the structural skeleton is placed at a grid of 21.0 m × 10.0 m. The height of the building is 7.0 m, measured from the floor to the lower face of the main beams. The presence of a seismic joint at the middle of the longitudinal direction allows to consider only half of the building of length L_{total} = 50.0 m.

The roof of the building is provided by precast prestressed girders (main beams) along the direction of 21.0 m and precast U-shaped beams (secondary beams) along the direction of 10.0 m. The cover of the roof is realized by Hollow Core Slabs, which are directly supported on the main girders. On the upper face of the slabs a layer of cast in situ concrete (6 cm thick) is poured ensuring the formation of a continuous and rigid diaphragm, according to the Greek Precast Code (B3.5.2.) about precast diaphragms.

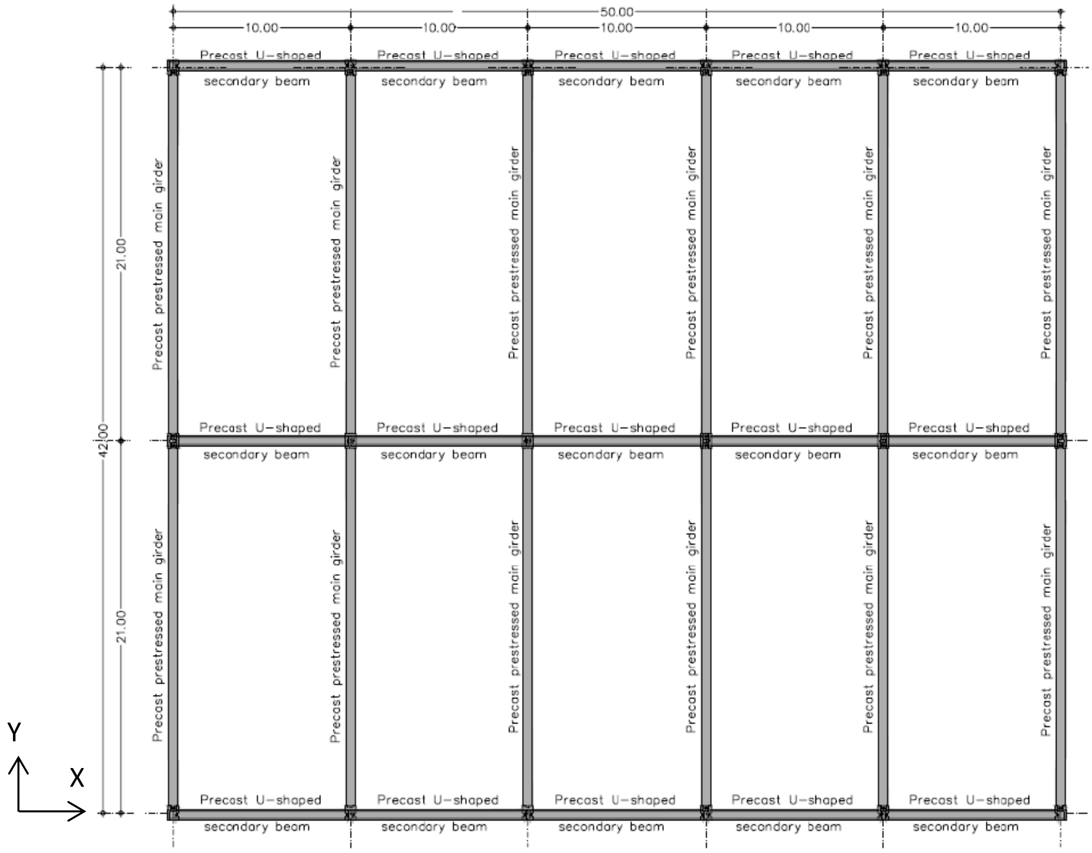

Figure 4.1. Plan view of the building.

The beam-column connections are provided by steel dowels bolted on the top. The gap between the body of the hole (at the beam end) and the body of the dowel is filled with proper concrete. All beams are placed on elastomer supporting pads provided on the top of the columns.

The perimeter of the building is assumed to be covered by precast “sandwich” cladding panel designed accordingly.

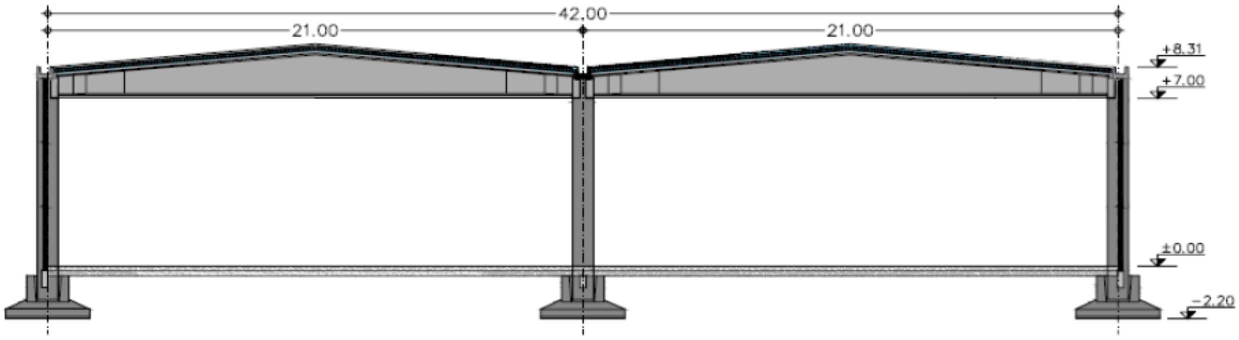

Figure 4.2. Vertical section of the building.

4.1.2 Structural analysis and dimensioning

The building of Fig. 4.1 and 4.2 has been designed according to Greek RC Code and the Greek Precast Code under the following assumptions:

- Steel class: B500C
- Concrete grade (precast): C30/37
- Loads:
  - Permanent roof load .... 0.30 kN/m^2
  - Live roof load. 1.50 kN/m2
  - Wind velocity... 25.00 m/s
- Total load effective to earthquake action
  - Total vibrating mass (14765 kN) = ... 1476500 kg
  - Peak ground acceleration = ... 0.25 g
  - Soil type: .... B
- Behaviour factor:
  - for the bare frame: *q* = ... 1.875

4.1.3 Numerical model

Modal and Response Spectrum analyses are performed using SAP2000. The EC8 elastic response spectrum for a_g = 0.24 g and soil type B is applied.

The numerical model consists of beam elements which represent the columns, the beams, the panels and the diaphragm. Since the analyses are elastic plastic hinges are not defined. Cladding panels are considered to be placed only in the X direction.

Frame Model

The structure is composed of precast columns, main girders and secondary beams (Fig. 4.3). The cross section of the latter in the original structure is shown in Fig. 43(c); this section is used in most analyses. However, some runs are performed with increased cross section of secondary beams, as explained in the ensuing. The columns are assumed fixed at their base, while diaphragmatic action is ensured at the roof level by massless X-braces. Following the precast concrete practice, pinned connections between beams and columns are adopted. Due to the presence of the panels, the frame elements are expected to behave elastically; therefore the stiffness may be considered uncracked. In the performed analyses the stiffness is taken equal to 75% of the geometrical for all buildings for comparison reasons.

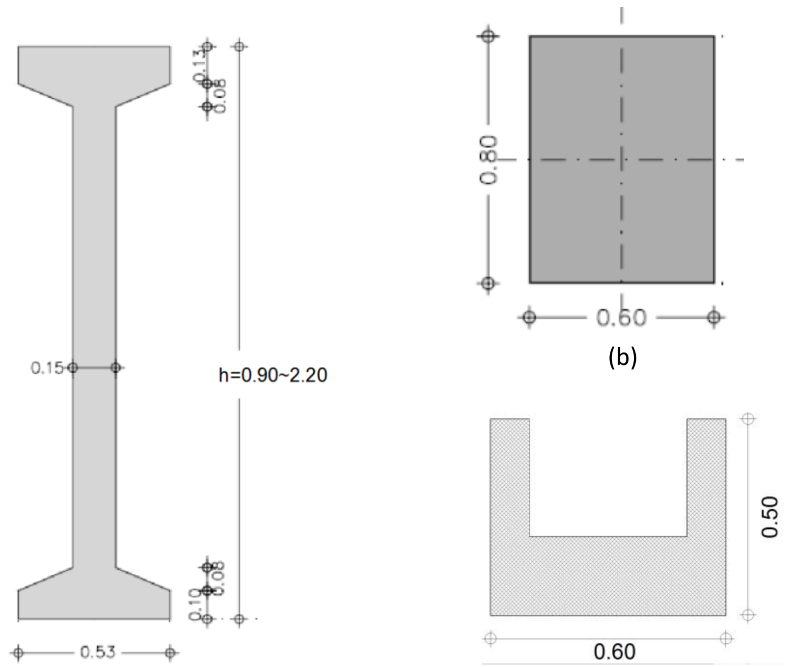

Figure 4.3. Elements' cross sections: (a) Main girder; (b) Column; (c) Secondary beam (original structure).

Panel Model

The configuration chosen is that of vertical or horizontal panels with fixed supports at each corner. The dimensions of the panels (L_{panel} and H_{panel}) are different in each case. However, the support's distances from the edges are constant in all cases examined and are shown in Fig. 4.4.

The thickness of the panels is taken equal to 0.15 m, which is the minimum required according to EC8 for ductile walls and for large lightly reinforced walls. However, this value may be incompetent to sustain the large forces transferred to the concrete.

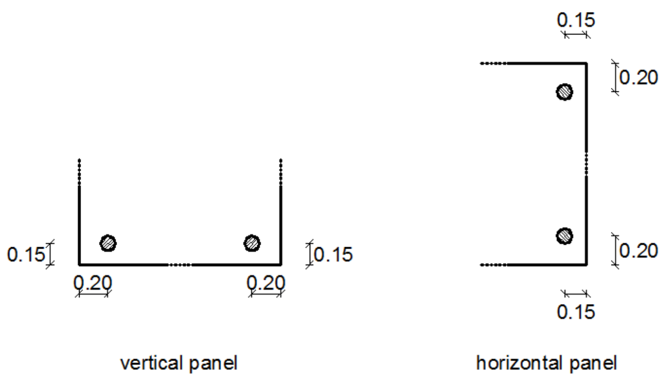

Figure 4.4. Distance of connectors from panel's edges.

Analyses are performed for both vertical panels connected to the beams, and horizontal panels connected to the columns. In the first case, 3 vertical panels with L_{panel} = 3.0 m and H_{panel} = 7.4 m are placed at each span of length 10.0 m (centreline distance of columns), as shown in Fig. 4.5. In the case of horizontal panels, 3 with L_{panel} = 2.0 m (measured in the vertical direction) and H_{panel} = 10.4 m (measured in the horizontal direction) are considered, as shown in Fig. 4.6.

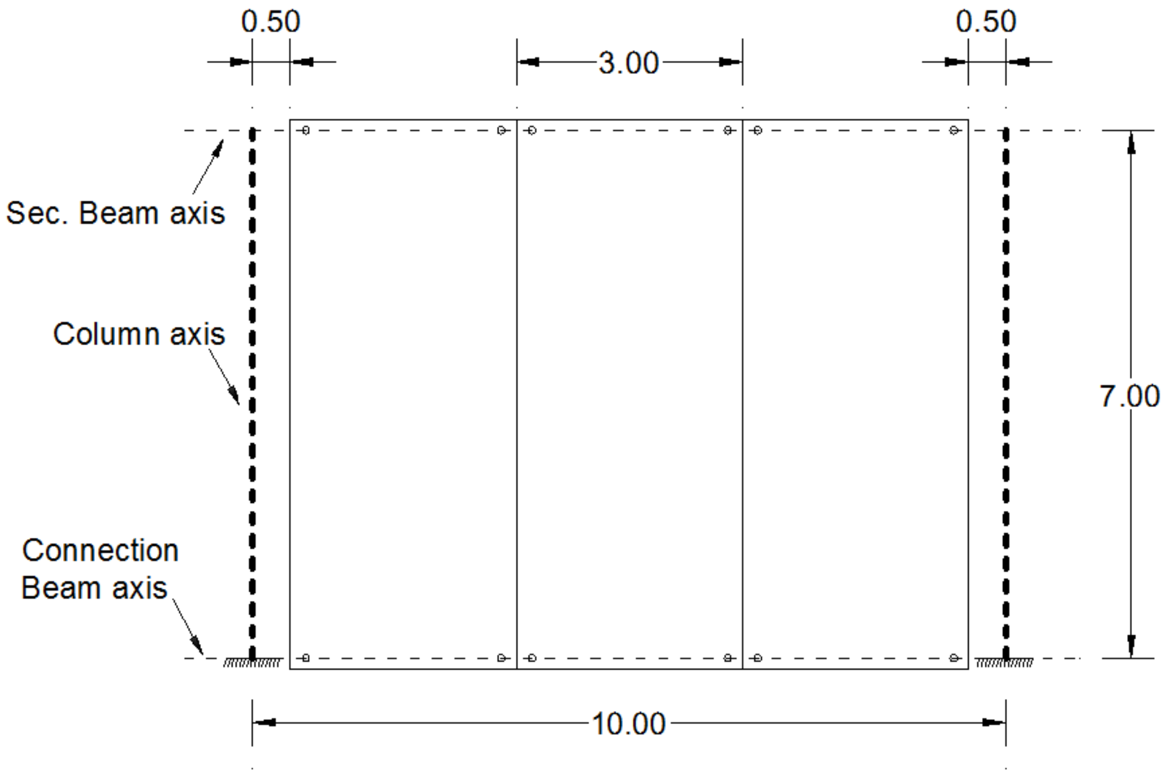

Figure 4.5. Vertical panel configuration.

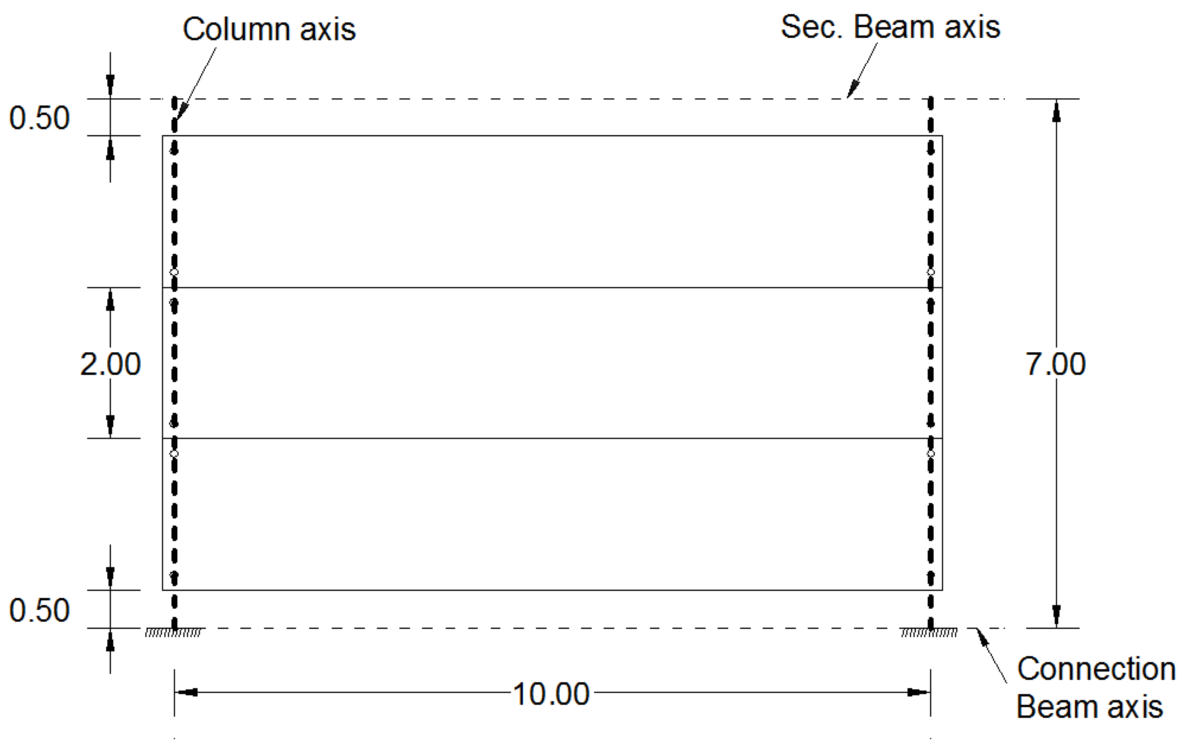

Figure 4.6. Horizontal panel configuration.

Each panel is modelled by 5 beam elements, as shown in Fig. 4.7. Element 1 coincides with the longitudinal axis of the panel and has the same cross section. The rest four elements model the effective width at the ends of the panel; two values are considered for the effective width, namely 1.0 m and 1.5 m. This "linear" model of the panels is verified by comparing the results with the results of analyses in which the panels are modelled by plate elements.

The connectors are modelled by elastic springs of varying stiffness, in order to investigate the effect of their deformability on the connection forces.

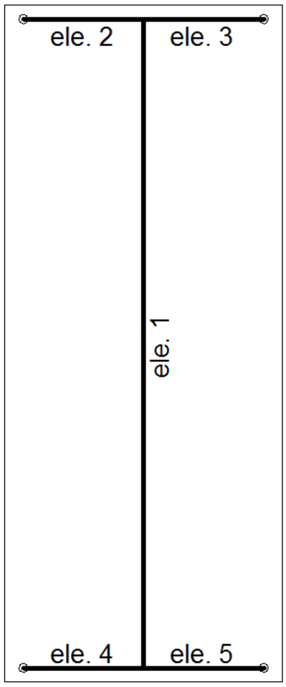

Figure 4.7. Model of panels.

4.1.4 Material properties

In all analyses, the mean strength of the concrete is taken into account, which is defined according to EN 1992-1-1 (Table 3.1 and Appendix C) (CEN, 2004a). Since there are no data available for reinforcement of the elements, reinforcement steel and confinement are not taken into account. The considered properties are summarized in Tables 4.1. The constitutive law for the concrete is depicted in Fig.4.8.

Table 4.1. Material properties considered for the concrete.

Parameter	**Value**
Modulus of Elasticity, E_c [GPa]:	33
Mean cylinder compressive strength of unconfined concrete, f_{cm} [MPa]:	38.0
Mean tensile strength of concrete, f_{ctm} [MPa]:	2.9
Deformation corresponding to f_{cm}, ε_{c1}:	0.0022
Ultimate deformation of unconfined concrete, ε_{cu1}:	0.0035

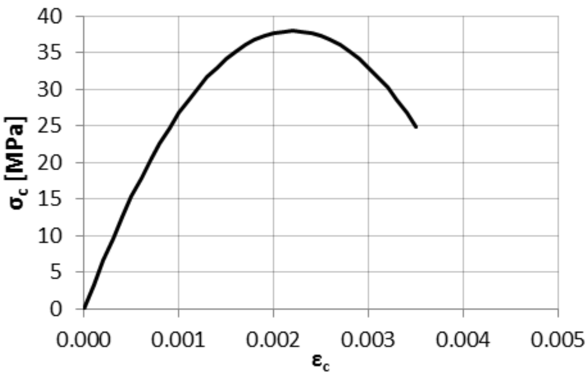

Figure 4.8. Stress-strain relation for the concrete considered in the analysis.

4.1.5 Results of the numerical analyses

As mentioned above, all analyses of the considered building are performed with SAP2000. A sketch of the numerical models used is shown in Fig. 4.9. Both vertical and horizontal panels are depicted, modelled as “beam” and the shell elements. The properties of the models were presented in the previous sections.

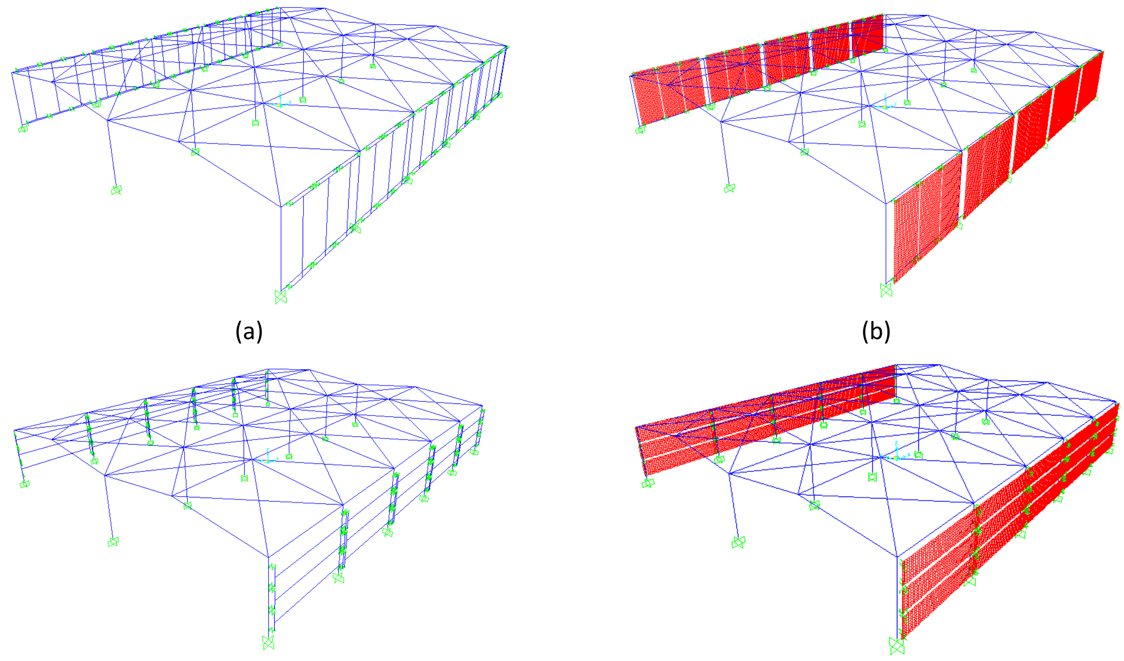

(a) (b) (c) (d)

Figure 4.9. SAP2000 models of the building analysed: (a) “beam” model of vertical panels; (b) shell model of vertical panels; (c) “beam” model of horizontal panels; (b) shell model of horizontal panels.

4.1.5.1 Modal Analysis

For comparison reasons, modal analyses are performed for the building with panels and the bare frame in which the panels contributed only as masses (un-connected panels). For the structure with vertical “beam” panels and effective width 1.0m and for the corresponding bare frame the 3D view of the most significant modes of vibration in direction X and Y is presented in Fig 4.10 and 4.11. The effect of the connectors’ stiffness in the eigen periods is shown in Fig. 4.12-4.15.

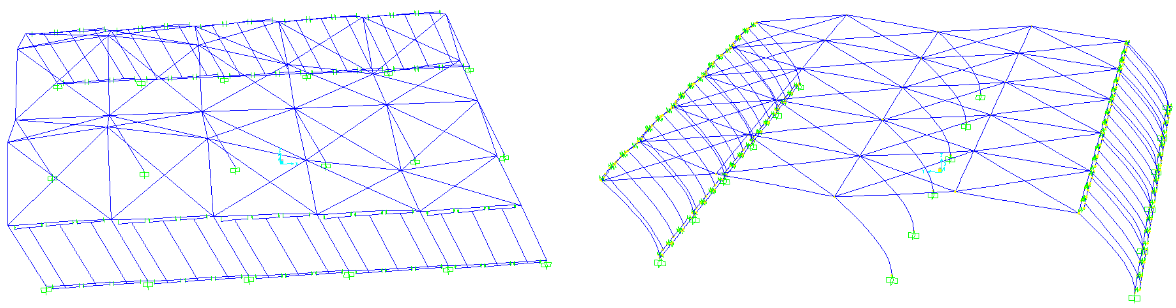

(a) (b)

Figure 4.10. Significant modes of vibration of the building with panels; (a) in direction X; (b) in direction Y.

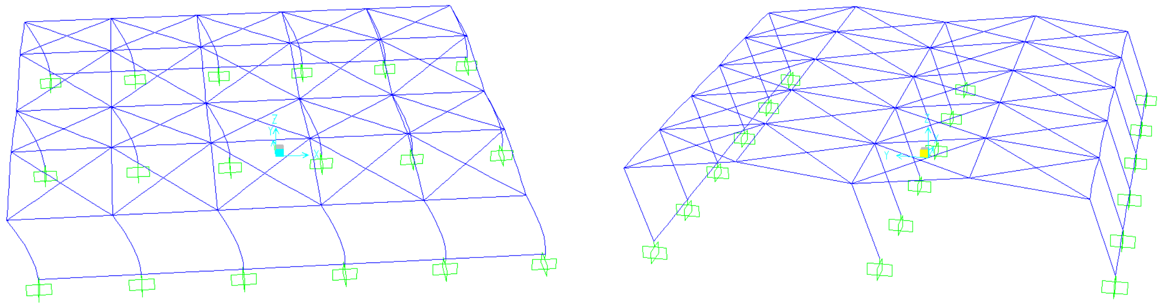

(a) (b)

Figure 4.11. Significant modes of vibration of the bare frame building; (a) in direction X; (b) in direction Y.

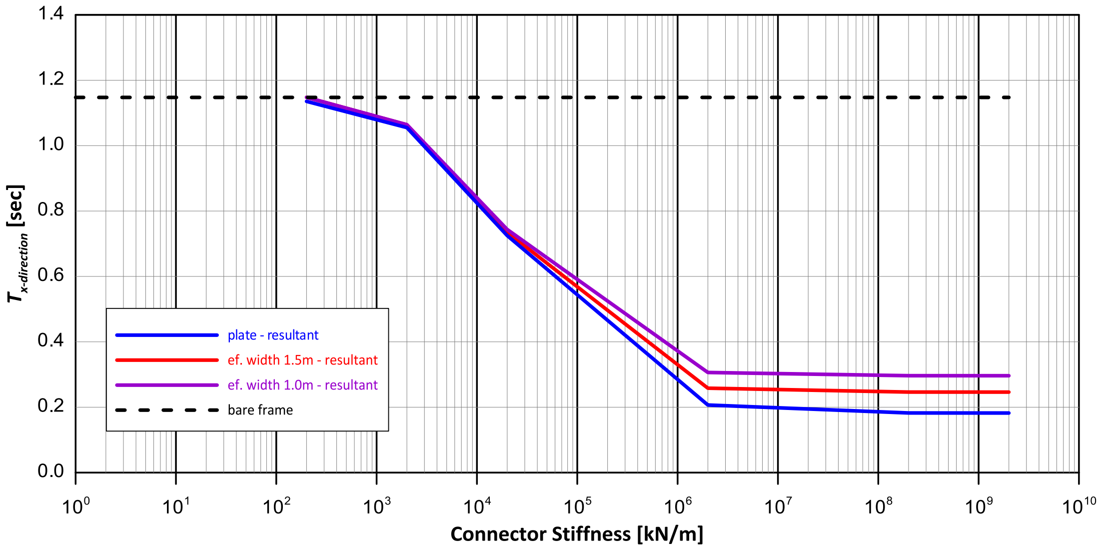

Figure 4.12. Period of the most significant mode of vibration in direction X for vertical panels.

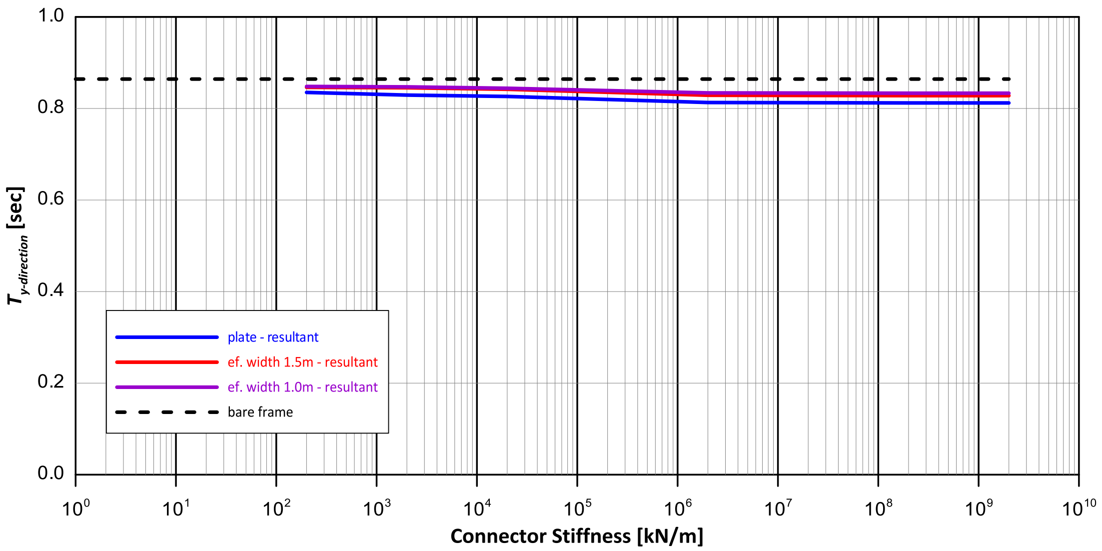

Figure 4.13. Period of the most significant mode of vibration in direction Y for vertical panels.

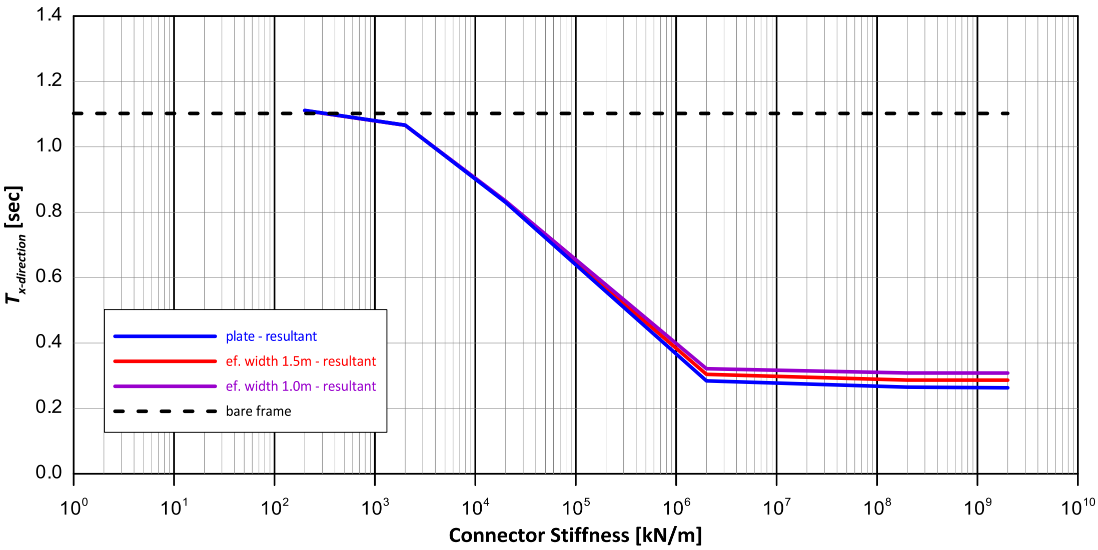

Figure 4.14. Period of the most significant mode of vibration in direction X for horizontal panels.

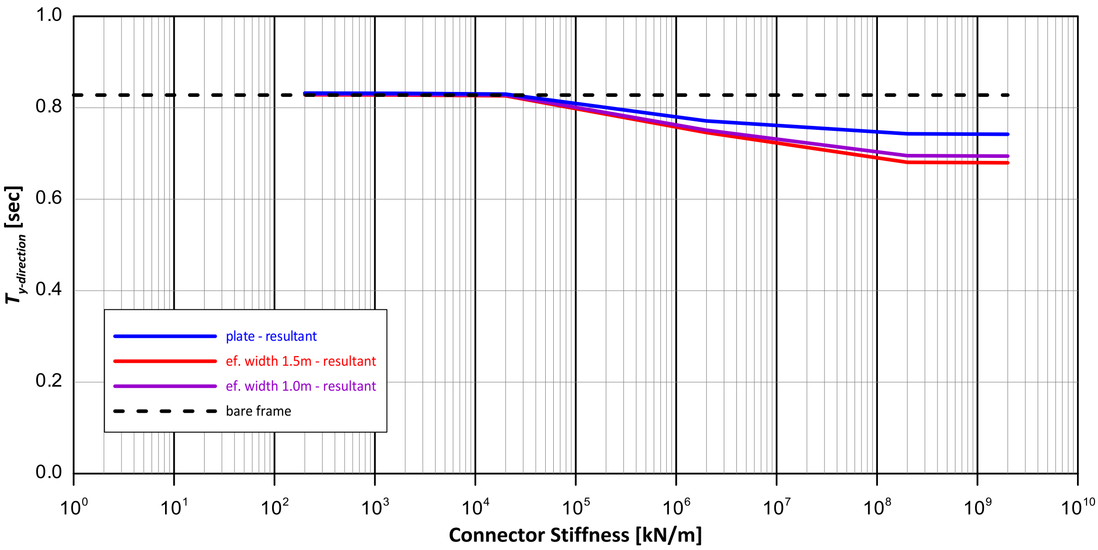

Figure 4.15. Period of the most significant mode of vibration in direction Y for horizontal panels.

4.1.5.2 Response Spectrum Analysis

The effect of the cladding is also examined through a Response Spectrum Analysis in the direction along which the panels are placed. The analyses for the vertical direction are not described in this thesis.

Forces induced to the connectors

The maximum resultant forces developed in the connections for different values of the connectors' stiffness, for vertical and horizontal panels are shown in Fig. 4.16 and 4.17 respectively. In both cases, the results for the F.E. and for the "beam" modelling of the panels are shown for comparison.

The vertical component of the connection force, $P_{i,v}$, is also shown in Fig. 4.16 with dashed line. It is evident that the vertical component almost coincides with the resultant, which is expected according to the results of the theoretical approach (remark 3).

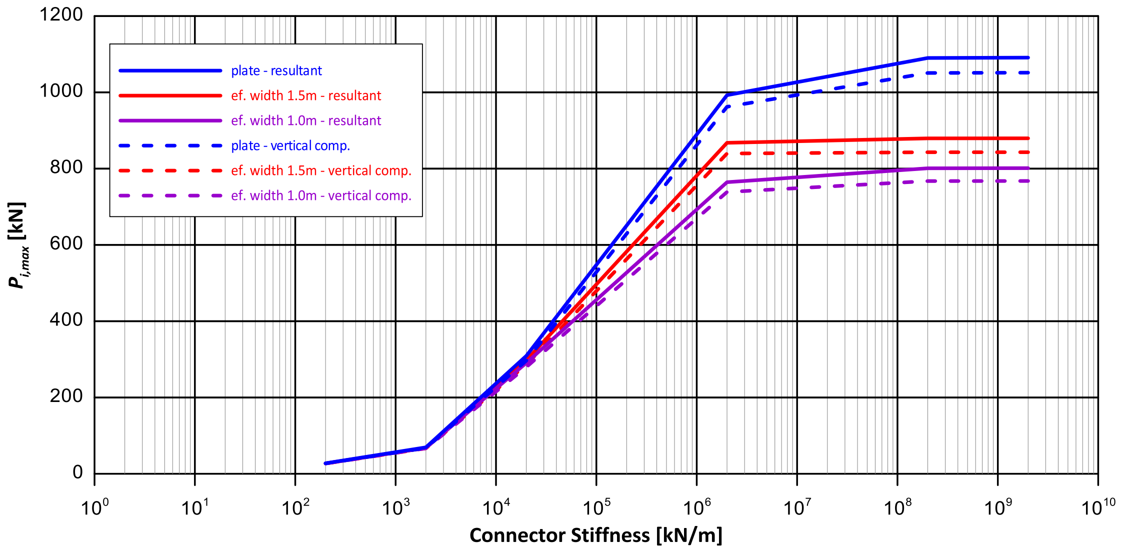

Figure 4.16. Maximum Forces in Vertical Panels

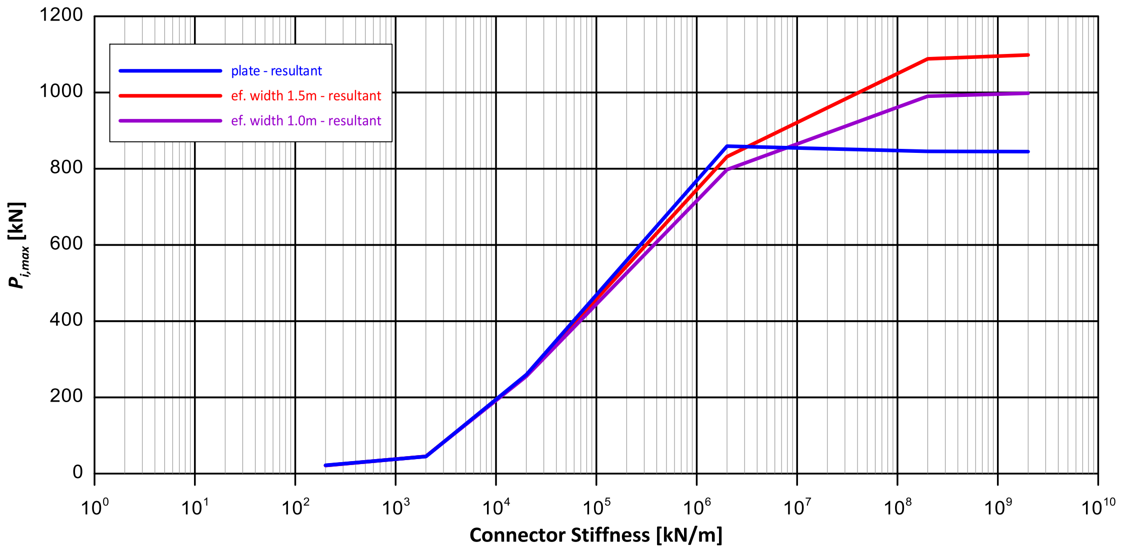

Figure 4.17. Maximum Forces in Horizontal Panels

It can be observed that the maximum forces induced to the connectors attain very large values for "rigid" connections, more than 1000 kN. However, these large values were observed only to the outer connectors of the first and the third panel, while in the rest connectors the forces were significantly lower. This large dispersion of the forces' magnitude is shown in the histogram (Fig. 4.18) of the calculated forces for the configuration with vertical panels, effective width 1.0 m and increased cross section of secondary beams. It is evident that the large values depicted in Fig. 4.16 and 4.17 correspond to few connectors only. In addition, it is not clear whether these large values are "real" or due to numerical instabilities caused by the large stiffness of the connectors. For this reason, the average values of the forces induced to all connectors are used in the following. The average forces are plotted in Fig. 4.19 and 4.20. Note that now, the accuracy obtained by the "beam" model of the panels is very satisfactory.

Comparing Fig. 4.19 and 4.20, it is observed that the forces induced to the connectors are 50% larger for horizontal panels than for vertical ones.

It is interesting to note that Fig. 4.16, 4.17, 4.19, 4.20 show that the forces induced to the connections decrease almost exponentially with decreasing stiffness of the connectors. This practically means that yielding of the connectors leads to relaxation of the forces, as expected; this, however, is accompanied by significantly increased displacements of the connectors, which might exceed the ductility capacity.

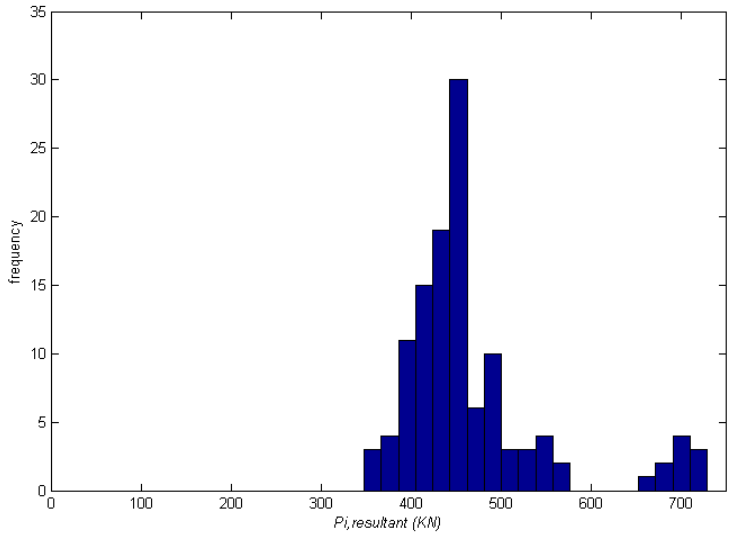

Figure 4.18. Histogram of resultant force at the connections

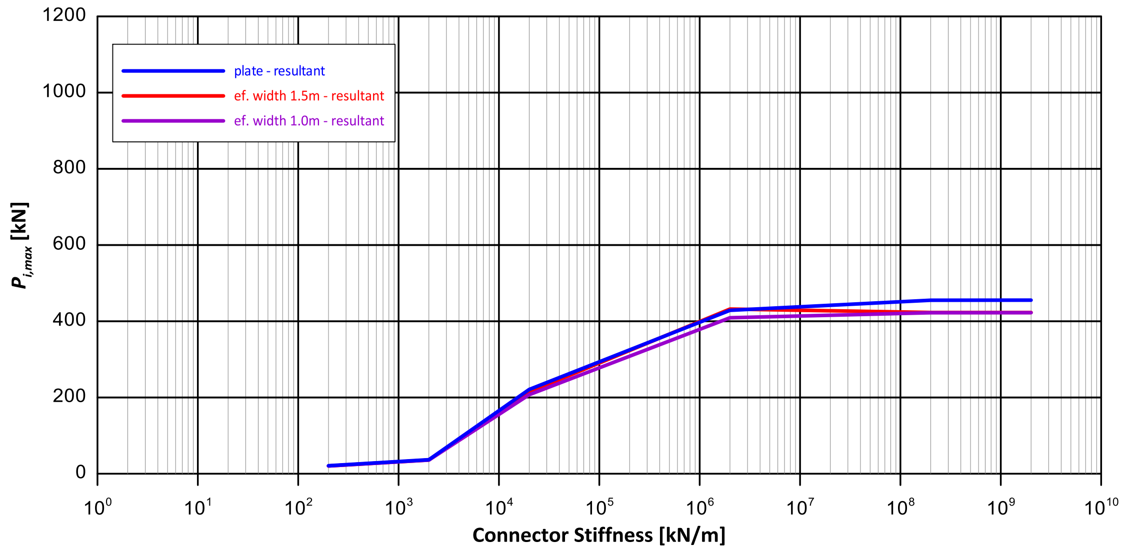

Figure 4.19. Average Forces in Vertical Panels

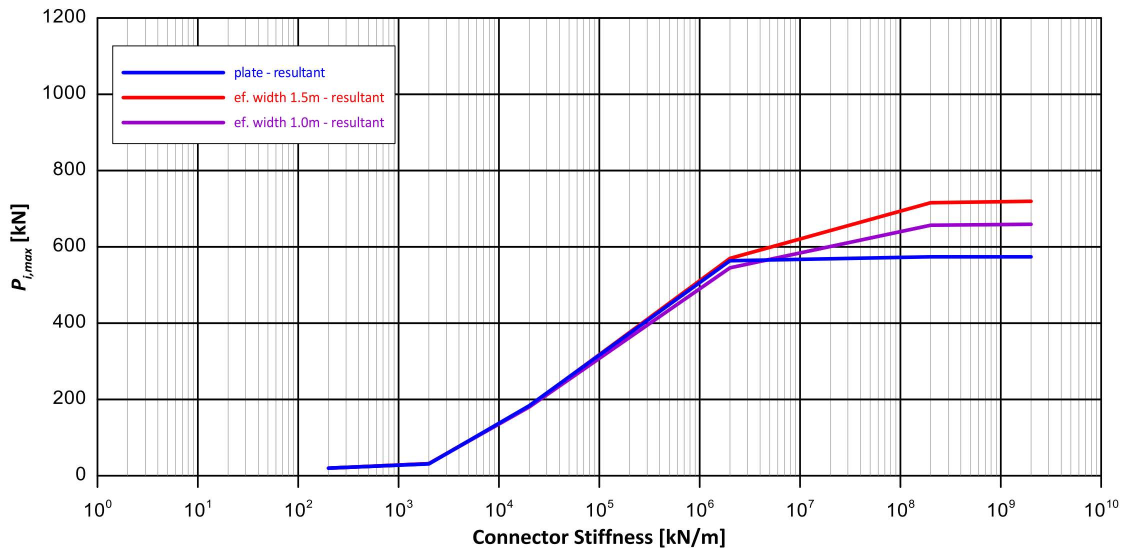

Figure 4.20. Average Forces in Horizontal Panels

Effect of number of panels, *n*

For vertical panels and for the "beam" model with effective width 1.0 m, the effect of the number of spans is examined by analysing the following cases:

- 2 panels per span (L_{panel} = 4.5 m) – 10 panels at each side
- 3 panels per span (L_{panel} = 3.0 m) – 15 panels at each side (original model)
- 6 panels per span (L_{panel} = 1.5 m) – 30 panels at each side

The results are shown in Fig. 4.21, where the vertical component of the connection force is also shown for comparison. As expected from the theoretical analysis, the forces induced to the connectors are only slightly affected by the number of the panels and their width L_{panel}. The small variation in P_i is attributed to the variation of the coefficient C_1 with L_{panel} (see Eqs (3.4) and (3.11)), since, in all cases, the distance of the connectors from the panel edges was kept constant (Fig. 4.4).

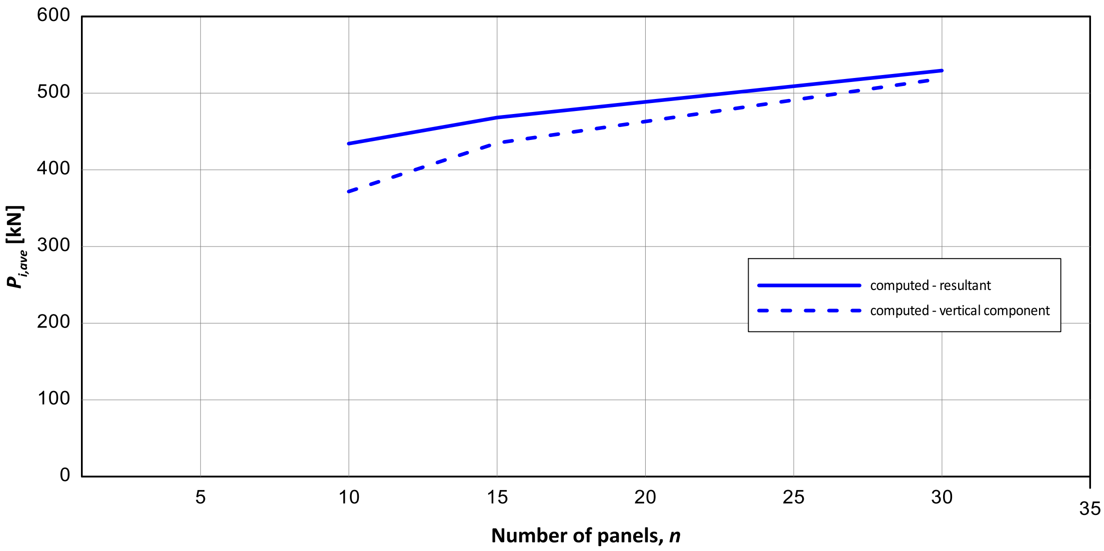

Figure 4.21. Effect of number of panels

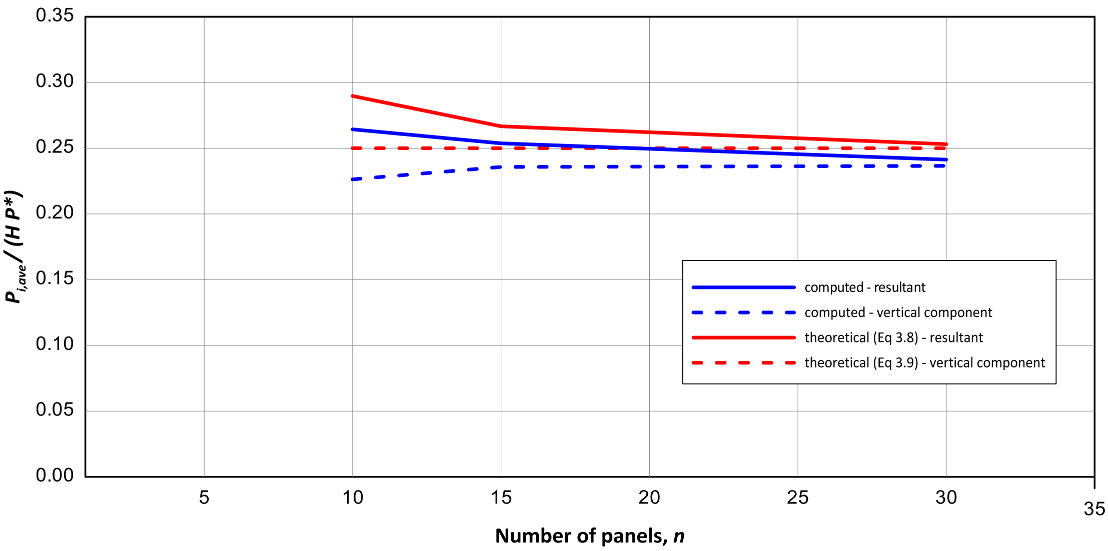

Figure 4.22. Effect of number of panels

The comparison of the numerical results with the theoretical predictions (Eqs (3.8) and (3.9)) is shown in Figure 4.22, in which the connection force Pi is shown normalized. It is seen that the average force

$P_{i,ave}$ is slightly lower than the theoretical prediction, which happens because, in the theoretical approach, the contribution of the columns to the base shear is neglected.

Effect of height of the panels, H

For vertical panels and the "beam" model with effective width 1.0 m, the effect of the height of the panels is examined by analysing the following cases:

- H = 5.0 m (H/L_{total} = 0.10)
- H = 7.0 m (H/L_{total} = 0.14) (original model)
- H = 10.0 m (H/L_{total} = 0.20)

The results are shown in Fig. 4.23, in which the variation of the ratio $P_{i,ave}$ / $(0.25P^*)$ with the height H is shown. It is reminded that, according to Eq. (3.11), this ratio is practically equal to H, which is verified by the numerical results.

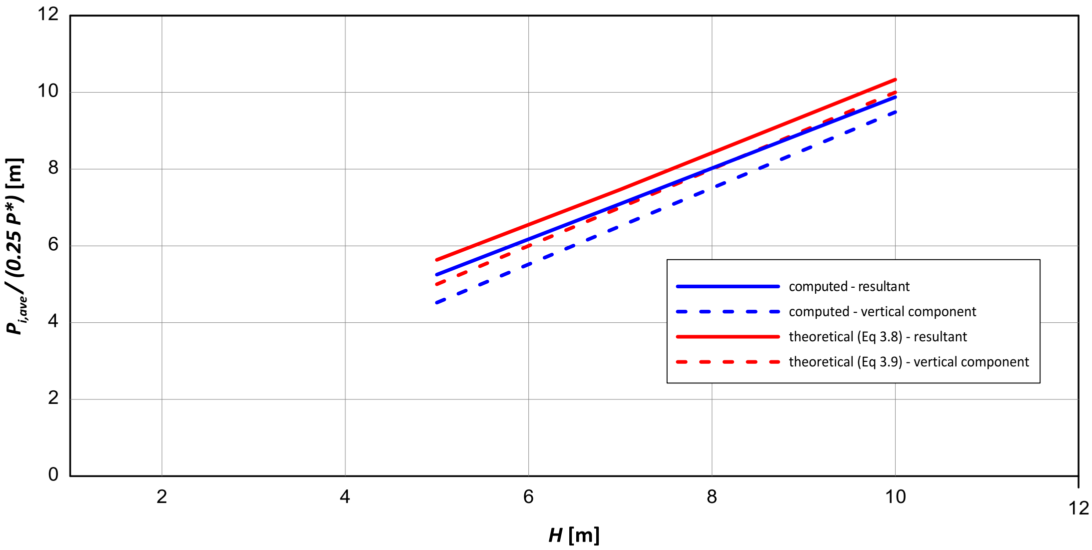

Figure 4.23. Effect of height of panels

Effect of the cross section of secondary beams

The above analyses show that the forces induced to the connectors are quite large and, thus, in the case of vertical panels connected to the beams, the beams must have the necessary strength and rigidity to accommodate these forces. In the original structure used, the secondary beams had a U-shape cross section, which was rather flexible (hereinafter referred to as "weak beam"). In order to examine whether this flexibility of the top beam affects the results, an analysis is performed with a much stronger beam (hereinafter referred to as "strong beam"), specifically with the same cross section with the foundation beam, namely 0.40 m × 0.60 m. The results are depicted in Fig. 4.24 and show that the effect of the cross section of the secondary beam on the average force induced to the connectors is not significant.

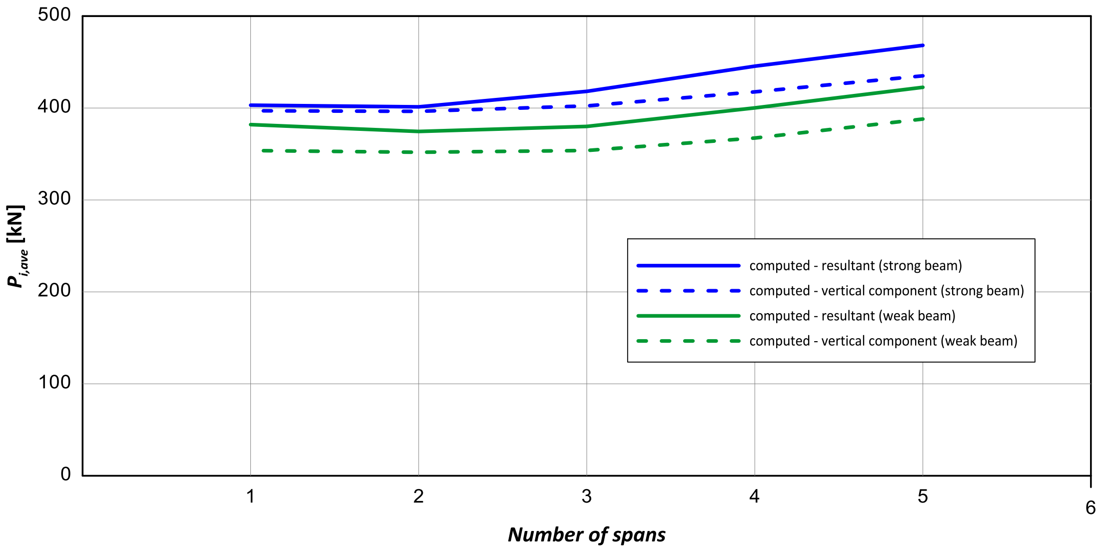

Figure 4.24. Effect of the secondary beam.

4.2 Industrial single-storey building – case B

4.2.1 Description

The analytical investigation is performed on several structural assemblies representing the most common typologies of precast buildings. Since the aim is to analyse how integrated connections play their role in the structural response, several building typologies are used in order to allow the comparison of the results.

Frame systems of structures for one-storey and multi-storey (low rise) buildings with industrial and commercial destination are considered. The following construction parameters are investigated in parametric analyses:

- *structural arrangement* (regular / not regular)
- *shape* ratio (elongated / intermediate / compact)
- *column height* (low 5 m and tall 8 m)
- *roof deck* (short beam with long roof elements / long beam with short roof elements)
- *roof diaphragm* (null / deformable / rigid)
- *cladding walls* (vertical / horizontal)
- *cladding walls coverage* (on four sides / on three sides)
- *number of connections at each panel* (three with vertical sliding at the top and four without relative displacements)
- *seismic action direction* (longitudinal / transversal)

As the combination of all the aforementioned parameters leads to a very large number of cases, only three representative cases (Fig. 4.25) are analysed. The analyses concern:

- One-storey building with height 7.5 m and length 60 m
- Two bays of 20 m span each (intermediate shape ratio)
- Long double T roof elements and short beams
- Null / Deformable / Rigid roof diaphragm
- Vertical cladding walls on four sides with 4 connections each
- Excitation: Tolmezzo (1976) in x- and y-direction for three intensities: 0.16 g, 0.36 g and 0.60 g

4.2.2 Structural analysis and dimensioning

The building of Fig. 4.25 (deformable roof diaphragm) is designed according to EC2 and EC8 under the following assumptions:

- Steel class: B450C
- Concrete grade: C45/55
- Longitudinal reinforcement cover: 30 mm
- Vertical loads:
  - TT70 roof element .... 3.80 kN/m^2
  - waterproofing etc. .... 0.40 kN/m^2
  - I beam (equivalent 0.4x0.8m2 cross section) .... 8.00 kN/m
  - cladding panels (panel height about 9m):
  - 4 kN/m2 × 9 m × 2.5 m = ... 90 kN/panel

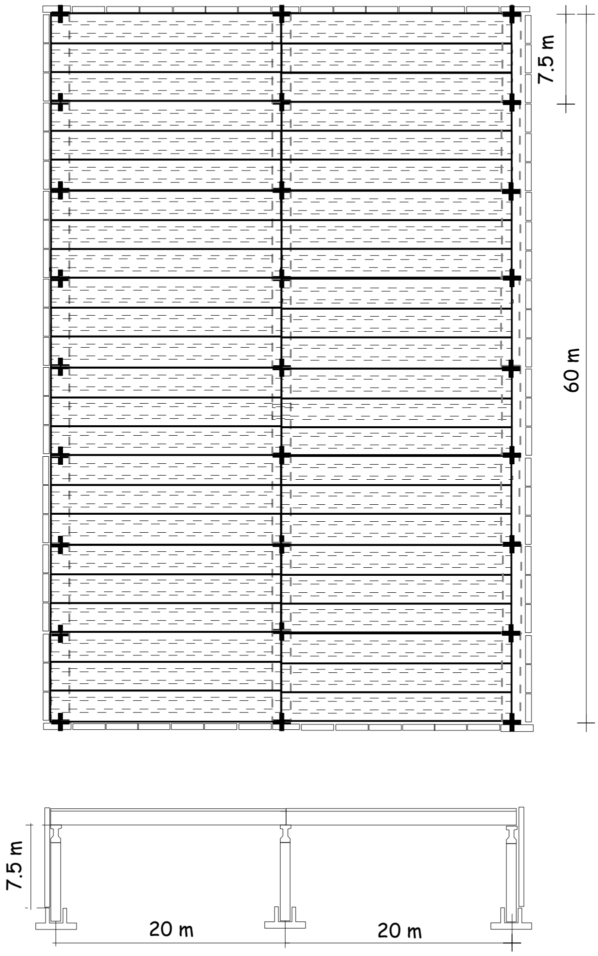

Figure 4.25. Plan view and cross section of the building that is analysed.

- Total load effective to earthquake action
  - (3.8 + 0.4) kN/m2 × 40 m × 60 m = ... 10080 kN
  - 8 kN/m × 3 × 60 m= .... 1440 kN
  - Cladding panels: 90 kN/panel × 80 panels = ... 7200 kN
  - 7200 kN × 0.8 (forfeit accounting for openings) .... 5760 kN
  - Half of the cladding panel weight is effective = ... 2880 kN
  - Effective ground acceleration = ... 0.30 g
  - Soil type: .... B
  - Total vibrating mass (14320 kN) = ... 1432000 kg

- Behaviour factor:
    - for the bare frame: q = ...3.0
    - for the panels: q = ...3.0

According to the design, the maximum static force equivalent to the earthquake is 2171 kN.

The cross section of the structural members is:
- Columns: Rectangular cross section 600 mm × 600 mm reinforced with 12∅22 (ρ_s = 1.27%) and stirrups ∅10/130 cm (Fig. 4.26).
- Beams: Rectangular cross section 800 mm × 400 mm.

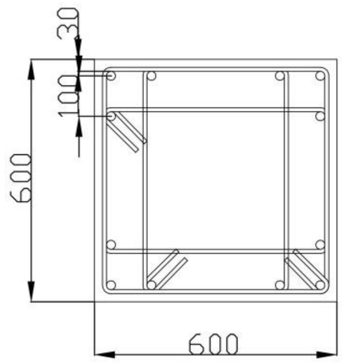

Figure 4.26. Detail of the column reinforcement.

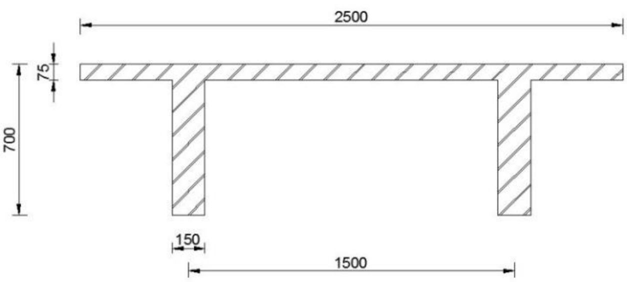

Figure 4.27. Cross section of TT70 roof element.

- Panels: Rectangular cross section 2500 mm × 20 mm.
- TT Floor: Elements TT70 are chosen with typical cross section as shown in Fig. 4.27.

There are three roof configurations with respect to the rigidity of the diaphragm. The roof-beam-column system is depicted in Fig. 4.28.

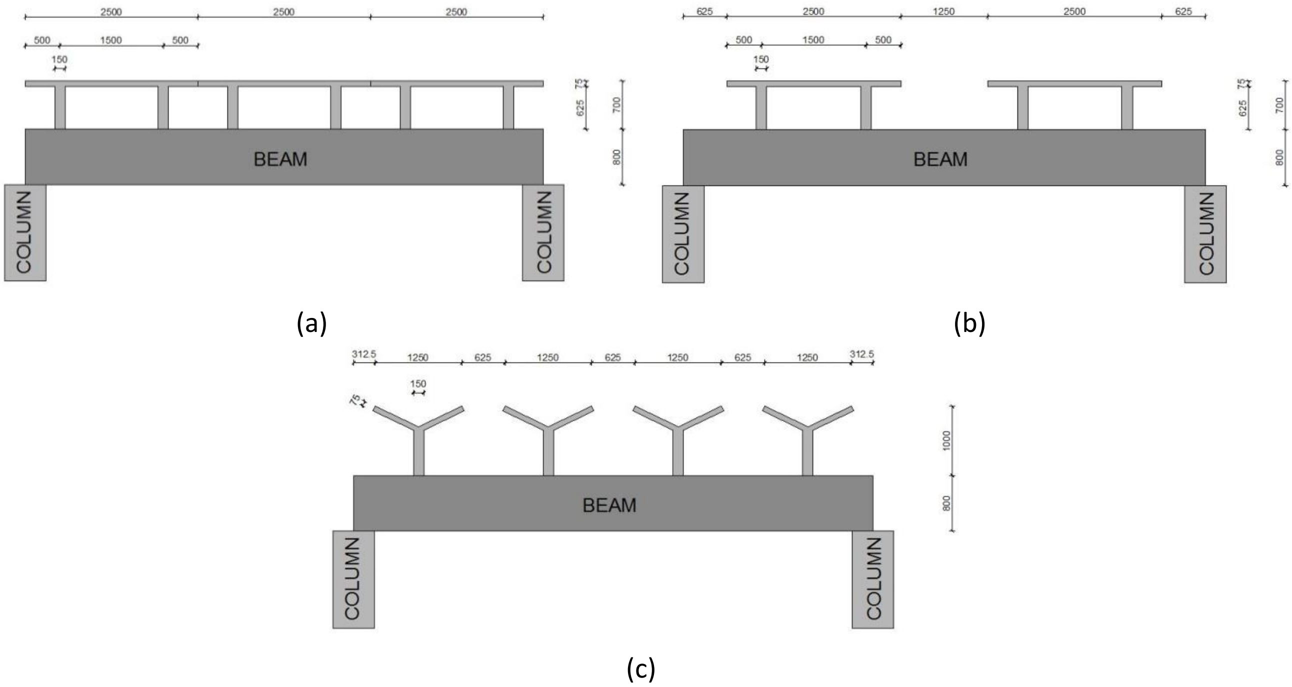

Figure 4.28. Roof Configurations; (a) rigid diaphragm; (b) deformable diaphragm; (c) null diaphragm.

It is noted that, in the integrated solution, the panels are placed above or under the beams (Fig. 4.29). For this reason, in the numerical analyses for fully connected panels the following modifications are made:

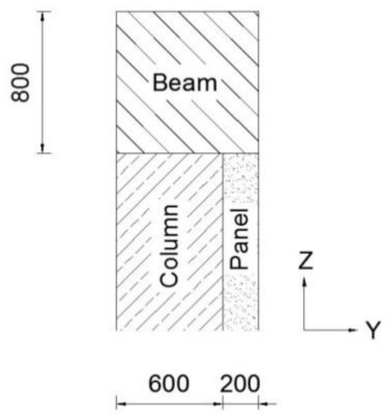

Figure 4.29. Considered relative position of column – beam – panel.

- The beam's width is increased to about 800 mm
- The height of the panel is assumed equal to the columns height (7.5 m)
- In the short side of the building, an extra beam is added for the fastening of the panels, which cannot be connected directly to the TT roof elements.

The panels are connected to the beams at four points (two at the top and two at the bottom). The connections are assumed of the "rebar type" (see section 8.2), as shown in Fig. 4.30. In this type of connection, rebars protrude from the beam to the panel or vice-versa and the bond is achieved with grout or resin infill.

For the design of these connections, the afore-mentioned simplified theoretical formula can be used. Specifically:

Using the EC8 spectrum for the seismic parameters described previously and for the fundamental period of the structure T1 = 0.50 sec (see section 4.2.6.1) the value of the base shear is:

$$P_{base} = m \cdot a_g \cdot S \cdot \frac{2.5}{q} = 14320 \times 0.30 \times 1.2 \times \frac{2.5}{3.0} = 4296\text{kN}$$

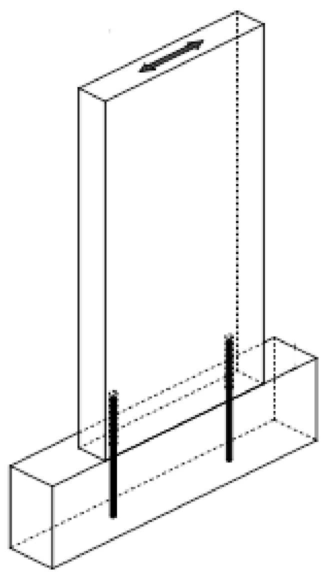

Figure 4.30. "Rebar type" connection between panel and beam (one half of the panel is shown).

Considering that:

- n = 24 (8 spans × 3 panels/span)
- L = 2.1 m (for panels of length L = 2.50 m)
- P_{base} = 6444 KN
- H = 7.5 m

equation (3.9) becomes:

$$P_i \cong 4296 \times \frac{7.5}{4 \times 24 \times 2.1} = 160\text{kN}$$

This is the force that acts to each connection, mainly in the vertical direction. Assuming that the connection is materialized with vertical reinforcement (Fig. 4.30), the required cross section of the rebar at each connection is:

$$A_s = \frac{160}{45/1.15} = 4.09\,\text{cm}^2$$

Thus, one rebar ∅25 is needed at each connection.

4.2.3 Numerical model

All the analyses are performed using OpenSees (McKenna et al., 2000) due to low computational cost and the generally high credibility of the specific software. Being an open source program, OpenSees allows the user to make alterations to the code, modify the constitutive laws of the materials, create new elements, etc. according to his needs.

The numerical model consists of beam elements which represent the columns, the beams, the roof elements and the panels. Probable places for plastic hinge formation are the bottom of the columns and the connections of the panels. Following the precast concrete practice, pinned connections between beams and columns are adopted. Therefore, beams are simply supported and are modelled with elastic elements. Details on the modelling of the rest connections between the various elements are given in the following sections.

The properties of the various elements and the materials are shown in Table 4.2.

Table 4.2. Element properties.

Property	Beam	Roof	Panel
Young's modulus, E [Gpa]:	36	36	36
Shear modulus, G [Gpa]:	14.4	14.4	14.4
Cross section area, A [m^2]:	0.640	0.375	0.500
Torsional moment of inertia, J [m^4]:	0.0577	0.0017	0.0063
Second moment of inertia about local z axis, I_z [m^4]:	0.0341	0.2035	0.0017
Second moment of inertia about local y axis, I_z [m^4]:	0.0341	0.0177	0.2604

Roof Model

Roof elements forming the null, the deformable and the rigid roof diaphragm consist of TT beams (Fig. 4.31) and are considered to behave elastically.

The connection between the TT roof elements and the beams is accomplished though the incorporation of two rigid beams and two extra elements that model the effective width of the slab of the TT element (Fig. 4.31). The cross section of these "effective width" elements is 75 mm × 1000 mm.

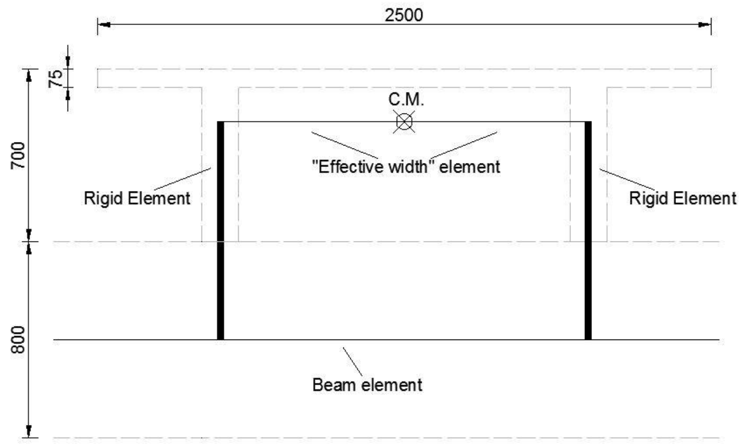

Figure 4.31. Model of TT roof elements.

Column Model

The columns are modelled as beam elements, while Distributed Plasticity method (described in section 4.2.4.2), with 5 integration points according to Gauss – Lobatto integration type is selected. The Coleman and Spacone regularisation technique is also applied.

Using the material characteristics the moment-curvature relationship was calculated for each column given the applied axial force. For the purpose of further analysis the curve was approximated with the tri-linear envelope which passes through the points corresponding to the concrete cracking, the yield of the reinforcement bar under tension and the concrete spalling (Fig. 4.32). The idealised curves for several different levels of axial force are shown in Fig. 4.33.

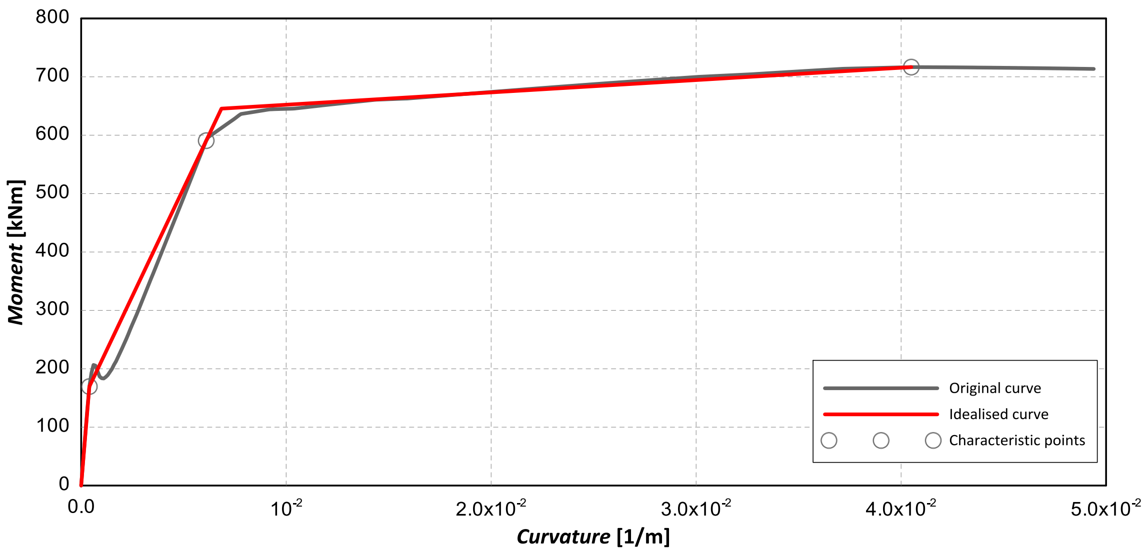

Figure 4.32. Original and idealized moment-curvature relationship of the column.

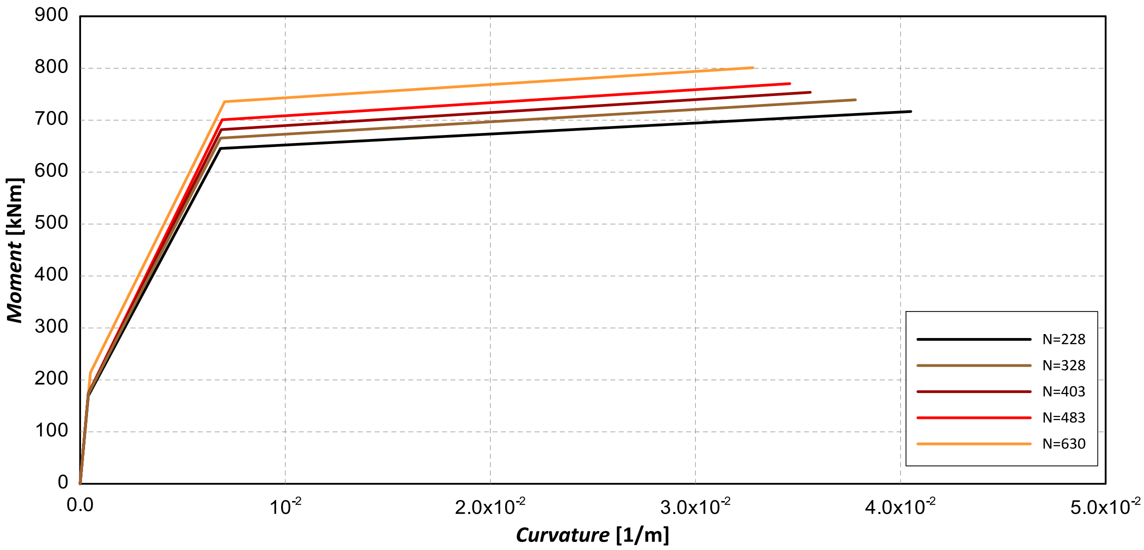

Figure 4.33. Idealized moment-curvature envelopes for different levels of axial force.

Panel Model

While the use of shell elements for modelling the behaviour of the panels would be a better choice from a theoretical point of view, beam elements are selected due to software limitations.

Each panel is modelled with 5 elastic beam elements (Fig. 4.34). The main element is placed at the centerline of the panel while the remaining four elements are used to materialize the connection with the beams modelling thus the "effective width" of the panel at its ends. Their cross section is 200 mm × 1000 mm.

In order to account for the inelastic response of the connections at each end of the panel, inelastic springs are considered at the ends of the main element (Lumped Plasticity model, see Fig. 4.35), the properties of which (Moment-Rotation law) is determined by an independent finite element analysis, as described in section 4.2.4.3. It is noted that, due to the joints that exist between the panel and the beams, the plastic hinges that are formed have, practically, zero length. For this reason, zero-length nonlinear springs are used to model the plastic hinges. In the out-of-plane direction, these springs behave elastically. In this way, the actual response is captured quite accurately.

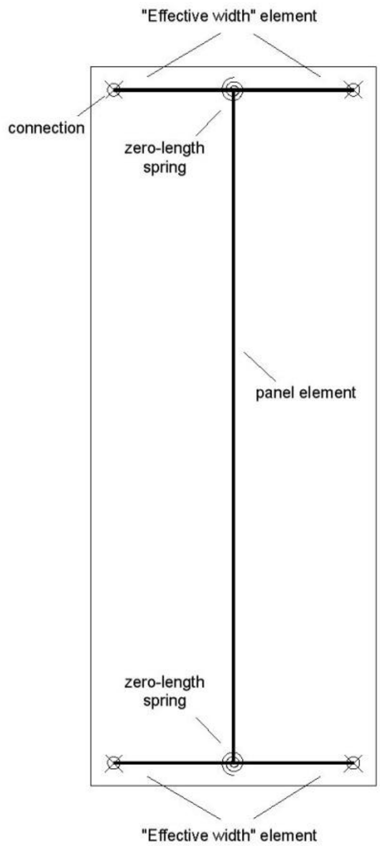

Figure 4.34. Model of panel elements.

4.2.4 Modelling the Inelastic Behaviour

4.2.4.1 Lumped Plasticity model

As mentioned above, Lumped Plasticity is used to model the plastic hinges at the ends of the panels. In this method, an elastic beam-column element is used to connect two zero-length plastic hinges positioned at the two edge nodes of the element (Fig. 4.35). In this way the nonlinear response is concentrated at the two ends of the element.

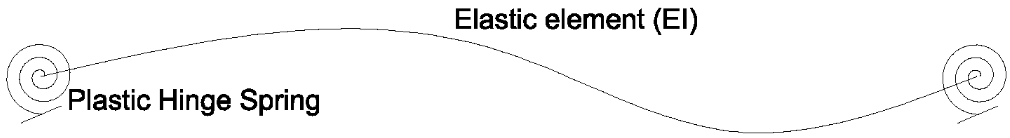

Figure 4.35. Lumped Plasticity Method.

Each Plastic Hinge Spring is defined as a pair of moments and chord rotations providing the envelope of the column response while hysteretic behaviour can also be assigned.

The drawback of the model is that linear distribution of bending moment and idealized curvature distribution have been usually assumed. Also, in order to define the rotation through the plastic curvature, the plastic hinge length is needed, making thus the result case sensitive. Moreover, the effect of the axial force in the moment-curvature diagram cannot be taken into account.

As mentioned above, the moment-rotation law used for the panel connections is derived by an independent finite element analysis (see section 4.2.4.3).

4.2.4.2 Distributed Plasticity model

Distributed Plasticity is used to model the plastic hinges at the columns. In this method, the distributed plasticity is obtained through the numerical integration along points spread in the element's length (Fig. 4.36).

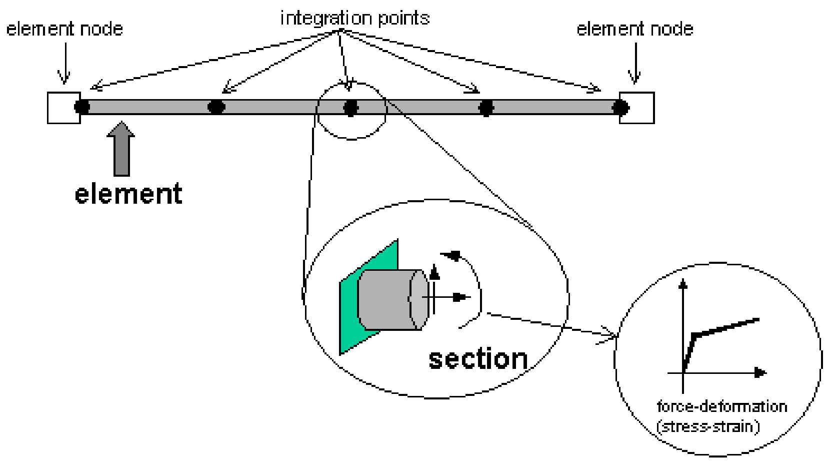

Figure 4.36. Distributed Plasticity Method (McKenna et al. 2000).

In OpenSees, the force-based beam-column elements allow a wide range of numerical integration types, such as Gauss – Lobatto, Gauss – Legendre, Gauss - Radau, Newton – Cotes etc., and number of integration points (IP). Usually, five points according to Gauss – Lobatto integration type are selected.

The position and the weights of Gauss – Lobatto integration points across the length [-1 1] are shown in Fig. 4.37.

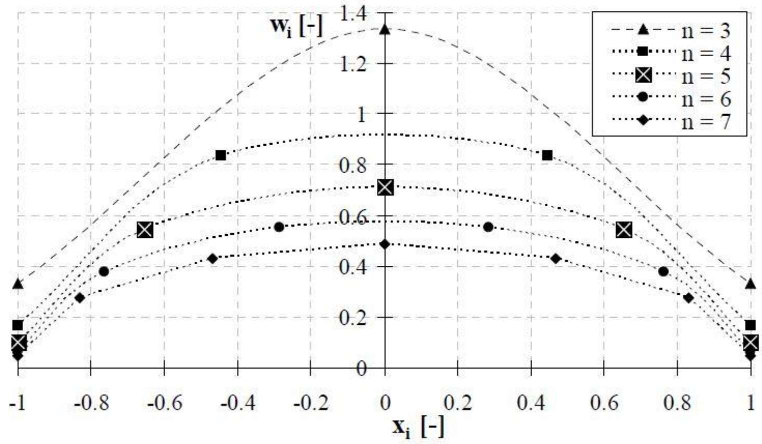

Figure 4.37. Position and the weights of Gauss – Lobatto integration points (Calabrese 2008).

When Distributed Plasticity is used, it is common to model the cross section using fibers. Specifically, the cross-section is divided into fibers and stress-strain relationships are defined for each of them producing thus moment-curvature diagrams that take into account the axial load.

This approach has various disadvantages, such as large computational cost and numerical instability, especially for dynamic analyses.

Localisation problems

Reinforced concrete frame elements, similarly to concrete solid elements, can lead to numerical inconsistencies that derive from localization problems. When the cross-section response starts softening or behaves perfectly plastic, the curvature tends to localize at a particular integration point, therefore the element response becomes non unique and depends on the number of integration points per element. On the contrary, for hardening materials plasticity usually spreads beyond a single integration point and numerical problems are limited to a non-smooth response if too few integration points are used.

The numerical problems encountered in force-based frame elements when plastic hinges form are nicely illustrated (Fig. 4.38 to 4.40) by Coleman and Spacone (2001) for the case of a steel cantilever beam under an imposed transverse tip displacement. A single force-based element is used for the entire member.

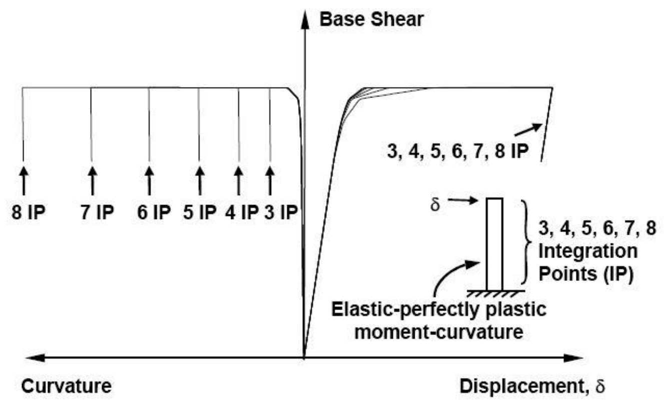

Figure 4.38. Cantilever beam with elastic-perfectly plastic section response (Coleman & Spacone 2001).

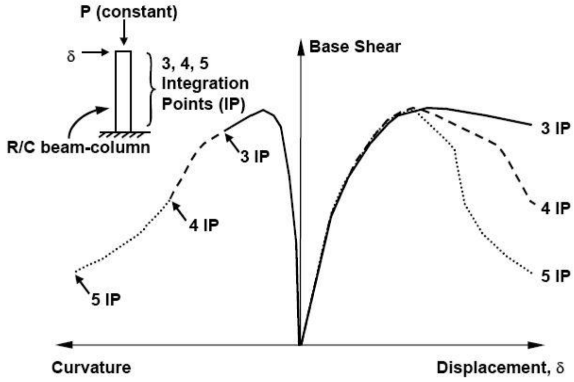

Figure 4.39. Cantilever beam with softening section response (Coleman & Spacone 2001).

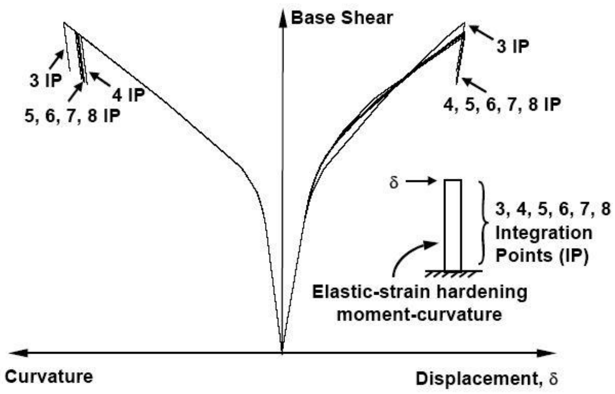

Figure 4.40. Cantilever beam with hardening section response (Coleman & Spacone 2001).

The loss of objectivity with elastic-perfectly plastic behaviour (Fig. 4.38) is attributed to the concentration of plastic deformation around the crucial integration point (i.e. the plastic hinge) while all the other integration points remain linearly elastic and do not see any change in either curvature or moment. However, the length of the base integration point and, thus, the plastic hinge length, is a function of the number of integration points used.

In the case of a softening moment-curvature response (Fig. 4.39), the loss of objectivity is more pronounced. As the number of integration points increases, the length of the first integration point decreases and increasing curvatures are required to achieve the same prescribed tip displacement. The concrete fiber compressive strains in the hinge region quickly increase resulting in rapidly degrading material stiffness. For larger numbers of integration points, the post-peak response becomes brittle and, with increasing numbers of integration points, snap-back may even occur.

The response of the hardening section behaviour (Fig. 4.40) is objective when not too few integration points are used. At both the element and the section levels the plasticity spreads to adjacent integration points and no abrupt response is obtained.

Regularisation techniques

Localisation effects in force-based elements have been discussed by Coleman and Spacone (2001), Scott and Fenves (2006) and others and propose various solution strategies. There are two main directions on how to re-establish the objectivity of the elements response.

The first one, proposed by Coleman and Spacone (2001) is an attempt to link the numerical problem with a physical material parameter, the constant fracture energy in compression, G_f^c. The idea of this regularisation process is to modify the uniaxial stress-strain relationship for concrete (in each integration point if possible) using the fracture energy in compression parameter G_f^c assuming thus a constant stress-displacement relationship rather than a constant stress-strain law.

Besides the regularization of the stress-strain law, in some cases there is still a need to post-process the results to obtain an objective prediction of the curvature demand in the plastic hinge region.

In case Kent and Park (1971) concrete law (Fig. 4.41) is used (a common selection in OpenSees) then the strain labelled ε_{20} is given by the following expression:

$$\varepsilon_{20} = \frac{G_f^c}{0.8 \cdot f_c' \cdot L_{IP}} - \frac{0.8 \cdot f_c'}{E} + \varepsilon_0 \tag{4.1}$$

where:

G_f^c is the fracture energy in compression;
f_c' is the concrete compressive strength;
L_{IP} is the length of the softening integration point;
E is the modulus of elasticity; and
ε_0 is the stain at the compressive strength.

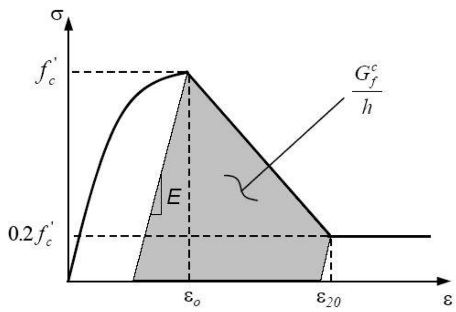

Figure 4.41. Kent and Park stress-strain law and compression fracture energy (Kent & Park 1971).

The second regularization procedure proposed by Scott and Fenves (2006) modifies the numerical integration scheme inside the plastic hinge at the extremities of the beam-column element. A modified Gauss-Radau (G-R) integration is used and the plastic hinge lengths are supposed to be known a priori. This method is incorporated within OpenSees software by the Beam with hinges element (Fig. 4.42).

In fact this specific element lies between the Lumped and the Distributed Plasticity method as it localizes plastic deformation at the element ends only but the plasticity is spread over specified hinge lengths.

In the performed analyses, the regularization technique of Coleman and Spacone (2001) is applied. Selecting concrete stress-strain law compatible with the Kent-Park (1971), equation (4.1) can be used to compute the "corrected" strain value. However, for the specific structure under consideration, the new value of ε_{20} practically coincides with the theoretical one, therefore no regularization is conducted.

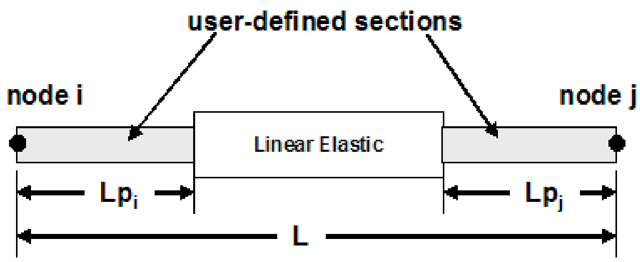

Figure 4.42. Beam with Hinges element in OpenSees (McKenna et al. 2000).

4.2.4.3 Moment – rotation law for the panel connections

As mentioned above, the Lumped Plasticity model is considered at the ends of the panels, in which the inelastic behaviour is modelled by zero-length springs. For the determination of the moment – rotation law that governs the behaviour of these springs, a special finite element analysis is performed using SAP 2000.

The model considered consists of one-half of the panel (up to its mid-height) and the beam to which it is connected. Both the panel and the beam are modelled with shell elements, while the rebars are modelled with beam elements. The joint between the panel and the beam is modelled with tensionless springs (gap elements).

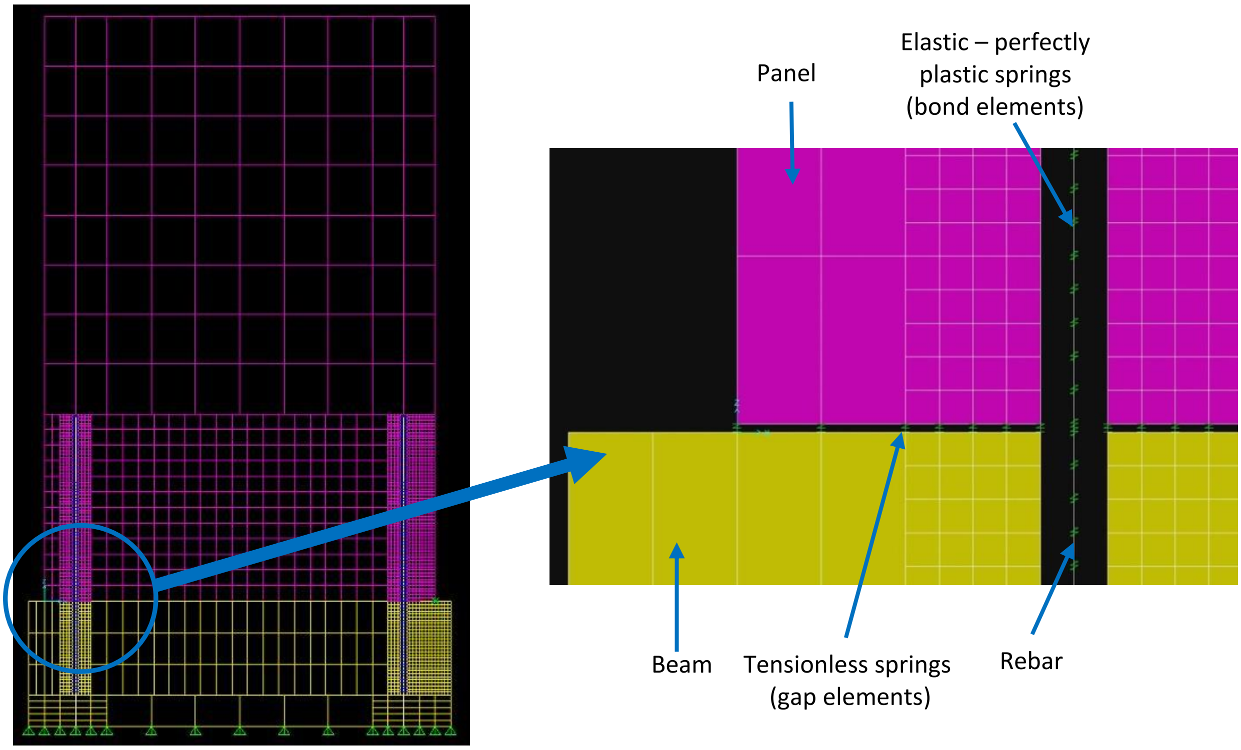

Figure 4.43. Model used for the analysis of the inelastic behaviour of panel – beam connections.

The nodes of the rebars are not connected directly to the corresponding nodes of the shell elements (panel and beam), but through nonlinear springs, in order to model realistically the bonding between the rebars and the surrounding concrete. The behaviour of these springs is elastic – perfectly plastic, thus the springs yield when the corresponding bond strength is exceeded. In this way, local loss of the bonding along the dowels can occur. In order to capture well the local de-bonding of the rebars, a quite dense mesh is applied around the rebars (max length = 20 mm). A sketch of the numerical model used in this analysis is shown in Fig. 4.43.

Response for monotonic loading (pushover)

The behaviour of the panel – beam connection under monotonically increasing the top displacement of the panel is shown in Fig. 4.44 (pushover capacity curve). It is noted that the shape of the obtained capacity curve from this analysis is quite similar with the one obtained during the experimental tests. The major drawback of the model is that the analysis ended in relatively small deformations, while the rebar was still in the hardening branch. Taking into account the displacements observed in the experiments (see section 9) the curve was linearly extrapolated up to the stress limit of the rebar steel. In general it can be said that, despite the fact that the considered model is not very accurate (shell elements instead of 3D ones, not exact representation of the reinforcement), it is capable to predict satisfactorily the behaviour of the connection.

The capacity curve (up to the failure of the rebar) is transformed to a bilinear curve using the equal area principle. The derived bilinear curve is shown in Fig. 4.44 with red line. After the exceedance of stress limit of the rebar steel total loss of capacity is assumed. The idealized curve is then transformed to a moment – rotation curve, which is shown in Fig. 4.45. This curve is used in the Lumped Plasticity model of the panels for the nonlinear analyses of the building with OpenSees.

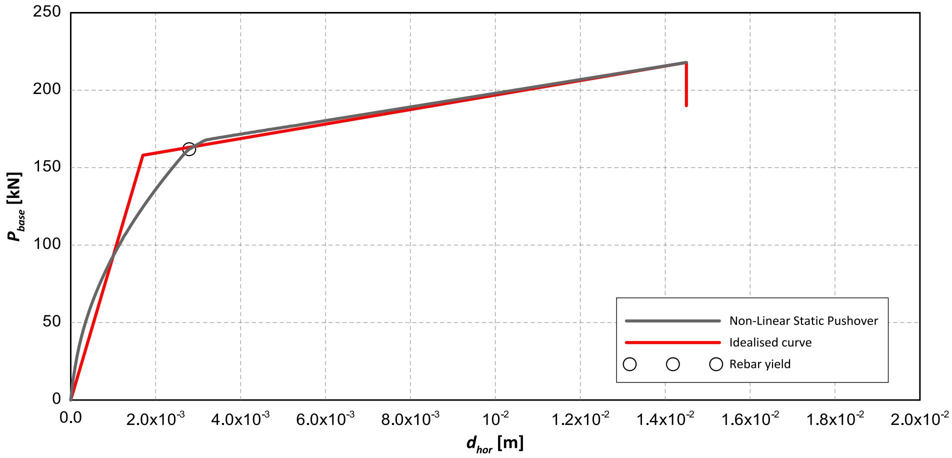

Figure 4.44. Force – displacement capacity of the panel – beam connection.

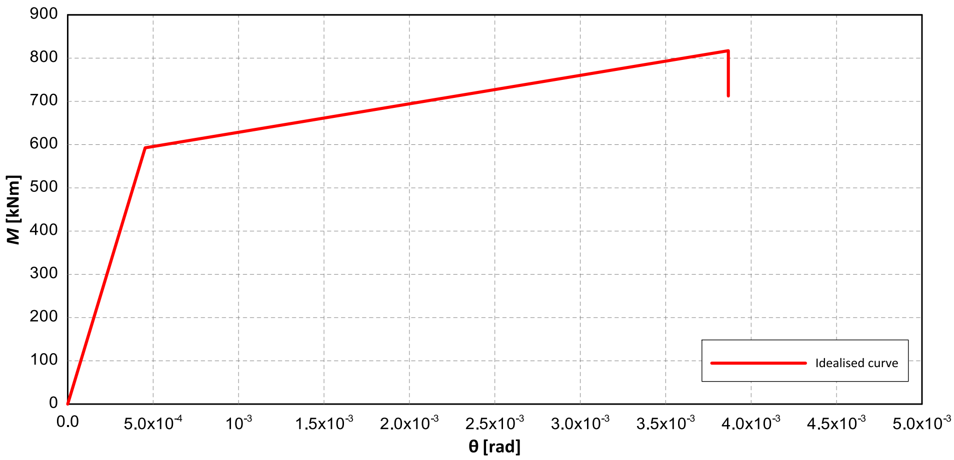

Figure 4.45. Idealized Moment – Rotation capacity curve of the panels' connections.

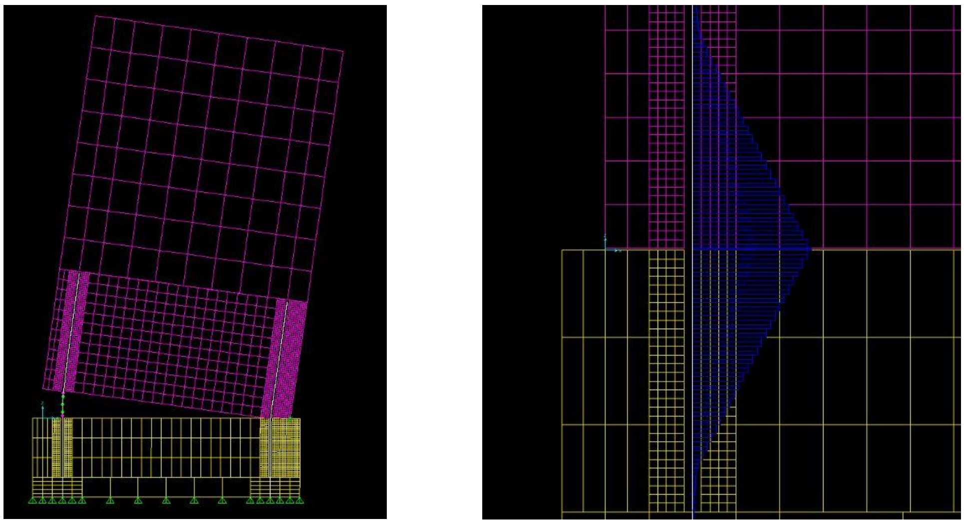

(a) (b)

Figure 4.46. Representative results: (a) deformed shape; (b) axial force induced to the rebar at the final step of the analysis.

Representative results of the analysis for the determination of the $M - \theta$ relationship of the panel – beam connections are shown in Fig. 4.46. In Fig. 4.46(a) the deformed shape of the model (exaggerated) is shown, while in Fig. 4.46(b) the axial force induced to the rebar at the final step of the analysis is depicted.

4.2.5 Material properties

In all analyses, the mean strength of the steel and the concrete is taken into account, which is defined according to EN 1992-1-1 (Table 3.1 and Appendix C) (CEN, 2004a) and EN 1998-2:2005 (Appendix E) (CEN, 2004b). The considered properties are summarized in Tables 4.3 and 4.4 while Fig. 4.47 and 4.48 show the considered constitutive laws for the concrete and the rebars, respectively.

Table 4.3. Material properties considered for the concrete.

Parameter	Value
Modulus of Elasticity, E_c [GPa]:	36
Mean cylinder compressive strength of unconfined concrete, f_{cm} [MPa]:	53.0
Mean cylinder compressive strength of confined concrete, $f_{cm,c}$ [MPa]:	65.4
Mean tensile strength of concrete, f_{ctm} [MPa]:	3.8
Deformation corresponding to f_{cm}, ε_{c1}:	0.0024
Ultimate deformation of unconfined concrete, ε_{cu1}:	0.0035
Deformation corresponding to $f_{cm,c}$, $\varepsilon_{c1,c}$:	0.0043
Ultimate deformation of confined concrete, $\varepsilon_{cu,c}$:	0.0193

Table 4.4. Material properties considered for the steel rebars.

Parameter	Value
Modulus of Elasticity, E_s [GPa]:	200
Mean yield strength of reinforcing steel, f_{ym} [MPa]:	517.5
Mean tensile strength of reinforcing steel, f_{tm} [MPa]:	648
Ultimate deformation of reinforcing steel, ε_{su}:	0.1000

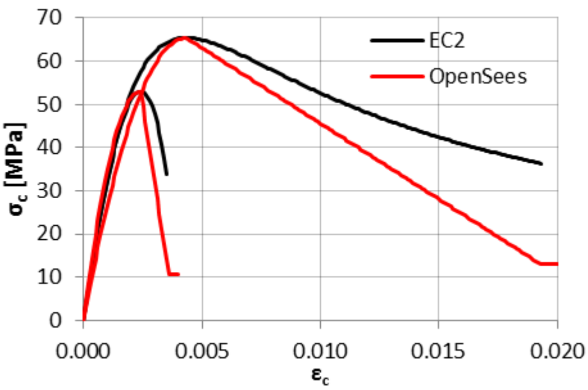

Figure 4.47. Stress-strain relation for the concrete considered in the analysis.

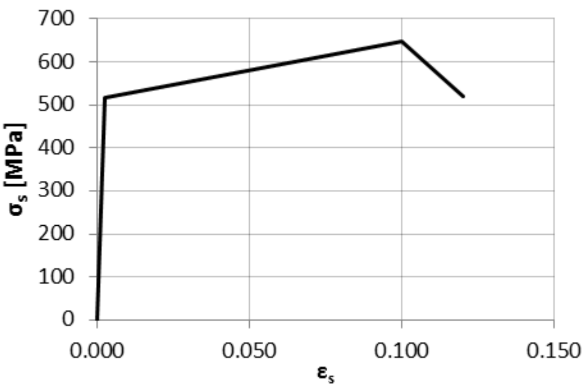

Figure 4.48. Stress-strain relation for the rebars considered in the analysis.

4.2.6 Results of the numerical analyses

As mentioned above, all analyses of the considered building are performed with OpenSees. A sketch of the numerical model for deformable diaphragm used is shown in Fig. 4.49. The properties of the model were presented in the previous sections.

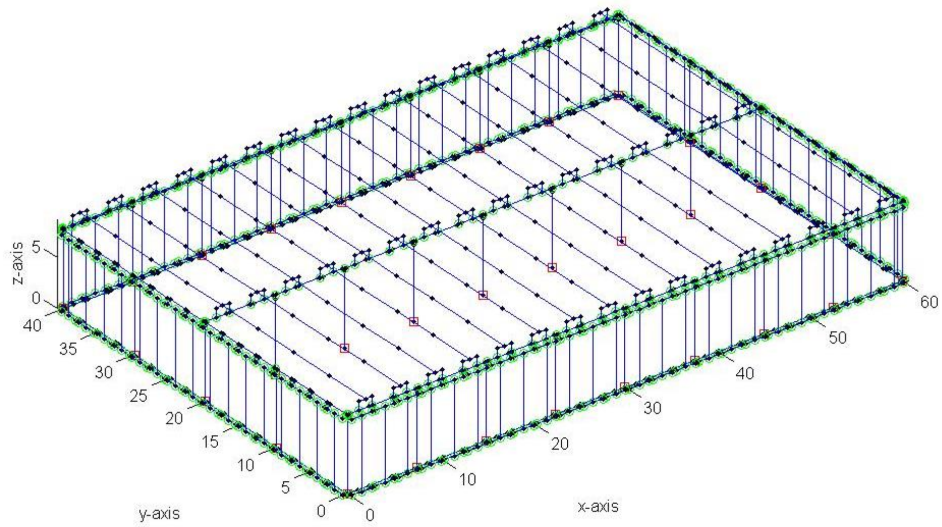

Figure 4.49. OpenSees model of the building analysed.

4.2.6.1 Modal Analysis

For comparison reasons, modal analyses are performed for the buildings with the panels and the bare frame in which the panels contributed only as masses (un-connected panels). The 3D view of the most significant mode of vibration in each direction is presented in Fig. 4.50 to 4.55. In the cases without panels, the stiffness of the elements is considered uncracked (for comparison reasons). The periods, the participation factors and the cumulative effective masses are summarized in Table 4.5.

As expected, the modes of vibration of the buildings with and without panels differ significantly. When the stiffness of the panels is neglected, the two first modes are translational (X and Y directions) and have practically the same period (around 1.09 sec for null, 0.87 sec for deformable and 0.95 sec for rigid diaphragm). It is evident that given the relatively higher stiffness of the diaphragm compering to the bare frame and the pinned connection of the columns, the system is forced to behave like a cantilever. The differences in the value of the periods lie in the difference in mass of the roof.

In case of the structures with panels, the effect of the diaphragm action depends on the configuration. As far as the X direction is concerned, the lack of connection between the roof and the beams on the transverse direction forces them to deflect more than the other elements. This deflection is bigger for the stiffer roof configuration. The corresponding mode of vibration is along the two first of the structure. As far as the Y direction is concerned, the most significant mode of vibration involves the in-plane deflection of the diaphragm. On the contrary, in the rigid configuration the stiffness shifts the period to lower values an only out-of-plane deflection is permitted.

Table 4.5. Dynamic characteristics of the buildings considered.

		Mode	Period [sec]	Participation Factors			Effective mass [%]		
				Dir X	Dir Y	Dir Z	Dir X	Dir Y	Dir Z
null diaphragm	With integrated panels	1	0.987	0.00	40.21	0.00	0	0.55	0
		2	0.959	-36.66	0.00	0.00	0.46	0	0
	With un-connected panels	1	1.093	46.14	0.00	0.00	0.72	0	0
		2	1.052	0.00	-46.52	0.00	0	0.74	0
deformable diaphragm	With integrated panels	1	0.495	0.00	-34.25	-0.01	0	0.51	0
		2	0.433	23.74	0.00	0.00	0.24	0	0
	With un-connected panels	1	0.881	40.19	-0.03	0.00	0.70	0	0
		2	0.875	0.03	40.23	0.00	0	0.70	0
rigid diaphragm	With integrated panels	1	0.417	-17.87	0.00	0.00	0.12	0	0
		8	0.302	0.00	-41.39	0.00	0	0.65	0
	With un-connected panels	1	0.965	-43.87	0.00	0.00	0.73	0	0
		2	0.956	0.00	-43.95	0.00	0	0.73	0

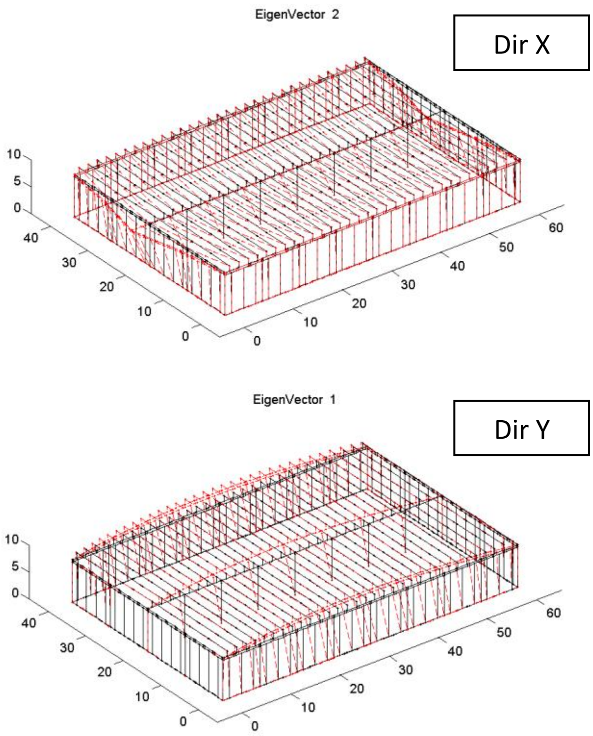

Figure 4.50. Two first modes of vibration for the building with integrated panels and null diaphragm.

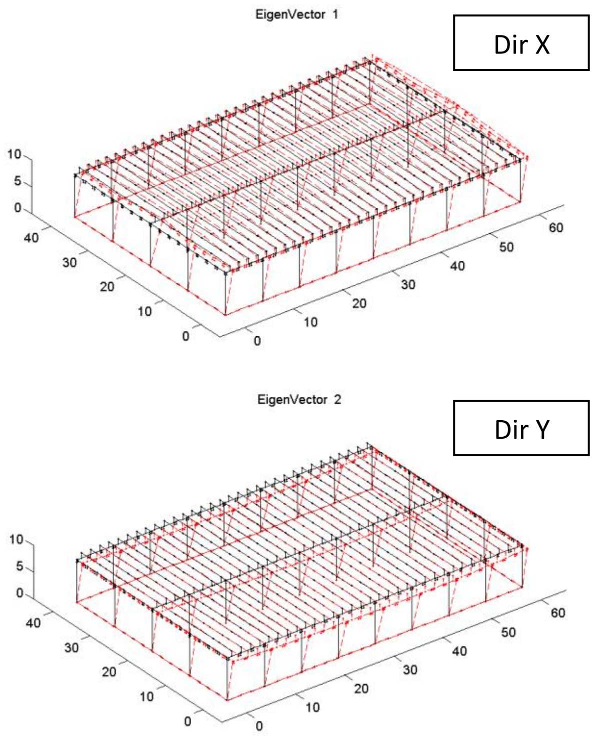

Figure 4.51. Three first modes of vibration for the bare frame and null diaphragm.

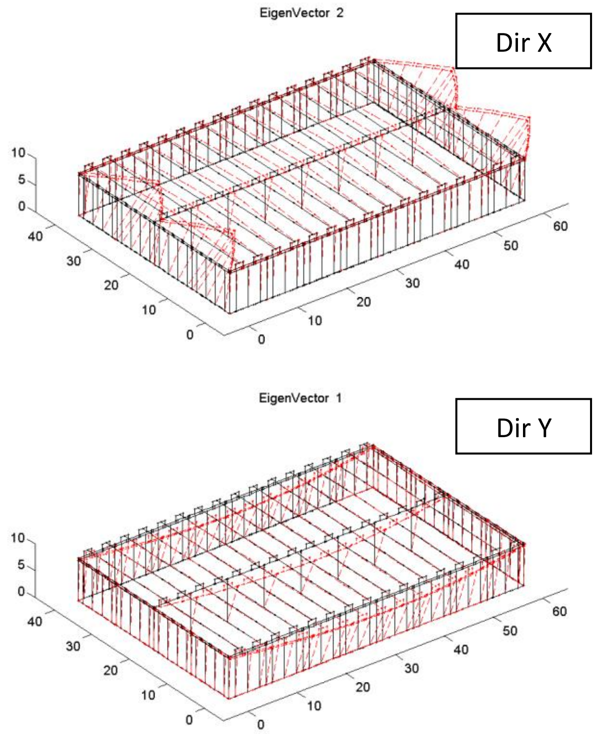

Figure 4.52. Two first modes of vibration for the building with integrated panels and deformable diaphragm.

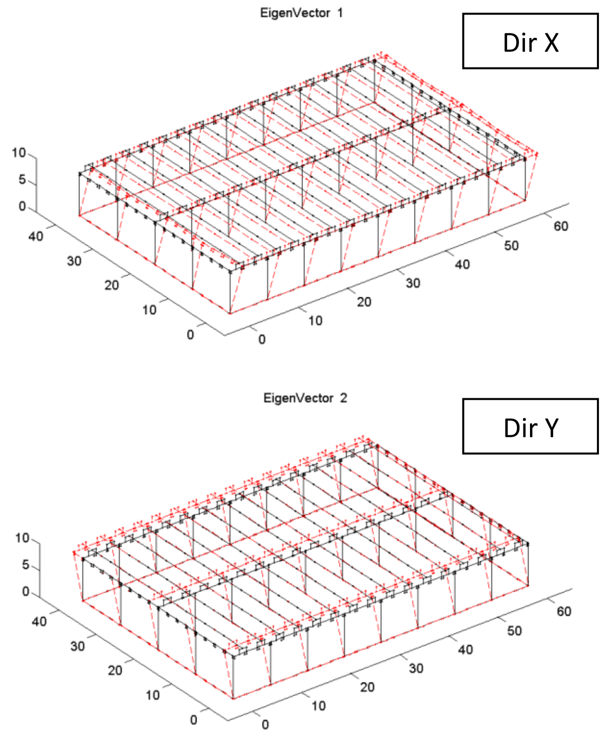

Figure 4.53. Three first modes of vibration for the bare frame and deformable diaphragm.

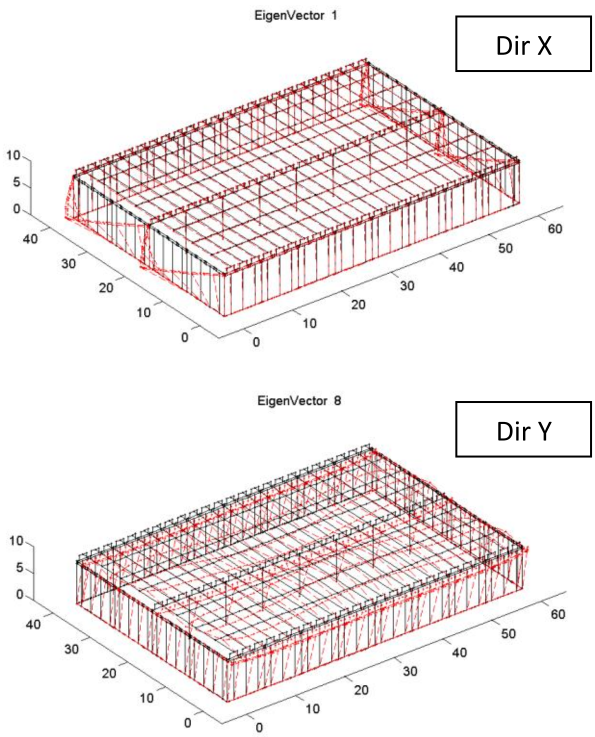

Figure 4.54. Two first modes of vibration for the building with integrated panels and rigid diaphragm.

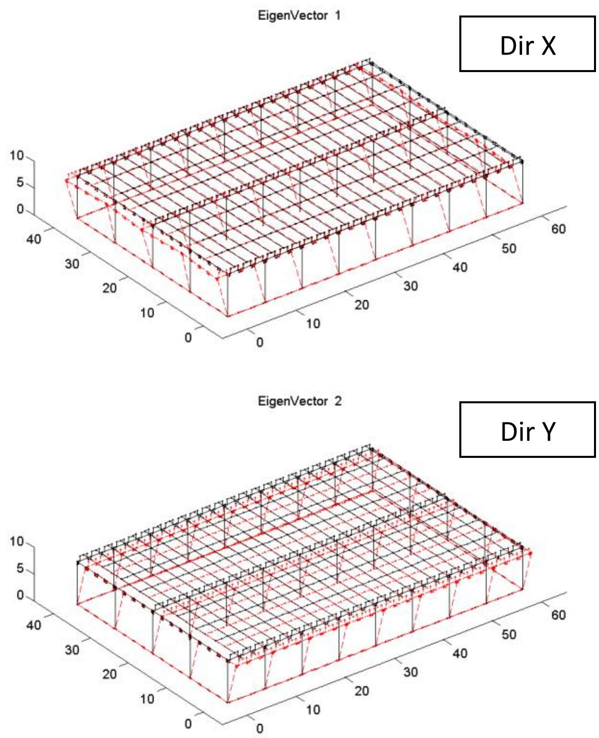

Figure 4.55. Three first modes of vibration for the bare frame and rigid diaphragm.

4.2.6.2 Static Pushover Analysis

Static pushover analyses are performed in the main directions of the buildings with the integrated panels and the un-connected panels. In these analyses, the loads are uniformly distributed on the top of the columns. For comparison reasons, modal analyses are performed for the building with the panels and the bare frame in which the panels contributed only as masses (un-connected panels).

The corresponding capacity curves (Base Shear vs. the displacement of the top of the columns in the exterior row) is represented in Fig. 4.56 to 4.58. As expected, the attained maximum load in the buildings with integrated panels is much larger than the one in the buildings with un-connected panels (more 3 to 4 times larger) provided that the large forces from the panels can be transferred through the diaphragm. Significant drop in the resistance of the buildings with panels is observed at relatively low top displacement (around 3 cm in the X and Y-direction for rigid and deformable diaphragm), which is attributed to the failure of the connections of the panels. In the Static Pushover in X-direction with null diaphragm the resistance drops for lower base shear and displacement as the failure mechanism differs. It is noted that the resistance in X-direction is about 20% larger than the one in the Y-direction, due to the larger number of panels in the longitudinal sides.

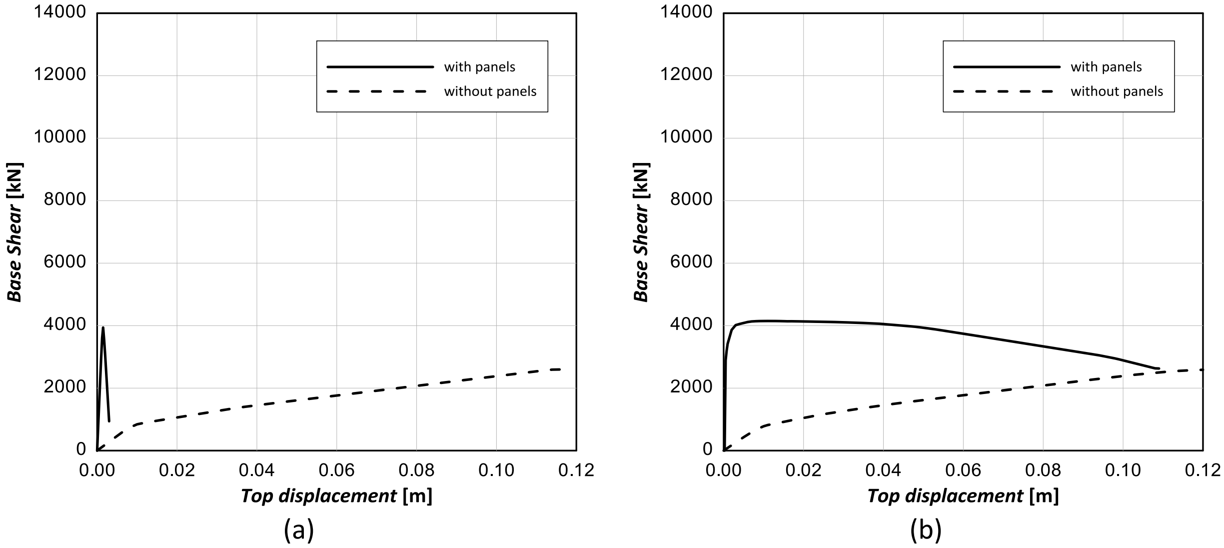

Figure 4.56. Static Pushover curves for structures with null diaphragm: (a) in X-direction; (b) in Y-direction.

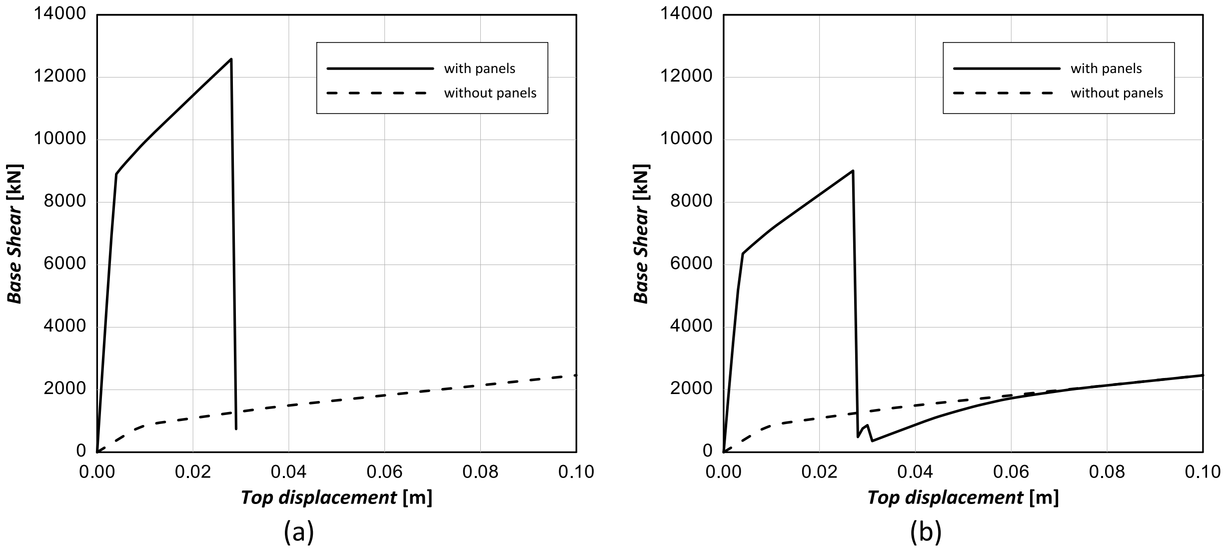

Figure 4.57. Static Pushover curves for structures with deformable diaphragm: (a) in X-direction; (b) in Y-direction.

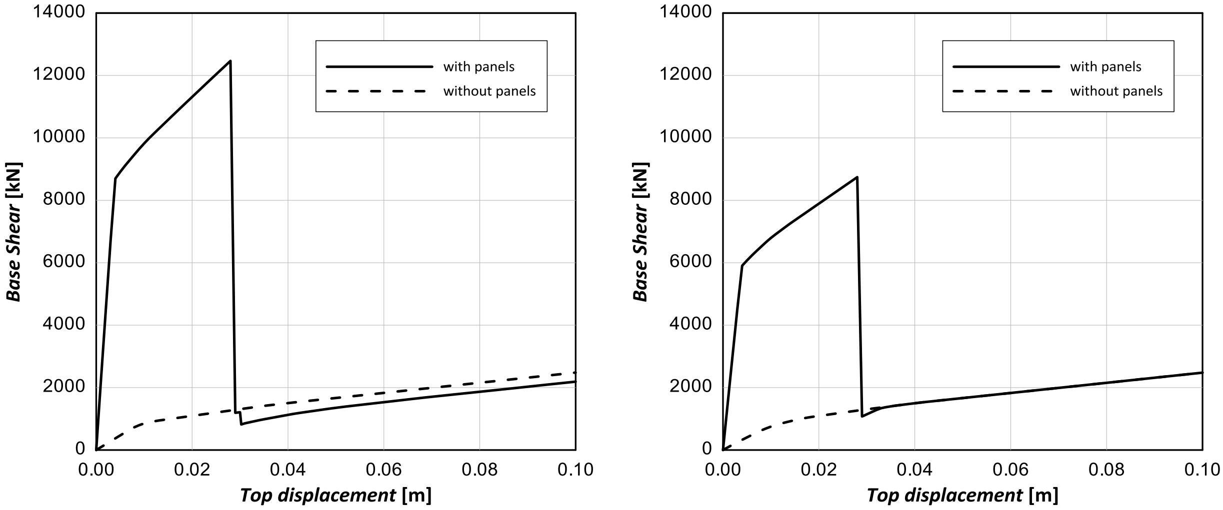

(a) (b)

Figure 4.58. Static Pushover curves for structures with rigid diaphragm: (a) in X-direction; (b) in Y-direction.

It is interesting to note that the failure of the connections of the panels occur almost simultaneously for all panels that are placed in the direction of loading. This is shown in Fig. 4.60 and 4.61, in which the moment at the connection of each panel (moment of the nonlinear spring, see section 4.2.4.3) versus the top displacement is shown. For each panel a separate curve is drawn; however, all the curves practically coincide and all connections fail at the same top displacement.

As mentioned above, in the case of loading in X-direction with null diaphragm the capacity curve shows an abrupt drop in lower deformation than in the other capacity curves. Additionally, the failure cannot be attributed to the local failure of the connections as they are still in the elastic branch (Fig. 4.59(a)). In absence of stiff diaphragm the deformation of the middle row columns is larger than those in the edges, forcing them to reach their capacity threshold sooner and causing numerical instability.

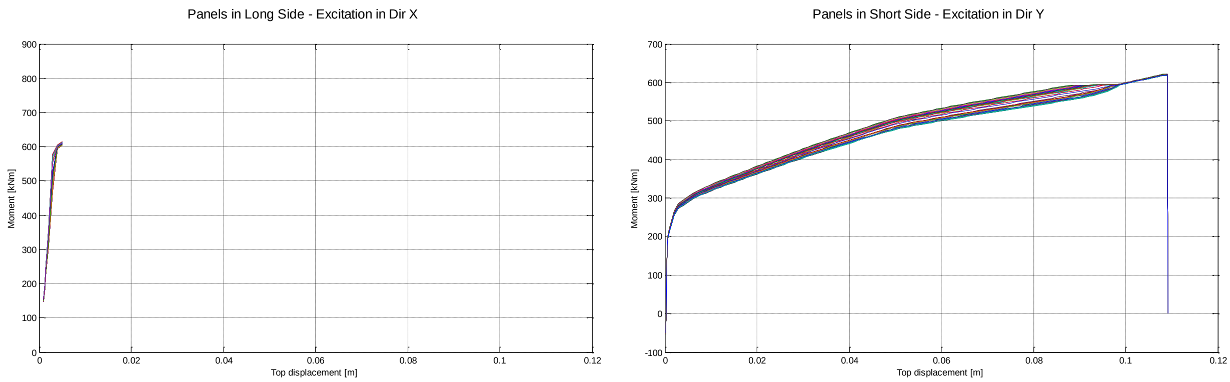

(a) (b)

Figure 4.59. Moment induced to the connections of the panels versus the top displacement in structures with null diaphragm: (a) panels of the long side for loading in the X-direction; (b) panels of the short side for loading in the Y-direction (different curve for each panel).

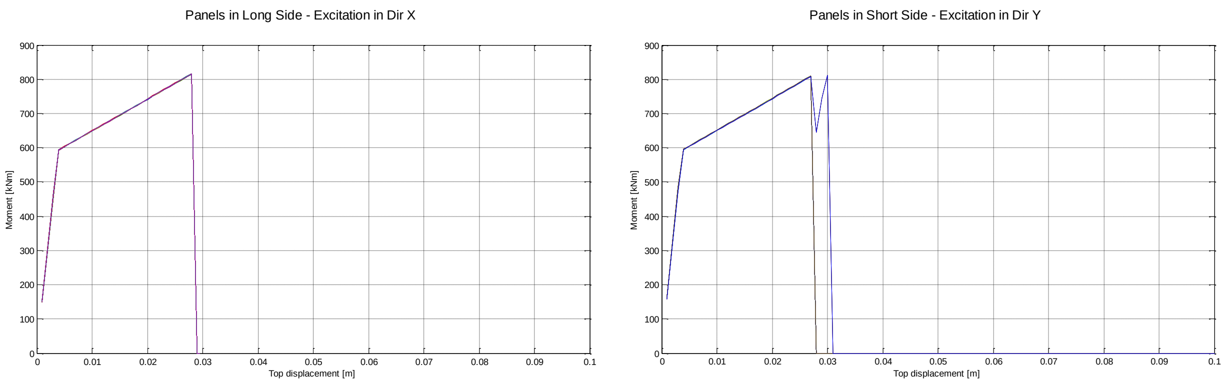

(a) (b)

Figure 4.60. Moment induced to the connections of the panels versus the top displacement in structures with deformable diaphragm: (a) panels of the long side for loading in the X-direction; (b) panels of the short side for loading in the Y-direction (different curve for each panel).

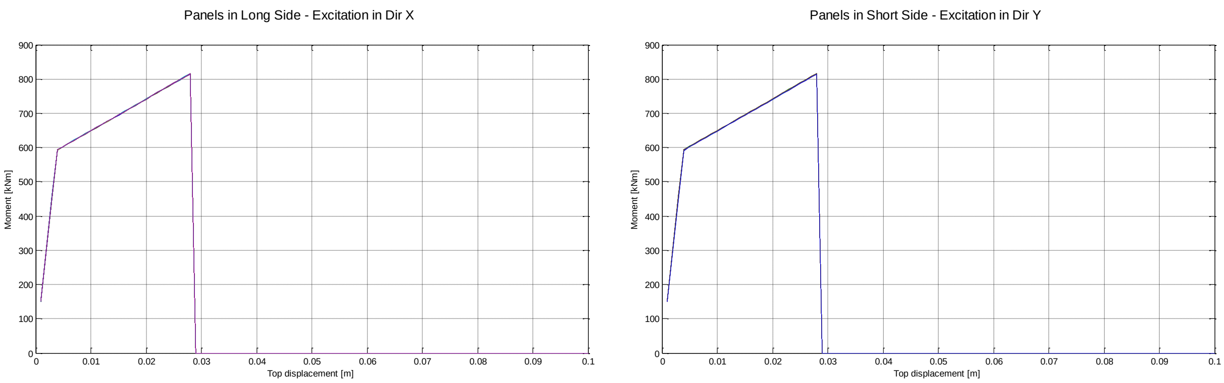

(a) (b)

Figure 4.61. Moment induced to the connections of the panels versus the top displacement in structures with rigid diaphragm: (a) panels of the long side for loading in the X-direction; (b) panels of the short side for loading in the Y-direction (different curve for each panel).

The difference between the middle and the edge row columns is presented in Fig. 4.62 to 4.64.

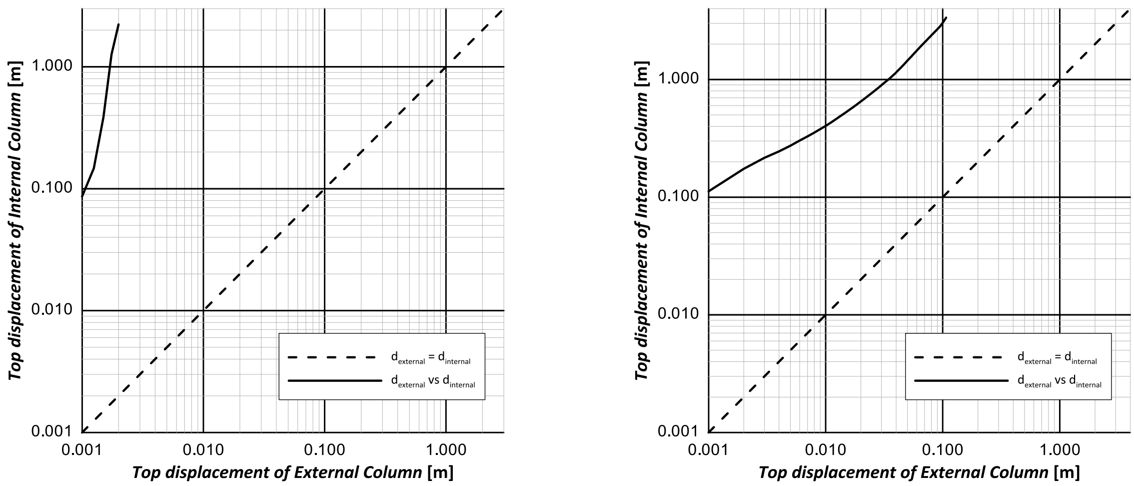

(a) (b)

Figure 4.62. Top displacement of internal columns versus the top displacement of external columns in structures with null diaphragm: (a) in X-direction; (b) in Y-direction.

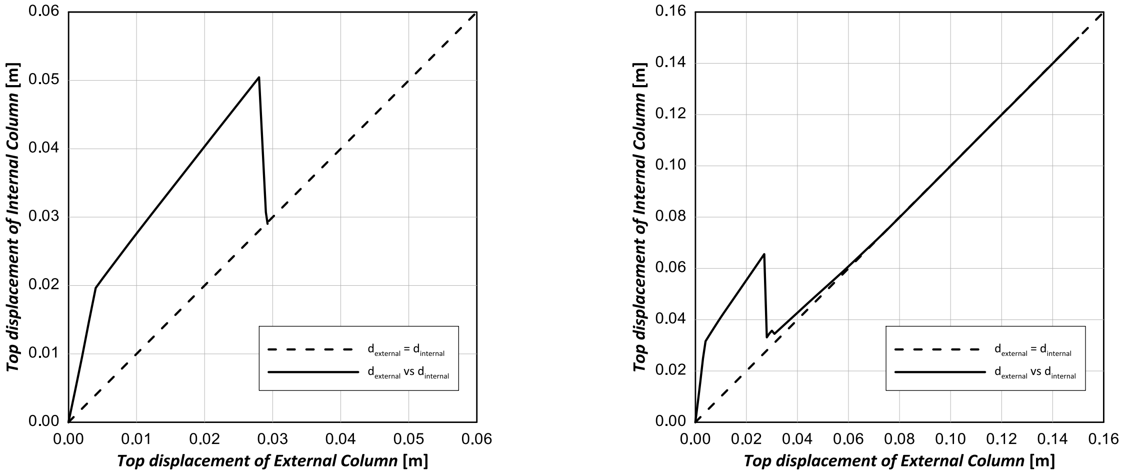

(a) (b)

Figure 4.63. Top displacement of internal columns versus the top displacement of external columns in structures with deformable diaphragm: (a) in X-direction; (b) in Y-direction.

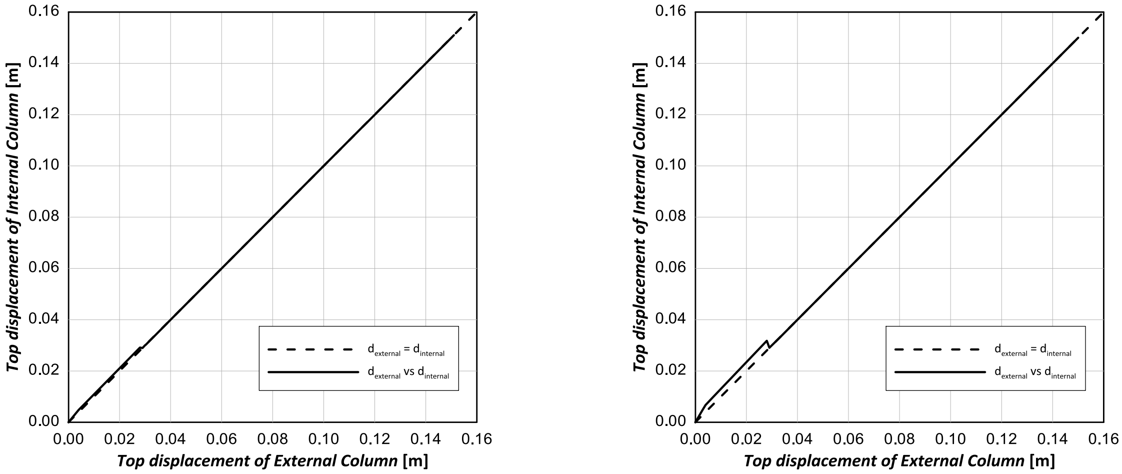

(a) (b)

Figure 4.64. Top displacement of internal columns versus the top displacement of external columns in structures with rigid diaphragm: (a) in X-direction; (b) in Y-direction.

4.2.6.3 Nonlinear Response History Analysis (NLRHA)

__Excitation__

For the nonlinear response history analysis, the modified Tolmezzo accelerogram (Fig. 4.65) is used. The record is modified to fit the Eurocode 8 spectrum (Fig 4.66) for soil type B. Three PGA (peak ground acceleration) intensities are taken into account: 0.18 g (corresponding to 0.15 g for soil type A), 0.36 g (corresponding to 0.30 g for soil type A) and 0.60 g (corresponding to 0.50 g for soil type A).

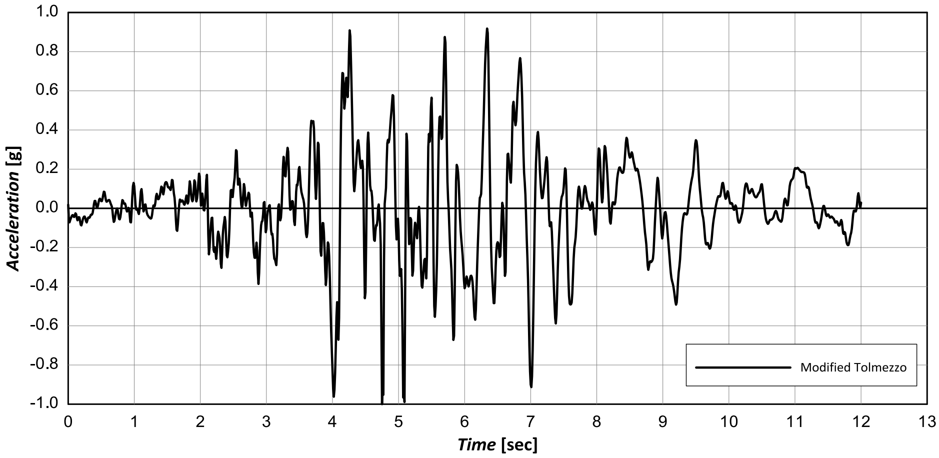

Figure 4.65. Modified Tolmezzo Accelerogram record used in the NLRHA.

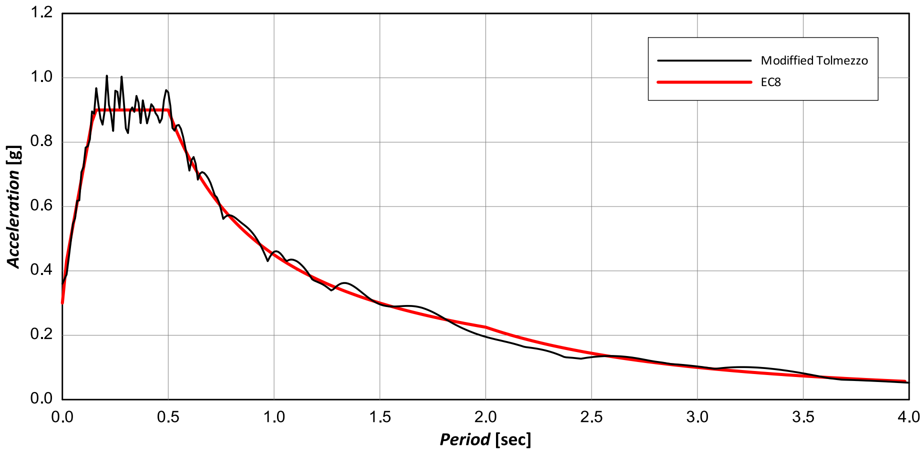

Figure 4.66. Comparison of the EC8 and the modified Tolmezzo spectra for PGA=0.36g.

__Results of the Nonlinear Response History Analysis__

In this section, the results of the nonlinear response history analyses of the buildings with panels with integrated connections for the afore-mentioned three seismic intensities of 0.18 g, 0.36 g and 0.60 g are presented.

The maximum values obtained from the analyses are tabulated in Tables 4.6 to 4.8. It is noted that in the null and deformable diaphragm there is a significant difference between the top displacement of the external columns and the one of the interior columns. This response is attributed to the much smaller deformation of the perimeter of the building compared to its middle, due to the large stiffness of the panels. Similarly, the shear forces induced to the external columns are much smaller than the ones of the interior columns. It is noted that the theoretical Eq. (3.9) provide a satisfactory estimation of the forces induced in the connections.

Table 4.6. Response of the building with panels with integrated connections (null diaphragm).

	X-direction			Y-direction		
Quantity(1)	**0.18 g**	**0.36 g**	**0.60 g**	**0.18 g**	**0.36 g**	**0.60 g**
External column top displacement [m]	0.0010	0.0020	0.0033	0.0009	0.0021	0.0042
Internal column top displacement [m]	0.0500	0.1046	0.1607	0.0489	0.0944	0.1586
Total Base Shear [kN]	2856.9	5686.5	9659.4	2203.5	4163.9	6715.8
Shear in one external column [kN]	38.2	62.0	85.6	66.1	103.9	137.9
Shear in one internal column [kN]	116.1	169.6	186.6	87.5	122.5	146.2
Shear in one extra column [kN]	49.5	72.2	90.6	3.1	5.6	8.8
Shear in one panel [kN]	42.6	84.3	138.7	33.8	64.0	103.1
Panels' vertical connection force(2) [kN]	126.1 (97.2)	204.2 (169.2)	305.8 (262.9)	108.2 (79.9)	162.7 (132.5)	233.8 (200.9)
Panels' resultant connection force(2) [kN]	130.4 (99.4)	215.3 (174.1)	326.3 (271.3)	112.5 (81.7)	174.2 (136.3)	253.4 (208.0)
Theoretical Panels' vertical force(3) [kN]	106.3	211.6	359.4	123.0	232.4	374.8

(1) In the table the maximum values obtained from the analyses are tabulated.
(2) The value inside the parenthesis represents the mean absolute value of the force in the connection.
(3) The value has been computed according to Eq. (3.9).

Table 4.7. Response of the building with panels with integrated connections (deformable diaphragm).

	X-direction			Y-direction		
Quantity(1)	**0.18 g**	**0.36 g**	**0.60 g**	**0.18 g**	**0.36 g**	**0.60 g**
External column top displacement [m]	0.0018	0.0034	0.0100	0.0023	0.0116	0.0757
Internal column top displacement [m]	0.0130	0.0251	0.0403	0.0290	0.0637	0.0921
Total Base Shear [kN]	4848.1	9023.7	12752.4	4491.0	8102.4	11043.6
Shear in one external column [kN]	41.7	62.9	77.3	34.3	48.4	95.8
Shear in one internal column [kN]	69.2	100.7	122.5	58.7	95.4	113.2
Shear in one extra column [kN]	109.9	158.9	178.7	7.6	27.4	61.6
Shear in one panel [kN]	75.3	144.0	187.5	103.6	188.8	258.2
Panels' vertical connection force(2) [kN]	190.2 (153.6)	321.1 (269.1)	403.6 (351.2)	234.5 (194.3)	390.5 (343.8)	516.9 (464.3)
Panels' resultant connection force(2) [kN]	198.5 (157.9)	339.6 (277.8)	426.8 (362.6)	248.3 (202.3)	420.3 (359.6)	560.4 (486.3)
Theoretical Panels' vertical force(3) [kN]	180.4	335.7	474.4	250.6	452.1	616.3

(1) In the table the maximum values obtained from the analyses are tabulated.
(2) The value inside the parenthesis represents the mean absolute value of the force in the connection.
(3) The value has been computed according to Eq. (3.9).

Table 4.8. Response of the building with panels with integrated connections (rigid diaphragm).

	X-direction			Y-direction		
Quantity[1]	**0.18 g**	**0.36 g**	**0.60 g**	**0.18 g**	**0.36 g**	**0.60 g**
External column top displacement [m]	0.0030	0.0059	0.0160	0.0052	0.0184	0.0849
Internal column top displacement [m]	0.0036	0.0071	0.0173	0.0086	0.0223	0.0854
Total Base Shear [kN]	7080.1	10665.8	14126.6	6900.7	9715.3	11723.7
Shear in one external column [kN]	40.4	55.0	68.2	20.9	38.6	76.8
Shear in one internal column [kN]	57.4	70.6	88.4	41.6	50.9	76.6
Shear in one extra column [kN]	93.5	145.8	173.6	15.9	31.5	65.0
Shear in one panel [kN]	124.3	169.2	196.8	165.7	202.6	260.4
Panels' vertical connection force[2] [kN]	277.6 (242.9)	367.9 (324.1)	419.2 (371.2)	349.1 (317.4)	414.2 (378.0)	520.4 (469.8)
Panels' resultant connection force[2] [kN]	292.1 (250.4)	389.3 (335.4)	448.2 (383.5)	375.0 (331.6)	454.2 (393.9)	563.1 (492.7)
Theoretical Panels' vertical force[3] [kN]	263.4	396.8	525.5	385.1	542.1	654.2

(1) In the table the maximum values obtained from the analyses are tabulated.
(2) The value inside the parenthesis represents the mean absolute value of the force in the connection.
(3) The value has been computed according to Eq. (3.9).

Representative hysteretic loops and are shown in the following figures. Results are presented separately for each direction and for each diaphragm configuration.

In Fig. 4.67 to 4.72, the hysteretic loops that represent the relationship between the total base shear vs. the displacement at several points of the roof are shown. Specifically, the shown displacements correspond to the top of the middle column of the exterior row (long side for X-direction and short side for Y-direction) and the top of the middle column of the interior row. As can be seen from the column in the exterior row, for PGA 0.36 g the structure experiences small inelastic response, while for PGA 0.60 g significant inelastic response is observed. The specific displacement is considered to represent satisfactorily the behaviour of the panels as it lies in same plane. On the contrary the displacement of the interior row is affected by the diaphragm action and it does not depict the inelastic behaviour of the structure as a hole.

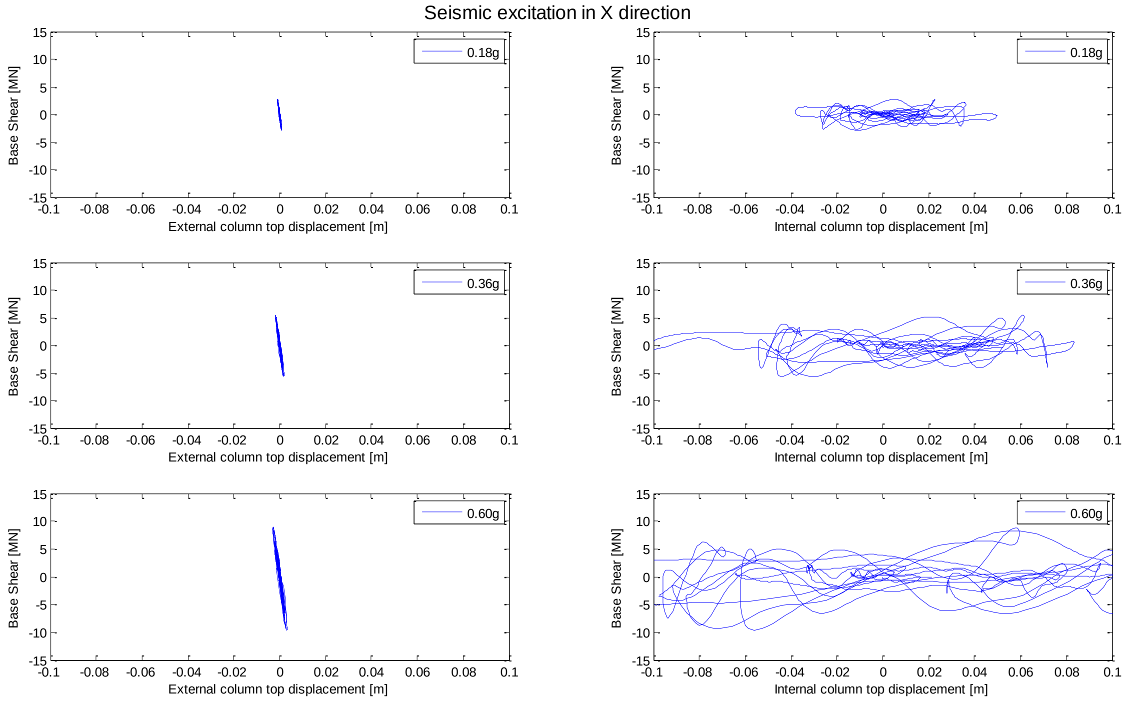

Figure 4.67. Hysteretic loops of the base shear vs. the top displacement at various positions for the seismic excitation applied in the X-direction. The null diaphragm configuration is considered.

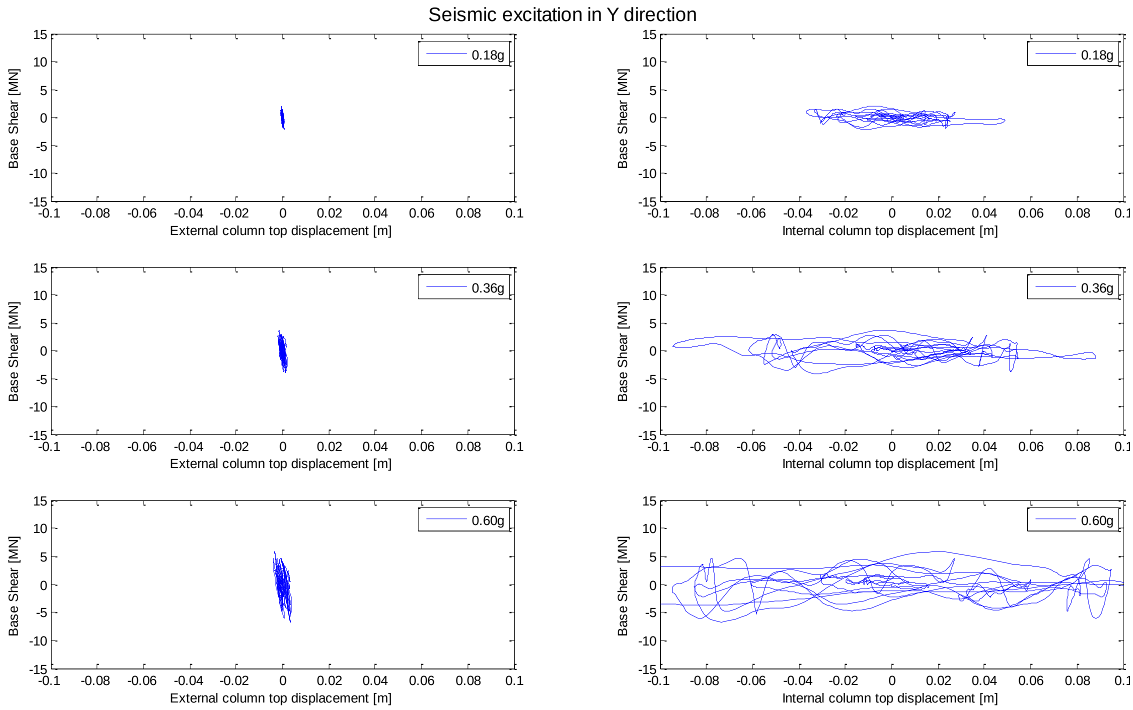

Figure 4.68. Hysteretic loops of the base shear vs. the top displacement at various positions for the seismic excitation applied in the Y-direction. The null diaphragm configuration is considered.

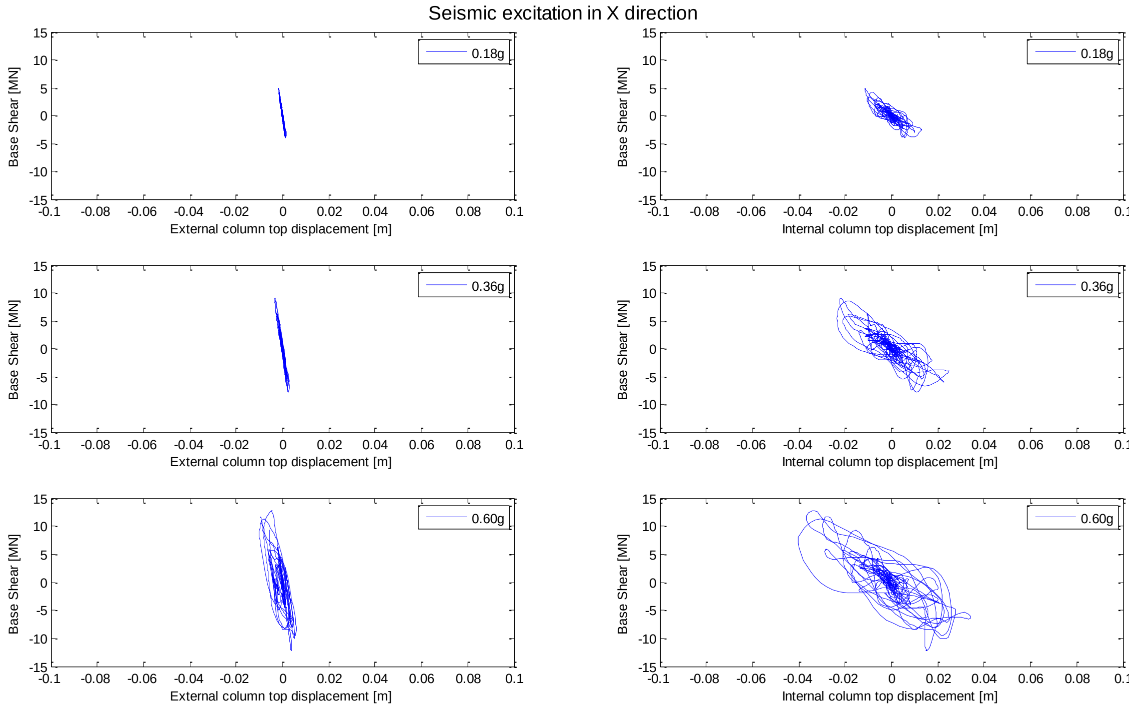

Figure 4.69. Hysteretic loops of the base shear vs. the top displacement at various positions for the seismic excitation applied in the X-direction. The deformable diaphragm configuration is considered.

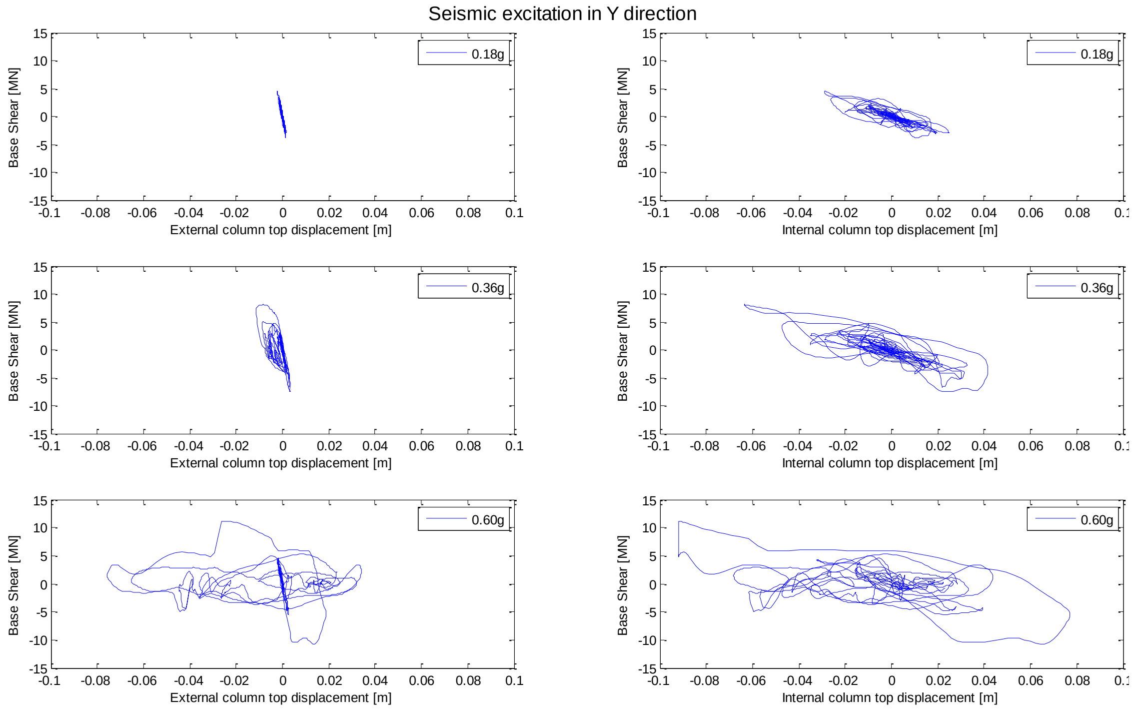

Figure 4.70. Hysteretic loops of the base shear vs. the top displacement at various positions for the seismic excitation applied in the Y-direction. The deformable diaphragm configuration is considered.

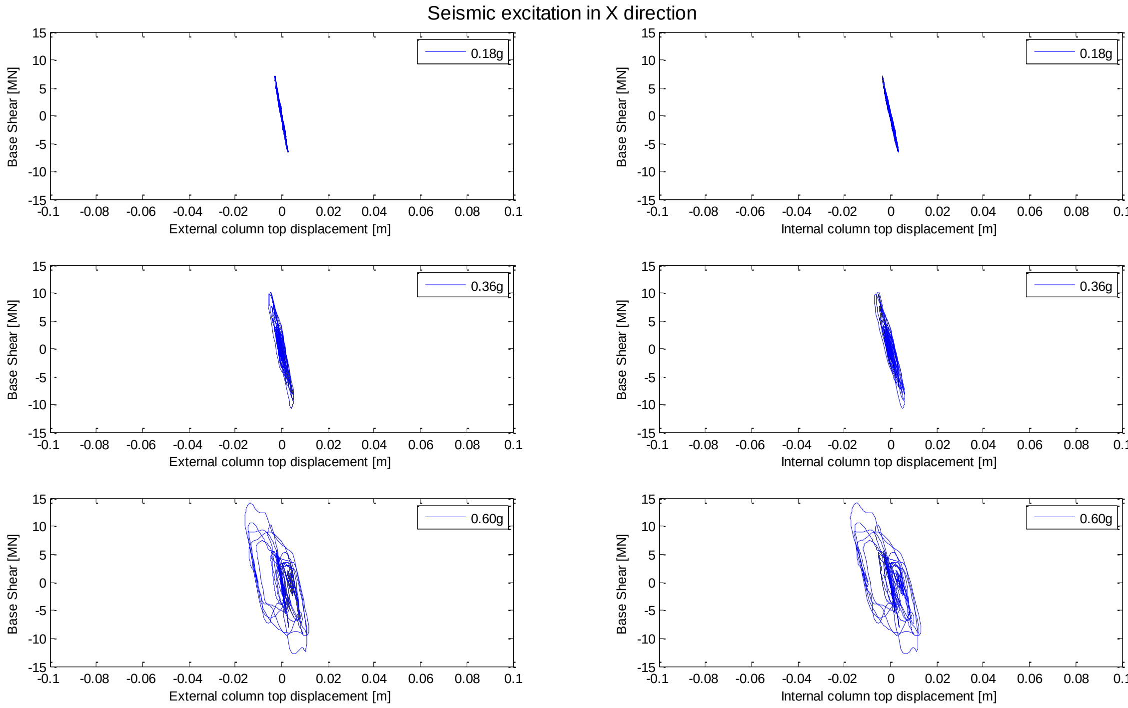

Figure 4.71. Hysteretic loops of the base shear vs. the top displacement at various positions for the seismic excitation applied in the X-direction. The rigid diaphragm configuration is considered.

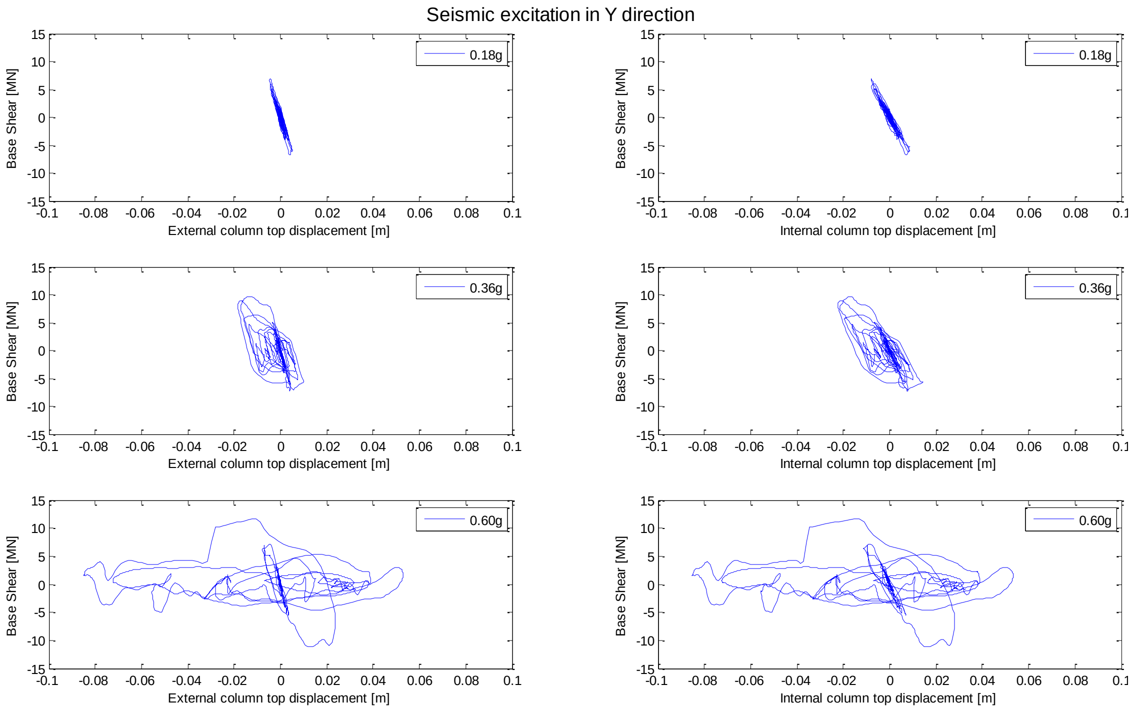

Figure 4.72. Hysteretic loops of the base shear vs. the top displacement at various positions for the seismic excitation applied in the Y-direction. The rigid diaphragm configuration is considered.

It is noted that the observed inelastic response of the structures for PGA = 0.18 g and 0.36 g is due to the inelastic response of the columns and not of the panels. In Fig. 4.73 to 4.75, the moment at the panels' ends versus the rotation is shown: in most of the cases the panel connections behave elastically even for PGA=0.36 g, but their response is highly inelastic for 0.60 g. Worth mentioning is the fact that in the null diaphragm the response of panels is elastic even for PGA=0.60g. It is reminded that the inelasticity of the panels is considered concentrated at the inelastic springs placed at their ends.

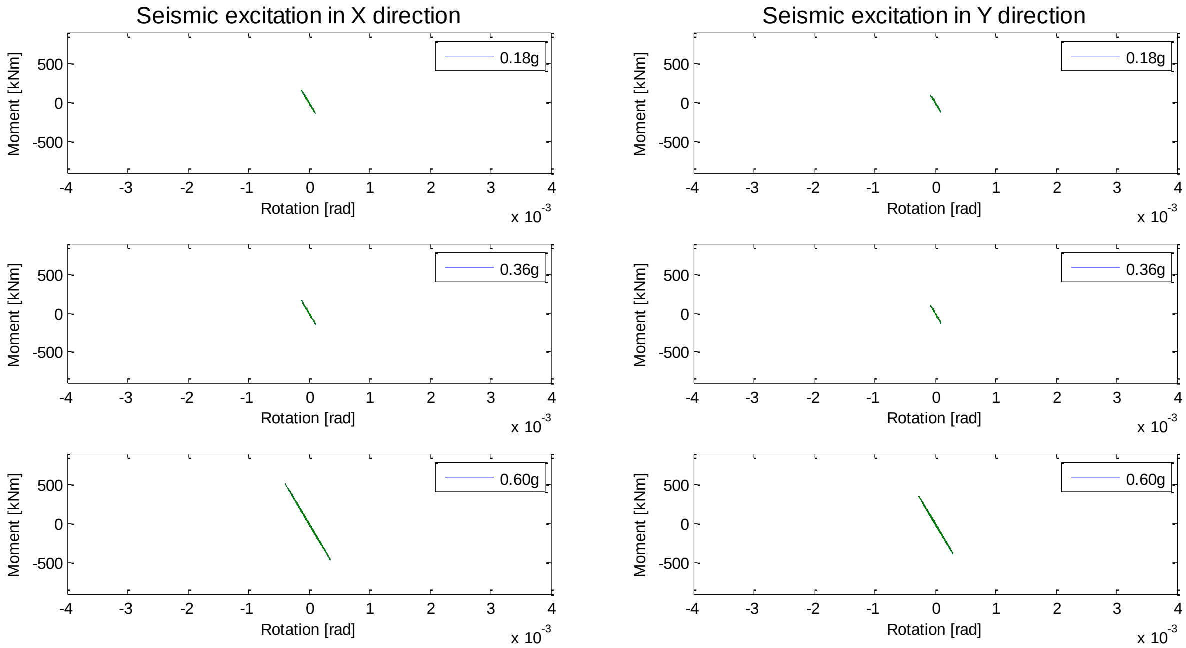

Figure 4.73. Moment – rotation hysteretic loops of the connections of the panels for the three levels of PGA and null diaphragm configuration considered.

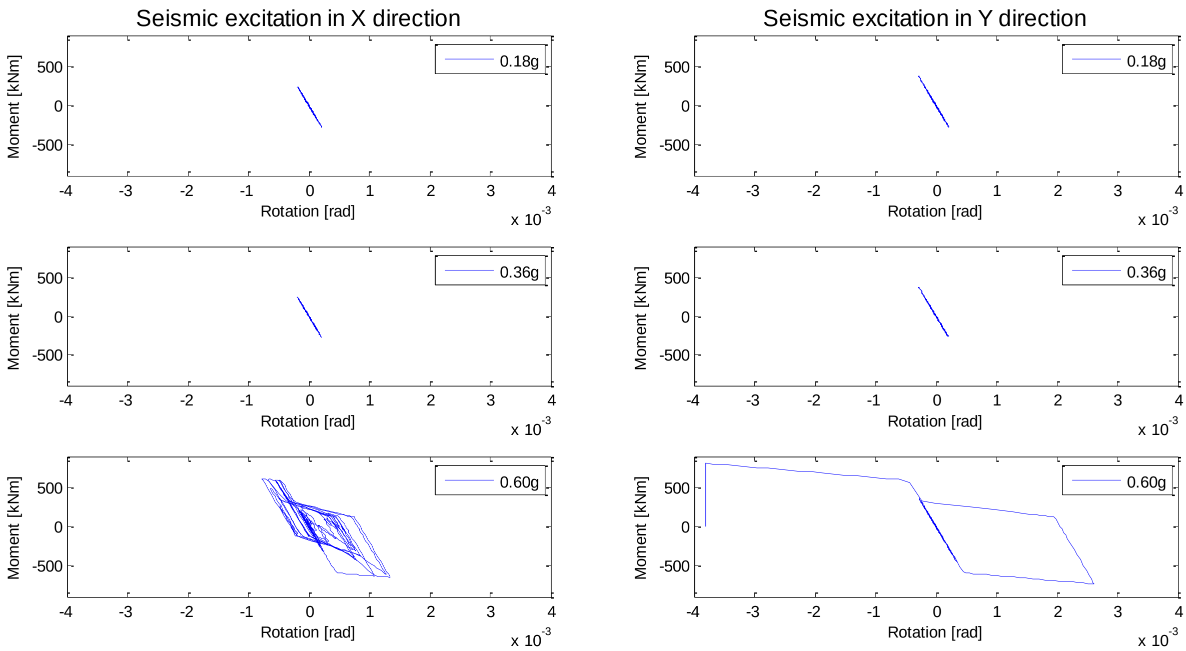

Figure 4.74. Moment – rotation hysteretic loops of the connections of the panels for the three levels of PGA and deformable diaphragm configuration considered.

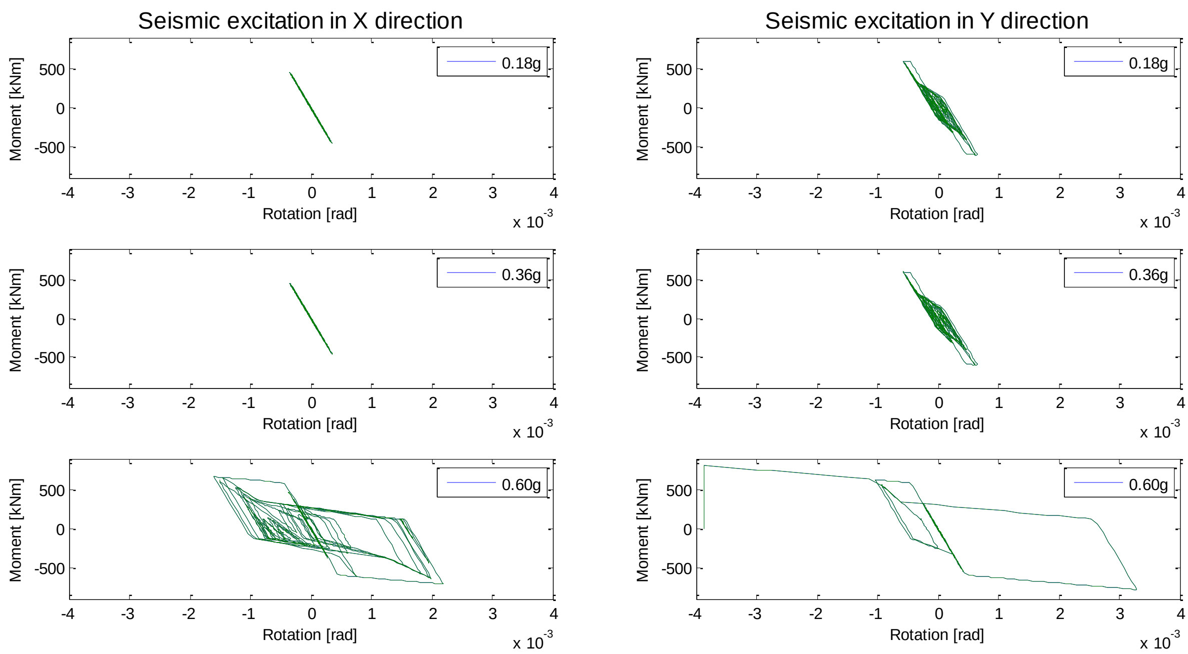

Figure 4.75. Moment – rotation hysteretic loops of the connections of the panels for the three levels of PGA and rigid diaphragm configuration considered.

On the contrary, some columns responded inelastically even for PGA = 0.18 g. As shown in Fig. 4.76 to 4.81, the columns that are enclosed by the panels behave elastically even for PGA = 0.36 g (for excitation in the direction of the panels), while the internal columns behaved inelastically even for PGA = 0.18 g. The extra columns that were placed at the mid-span of the short sides suffered severe inelastic response.

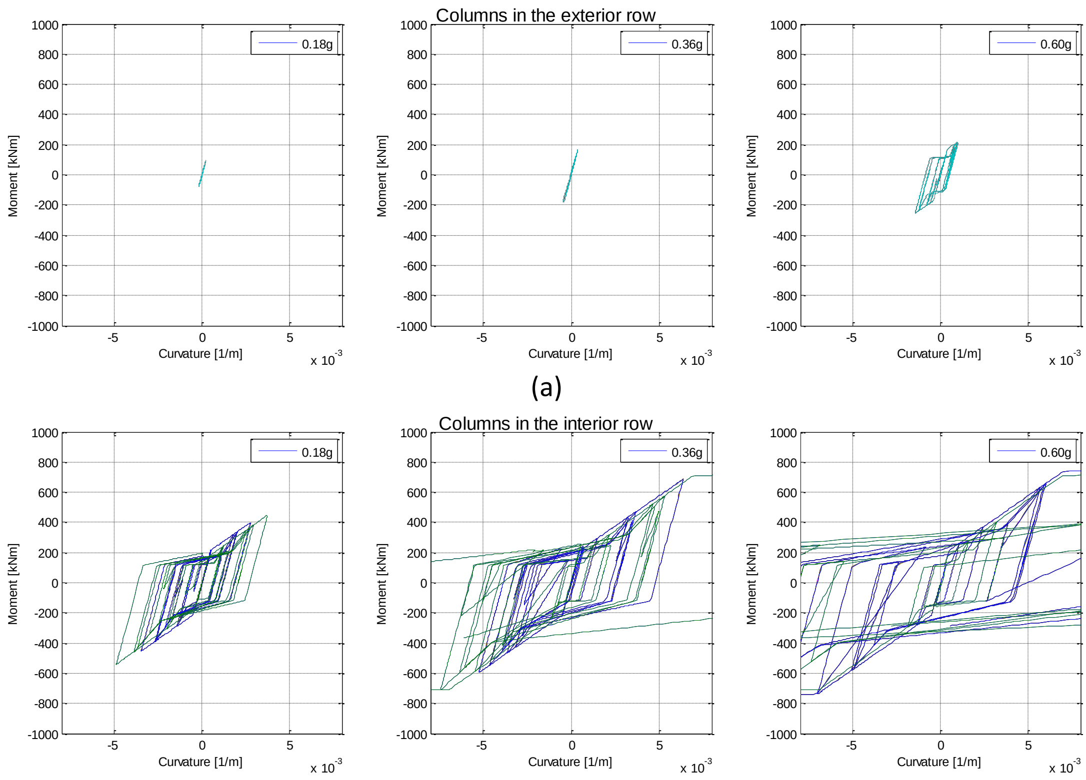

(a)

(b)

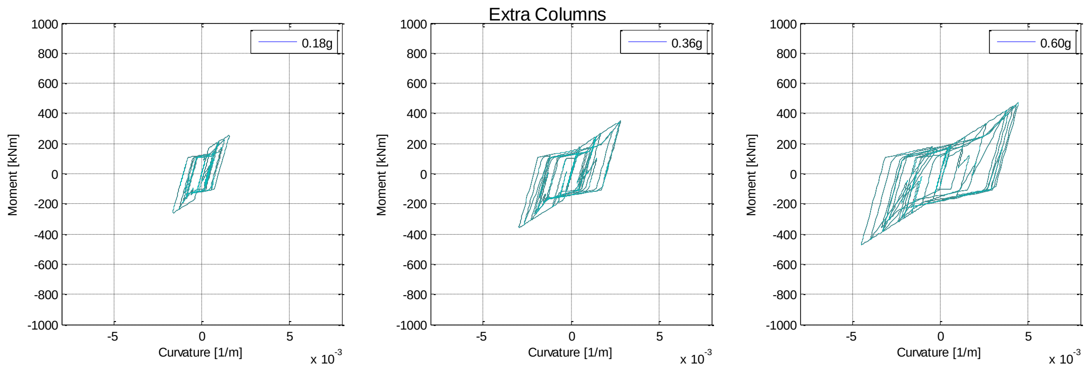

(c)

Figure 4.76. Moment – curvature hysteretic loops at the bottom of columns of the building with null diaphragm for excitation in the X-direction: (a) columns in the exterior row; (b) columns in the interior row; (c) extra columns (different curve for each column).

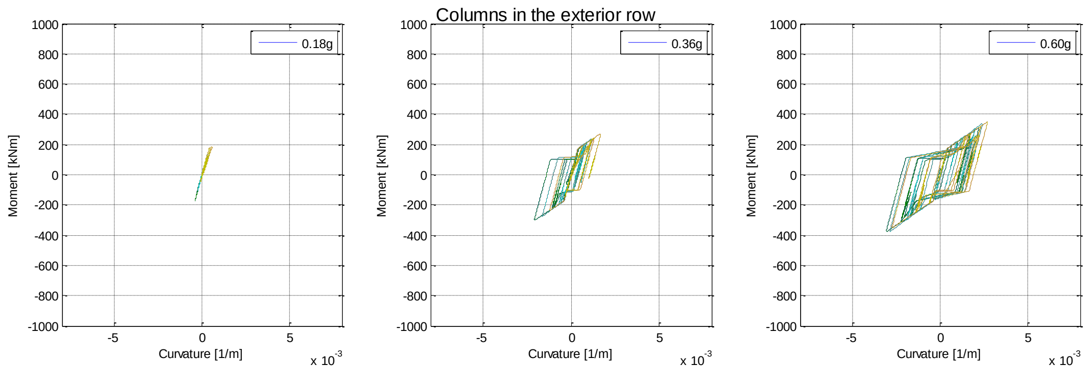

(a)

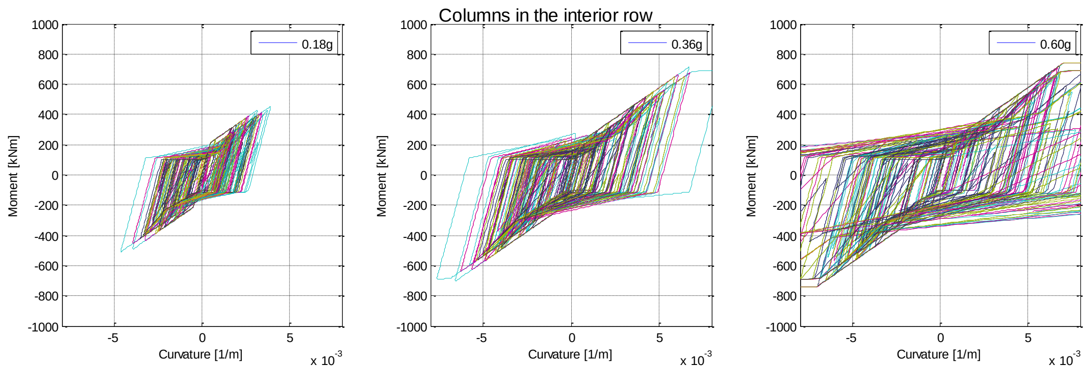

(b)

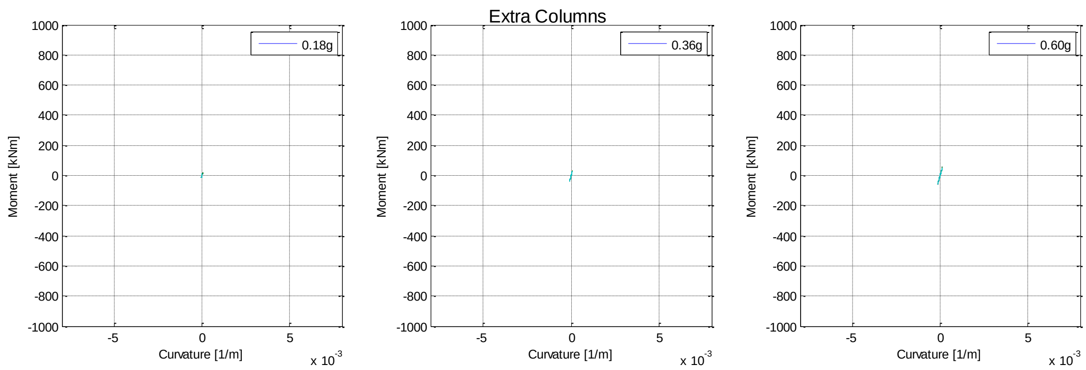

(c)

Figure 4.77. Moment – curvature hysteretic loops at the bottom of columns of the building with null diaphragm for excitation in the Y-direction: (a) columns in the exterior row; (b) columns in the interior row; (c) extra columns (different curve for each column).

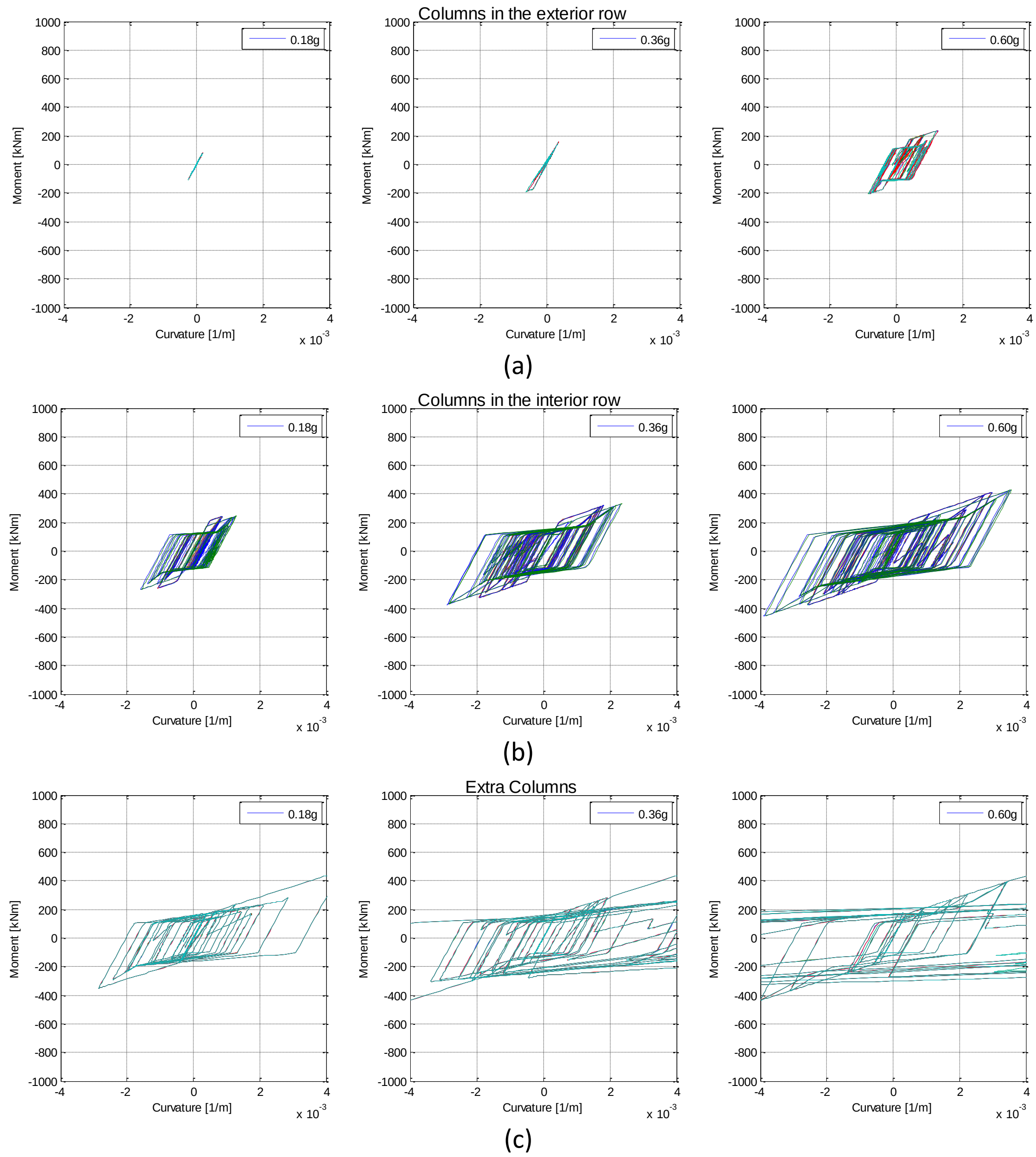

Figure 4.78. Moment – curvature hysteretic loops at the bottom of columns of the building with deformable diaphragm for excitation in the X-direction: (a) columns in the exterior row; (b) columns in the interior row; (c) extra columns (different curve for each column).

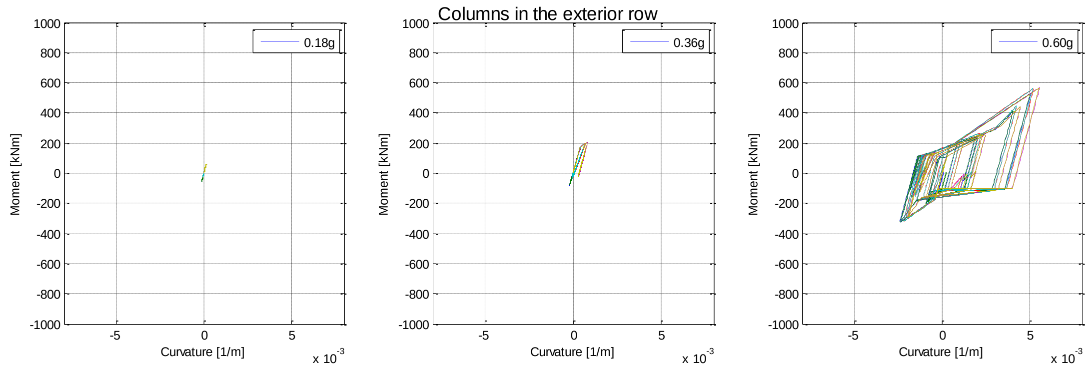

(a)

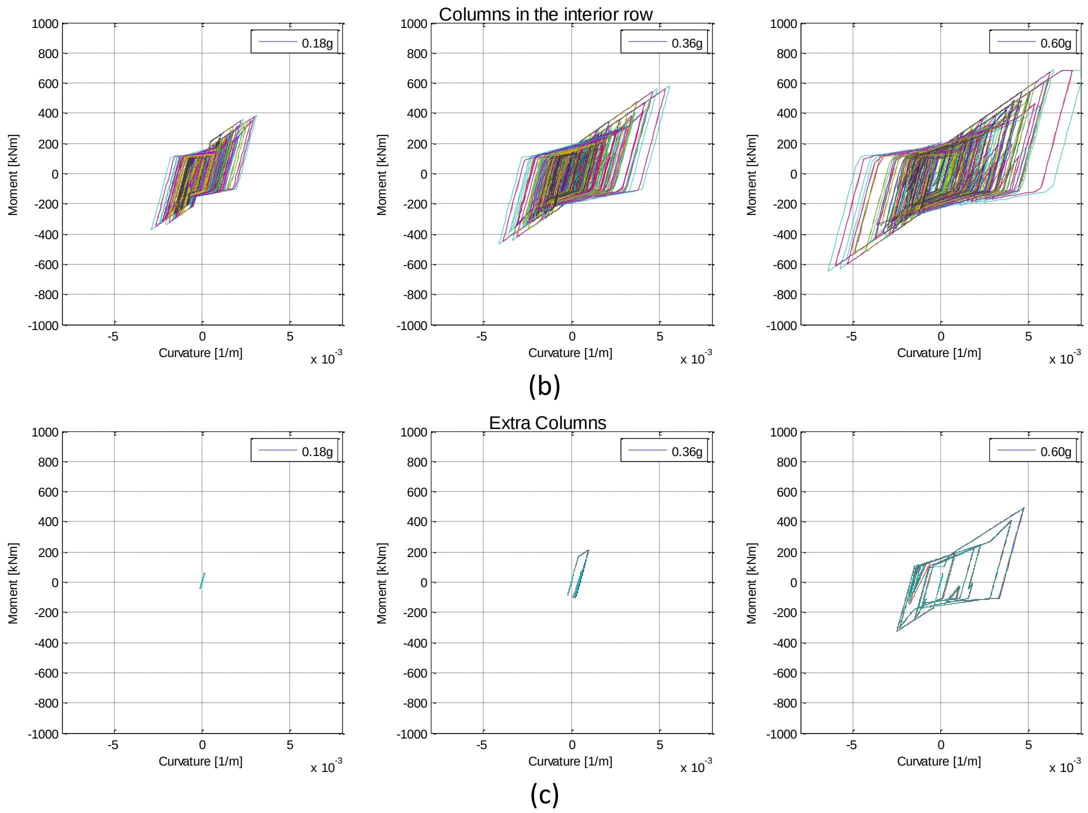

Figure 4.79. Moment – curvature hysteretic loops at the bottom of columns of the building with deformable diaphragm for excitation in the Y-direction: (a) columns in the exterior row; (b) columns in the interior row; (c) extra columns (different curve for each column).

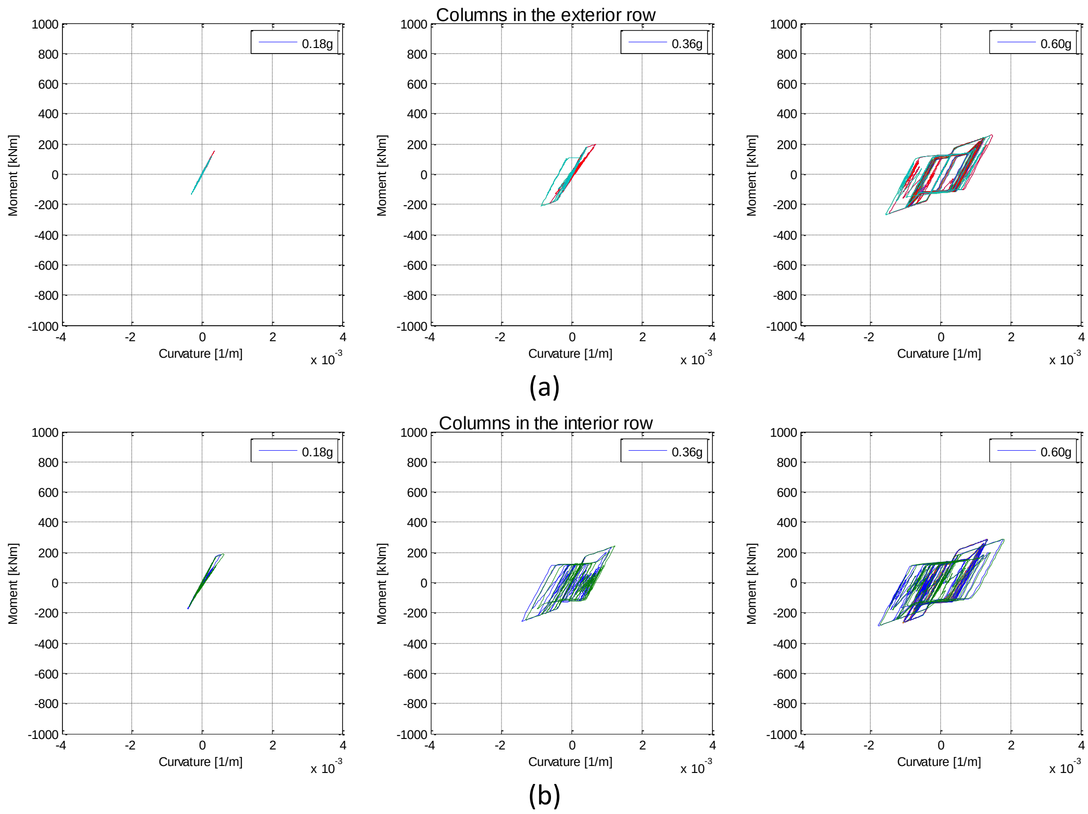

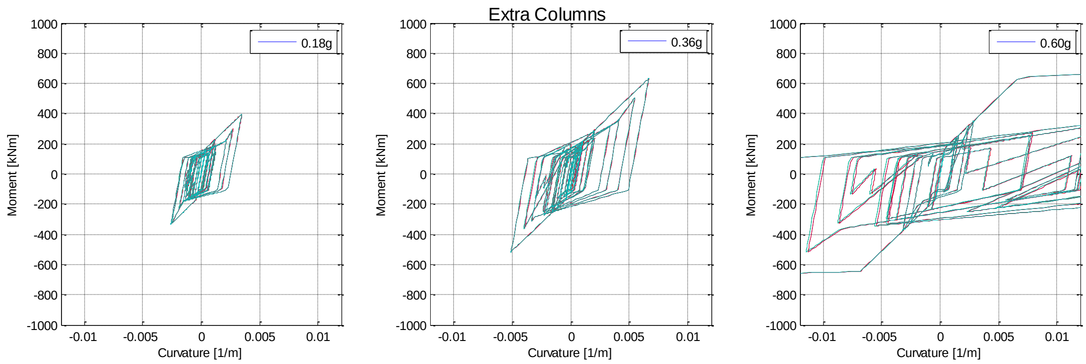

(c)

Figure 4.80. Moment – curvature hysteretic loops at the bottom of columns of the building with rigid diaphragm for excitation in the X-direction: (a) columns in the exterior row; (b) columns in the interior row; (c) extra columns (different curve for each column).

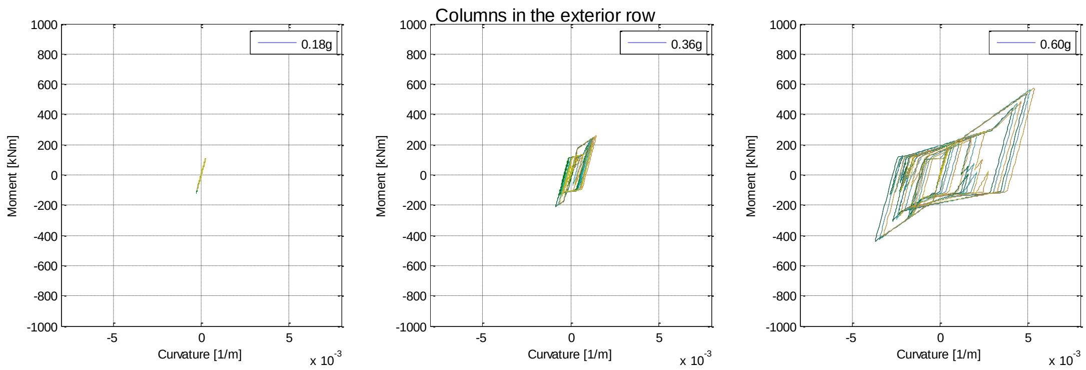

(a)

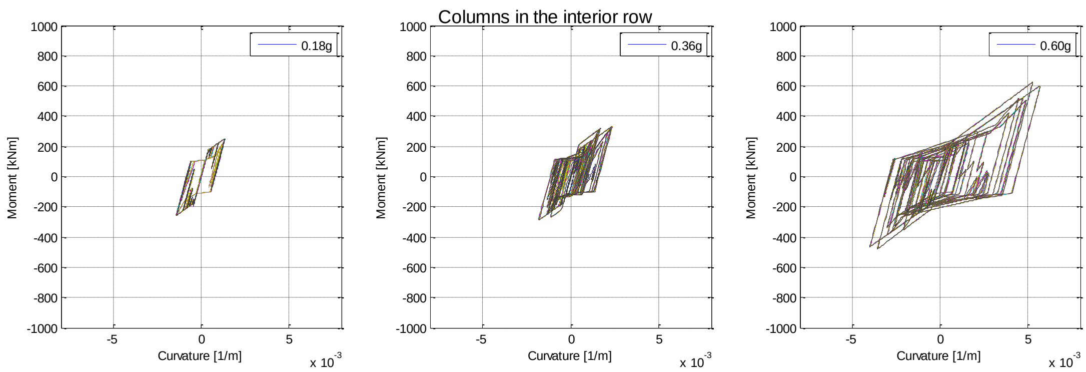

(b)

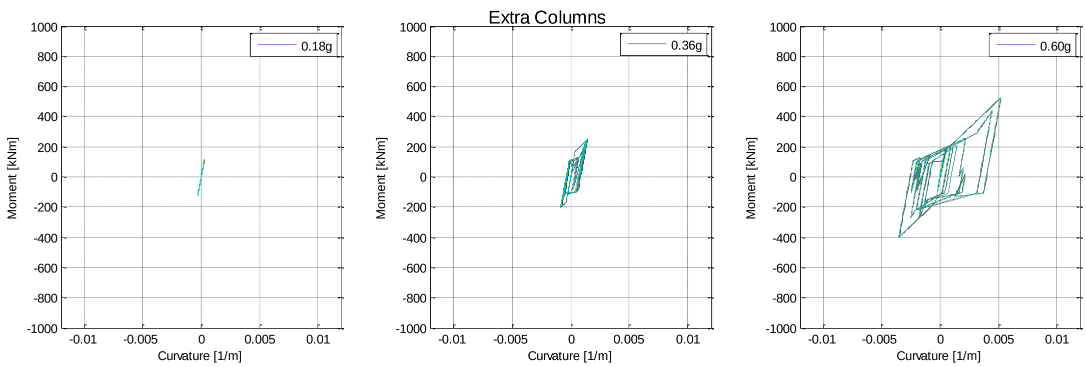

(c)

Figure 4.81. Moment – curvature hysteretic loops at the bottom of columns of the building with rigid diaphragm for excitation in the Y-direction: (a) columns in the exterior row; (b) columns in the interior row; (c) extra columns (different curve for each column).

5 Conclusions

From the results of the performed analyses the following conclusions can be drawn:

- Buildings with integrated panel connections were considerably stiffer than the similar building with isostatic connections, resulting in increase of the seismic loads.

- The force induced to each connection is proportional to the vertical distance of the connections, i.e., the height of the storey, but independent of the width of the panels. This practically means that the connection forces cannot be reduced by using more panels of smaller length or less panels of larger length. However, the connection forces greatly depend on the “coverage” of the external sides by panels and increase significantly in case of sides with long openings, i.e., sides partially covered with panels.

- The major component of the force induced to each connection is in the vertical direction. Bearing this in mind, in “rebar type” connections the inelastic response is mainly governed by the response of the dowels in tension.

- A large dispersion in the value of the forces induced to the connections is observed when the “rigid connection” assumption is adopted. On the other hand, the dispersion is decreased significantly when more realistic moment – rotation laws are used.

- Even for small top displacements, and significantly prior to the yielding of the connection rebars, the bond between the rebars and the surrounding concrete in the vicinity of the joint reached its maximum strength. As the top displacement was increasing, the bond loss was propagating along the rebar.

- In the bare frame systems, the roof diaphragm configuration does not affect the response of the building as the diaphragm is relatively stiffer than the frame. Since the columns are hinged on the top, the fundamental mode of vibration in these cases is that of the cantilever. On the contrary, in systems with integrated panels the diaphragm has a profound effect in the transmission of the forces and its configuration affects the overall response.

- The capacity (pushover) strength of the structure show an abrupt loss of the strength when the panel connections fail. The monotonic loading results also show that this failure occurs almost simultaneously for all panels aligned in the loading direction.

- The nonlinear time history analyses using the modified Tolmezzo record show that the connections behave elastically even for PGA equal to 0.36 g. However, for the higher seismic intensity examined (PGA = 0.60 g) they enter the inelastic region, with exception the null roof configuration.

- For all roof configurations examined it is observed that much larger forces are induced to the columns which are not connected to the panels aligned in the loading direction compared with the corresponding forces induced to the outer (façade) columns. The former behaved inelastically even for the lowest seismic intensity examined (PGA = 0.18 g).

- Similarly, due to the flexibility of the roof diaphragm in null and deformable configurations the displacements at the above-mentioned inner columns are much larger than those on the outer columns. The differences are significantly lower in case of rigid diaphragm.

6 References

Alemdar, B. N. *Distributed Plasticity Analysis of Steel Building Structural Systems*. Ph.D. Thesis, Georgia Institute of Technology, Atlanta, 2001.

Calabrese A. *Numerical Issues In Distributed Inelasticity Modelling of RC Frame Elements For Seismic Analysis*. Master Degree Dissertation, Istituto Universitario di Studi Superiori di Pavia, Università degli Studi di Pavia, 2008.

Coleman, J., Spacone, E. Localization issues in force-based frame elements. *Journal of Structural Engineering*, ASCE, 2001, 127(11): 1257-1265.

European Committee for Standardization (CEN). *Design of concrete structures – Part 1-1: General rules and rules for buildings*. Eurocode 2, EN 1992-1-1, 2004.

European Committee for Standardization (CEN). *Design of structures for earthquake resistance – Part 1: General rules, seismic actions and rules for buildings*. Eurocode 8, EN 1998-2, 2004.

European Committee for Standardization (CEN). *Design of structures for earthquake resistance – Part2: Bridges*. Eurocode 8, EN 1998-2, 2004.

Fajfar, P., Fischinger, M. Non-linear seismic analysis of RC buildings: Implications of a case study. *European Earthquake Engineering*, 1987, 1: 31-43.

Fischinger, M., Kramar, M., Isaković, T. Cyclic response of slender RC columns typical of precast industrial buildings. *Bull. Earthquake Eng.*, 2007, Springer, 6: 519-534.

Fischinger, M., et al. Catalogue on the existing cladding panel systems and connections in precast buildings with the identification of their possible seismic deficiencies. SAFECLADDING: Improved fastening systems of cladding wall panels of precast buildings in seismic zones, Deliverable 1.1, 2013, FP7 Project No. 314122.

International Federation for Structural Concrete (fib). *Practitioners' guide to finite element modelling of reinforced concrete structures*. Fib Bulletin 45, State-of-art report prepared by Task Group 4.4.

Kent, D.C. and Park, R. (1971), "Flexural Members with Confined Concrete*," Journal of the Structural Division*, ASCE, 1971, 97(ST7): 1969-1990.

Mazzoni, S., McKenna, F., Scott, M. H., Fenves, G., et al. *OpenSees Command Language Manual (2007)*

McKenna, F., Fenves, G. L., Scott, M. H., and Jeremic, B. *Open System for Earthquake Engineering Simulation (OpenSees)*. Pacific Earthquake Engineering Research Center, University of California, Berkeley, CA, 2000.

Paulay, T., Priestley, M. J. N. *Seismic Design of Reinforced Concrete and Masonry Buildings*, New York, John Wiley & Sons, 1992.

Scott, M.H. and G.L. Fenves. Plastic Hinge Integration Methods for Force-Based Beam-Column Elements. *Journal of Structural Engineering*, 2006, ASCE, 132(2): 244-252.

Takeda, T., Sozen, M. A., Nielson, N. N. Reinforced concrete response to simulated earthquakes. *Journal of the Structural Division*, 1970, ASCE, 96(12): 2557–2573.

EXPERIMENTAL PART

7 Calculation of the expected connections' forces

In order to decide on the tests that should be performed, additional analytical investigation was carried out for the estimation of the magnitude of the expected forces to be induced to the connections of integrated systems under seismic action. A detailed analytical investigation for several types of buildings is presented in section 4. The procedure described below is based on the theoretical estimation of the average forces through Eq. (3.9) and on the Nonlinear Response History Analysis (NLRHA) in which the inelasticity is limited to the columns' behaviour.

7.1 Case studies

7.1.1 Typical residential building

As a first example, let us consider a 3–storey building with plan dimensions 10.0 m × 20.0 m and storey height of 3.50 m. The panels are of dimensions L_{panel} = 2.00 m and H_{panel} = 3.00 m, thus, adopting the distances of the connections from the edges shown in Fig. 4.4, L = 1.60 m and H = 2.70 m. Due to probable openings, it is assumed that only a portion of each side of the perimeter is covered by panels, specifically it is considered that n = 3 in the short direction and n = 7 in the long direction. Then, Eq. (3.9) gives:

$$P_i = 0.141 \cdot P_{base} \quad \text{in the short direction} \tag{7.1a}$$

$$P_i = 0.060 \cdot P_{base} \quad \text{in the long direction} \tag{7.1b}$$

Considering an average floor weight of w = 10.0 kN/m^2 for all stories and that the ground acceleration is a_g=0.24 g and the soil category is B (S = 1.20), and assuming that the spectral amplification is $S_e/(S \cdot a_g)$ = 2.5 (horizontal branch of the spectrum and elastic behaviour, q = 1.0), the total base shear is: P_{base} = 4320 KN. Then, Eqs. (7.1a) and (7.1b) lead to the following connection forces at the ground floor:

$$P_{i,\text{base}} = 608 \text{ kN in the short direction}$$

$$P_{i,\text{base}} = 260 \text{ kN in the long direction}$$

At the upper floors, the forces that will be induced to the connections will be smaller, since the storey shear forces will be smaller. For example, assuming a linear distribution of the seismic loads, the shear force at the upper third floor will be: P_3 = 4320×10.50/(3.50+7.00+10.50) = 2160 KN. Then for the same configuration of panels, the connection forces will be:

$$P_{i,\text{3rd}} = 304 \text{ kN in the short direction}$$

$$P_{i,\text{3rd}} = 130 \text{ kN in the long direction}$$

7.1.2 Industrial single-storey building – case A

As a second example, the building described in section 4.1 is considered. Let us assume that 3 vertical panels of 3.00 m width and 7.40 m height are placed at each span of length 10.00 m (axial distance of columns), as shown in Fig. 4.5, and that the distances of the connections from the panels' edges are as shown in Fig. 4.4. Then, L_{total} = 100.00 m; H = 6.70 m; L = 2.60 m; n = 30 and Eq. (3.9) gives:

$$P_i = 0.021 \cdot P_{base} \tag{7.2}$$

Considering an average roof weight of w = 7.5 kN/m^2 and that the ground acceleration is a_g=0.24 g and the soil category is B (S = 1.20), and assuming that the spectral amplification is $S_e/(S \cdot a_g)$ = 2.5 (horizontal branch of the spectrum and elastic behaviour, q = 1.0), the total base shear is: P_{base} = 22680 kN. Then, Eq. (7.2) gives:

$$P_i = 476 \text{ kN}$$

It is noted that the above value is the **expected average force** at each connection. The numerical analyses presented in previous sections showed that the distribution of the forces induced to the connections is not uniform and that significantly larger forces, up to 50% larger, can develop at some connections.

7.1.3 Industrial single-storey building – case B

As a third example, one of the industrial buildings analysed in section 4.2 is considered. In the present analysis, the roof diaphragm is considered rigid, which offers an upper limit of the panel forces.

In this investigation, the behaviour of the connections was assumed elastic and all inelasticity was limited to the columns' behaviour. The maximum forces induced to the connections are tabulated in Table 1.

Table 7.1. Maximum vertical forces induced to the panel connections [kN].

PGA	X - direction	Y - direction
0.18 g	231	369
0.36 g	471	714
0.60 g	789	1233

8 Description of the experimental investigation

8.1 Description of the specimens

The specimens modelled the connection at one end of the panel with the beam. For this reason, panels of “half-height” were tested with the force applied at their free top. It is noted that, for prototype panels with four point connections, the panel behaves as a beam clamped at both ends and the zero moment location is around the mid-height.

The height of the panel specimens was 2.67 m, their width was 1.50 m, and their thickness was varying from 0.18 to 0.25 m, depending on the type of the connection. The beams were of cross section 0.40 m × 0.60 m and were securely fastened to the strong floor of the Laboratory.

The width of the specimens is considered small for typical panels used in industrial buildings. However, the experimental campaign aimed at investigating the behaviour of the connections under monotonic and cyclic loading. For this reason, and in order to reduce the size of the specimens, a relatively small width was chosen, which, however, was long enough to prevent interaction effects between the two connections.

The panels were placed *inside* the front face of the beam (Fig. 8.1(a) & 8.1(b)). This configuration does not necessarily imply that the panels are also placed inside the front face of the columns. However, if it is decided to place the panels outside of the columns, the beams must be wider than the columns in order to achieve the configurations shown in Fig. 8.1.

8.2 Types of connections examined

As mentioned above, the forces induced to the panel connections are practically applied in the **vertical direction**. Concerning the expected forces that can develop during earthquakes, the analyses showed that, for the design seismic loads, they can be quite large and may reach the value of **600 kN.** For larger earthquakes, significantly larger values can be attained, depending on the dimensions of the building.

Based on these observations, several types of connections were selected to be tested, specifically:

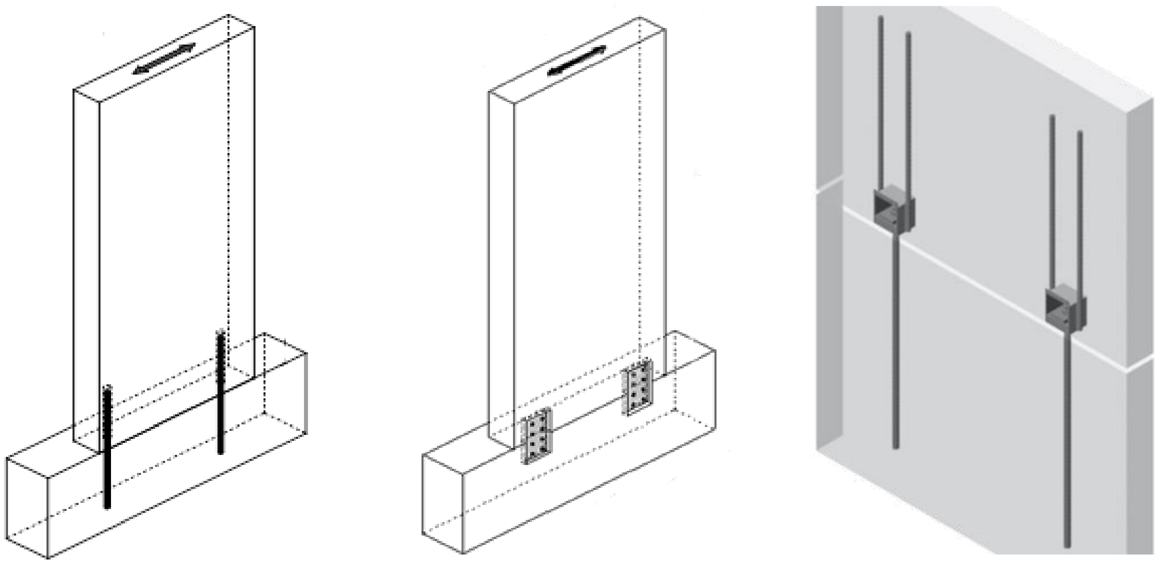

(a) (b) (c)

Figure 8.1. (a) “rebar connections”; (b) “steel plate connections”; (c) industrial type wall shoe.

1. Connections made of rebars, which are denoted as “rebar connections” (Fig. 8.1(a))
2. Connections made of bolted steel plates, which are denoted as “steel plate connections” (Fig. 8.1(b))
3. Industrially manufactured connecting mechanisms, as the wall shoes shown in Fig. 8.1(c), which are denoted as “industrial connections”

The “rebar connections” can be materialized using vertical reinforcement bars that are stressed mainly in tension during the loading. The bars protrude from the panels to the beams or vice versa and the gap between the bars and the ducts is filled with epoxy resin or high strength grouting. The proposed configuration is shown in Fig. 8.1(a).

An important drawback of this type of connection is the mounting difficulties rising from the protruding bars. To overcome this problem, three-point connections can be used which, however, increase the capacity demand as mentioned in the previous section.

On first sight, this type of connection simulates a monolithic connection of the panel with the beam, since the bars provide the tensile strength in the tension zone, while the concrete provides the resistance in the compression zone (Fig. 8.2). However, its behaviour is quite different, due to the joint at the panel-beam interface. This issue is discussed in the ensuing, when the experimental results are presented.

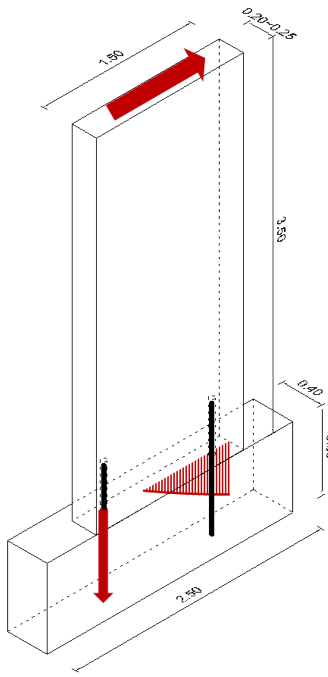

Figure 8.2. Forces and stresses that develop in “rebar connections” during loading.

The “steel plate connections” can be materialized using steel plates that are connected with other steel plates embedded in the beam and the panel by adequate number of bolts. The plates embedded in the concrete are welded to reinforcement bars so that the connection forces are gradually transferred the concrete away from the joint. A possible configuration of this connection is shown in Fig. 8.3.

The number of bolts and their distance must be appropriate to prevent local damage to the concrete. Also, using capacity criteria for the design of the steel plates, the shear failure of the bolts can be avoided. In this way, the behaviour of the connection is ruled by the behaviour of the steel plate. An advantage of this connection is that the steel plate can be easily substituted in case of damage. It is also noted that this connection does not pose any difficulties in the mounting of the panels.

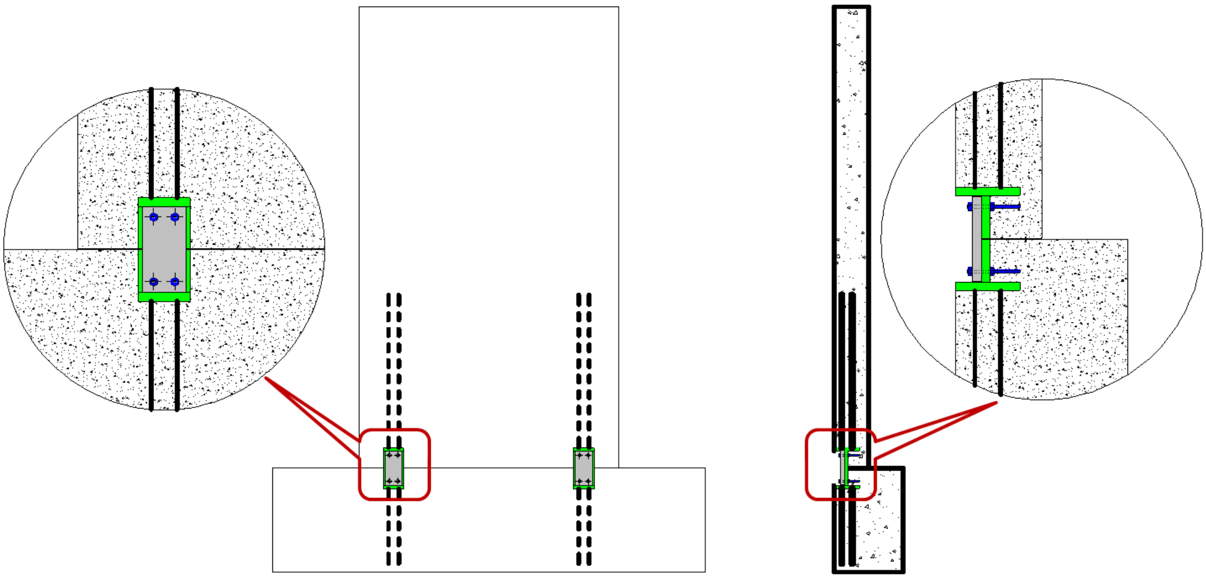

Figure 8.3. Proposed configuration of "steel plate connections".

8.3 Design of the specimens

8.3.1 Assumptions

The specimens were designed for concrete grade C30/37 and steel grade B500C in accordance to EN 1992-1-1 and EN 1998-1. The design of the specimens was made assuming "rebar connections".

In order to avoid undesirable modes of failure in the panel or the beam away from the joint region, capacity design criteria were applied for the calculation of the required reinforcement of the specimens. Therefore, the design was performed for horizontal force imposed at the top of the panel (Fig. 8.2) that corresponds to the maximum expected yielding of the connection rebars, i.e., when their tensile stress reaches the mean value f_{ym} = 575 kPa increased by an overstrength factor of 30%.

8.3.2 Numerical Analysis

In order to quantify the forces induced to the specimen during loading, a finite element analysis was performed using SAP 2000 software. A similar model was also used in previous sections for determining the moment – rotation law that governs the behaviour of panels.

The numerical model considered consisted of the panel, the beam and the connection to the strong floor of the lab. The panel was model with shell elements, the beam with solid elements and the dowels with beam elements. The joint between the panel and the beam was modelled with tensionless springs (gap elements). Gap elements were also used for the contact between beam and strong floor whereas the actual fastening with rods was modelled through elastic beams. A sketch of the numerical model used in the analysis is shown in Fig. 8.4.

No yielding in tension of the concrete was considered in order to calculate the required reinforcement to bear the corresponding forces. To this end, the maximum developed stresses σ_{max} were calculated (Fig. 8.5) and vertical reinforcement was placed symmetrically around the connection rebars in both the panel and the beam to take the corresponding tensile forces.

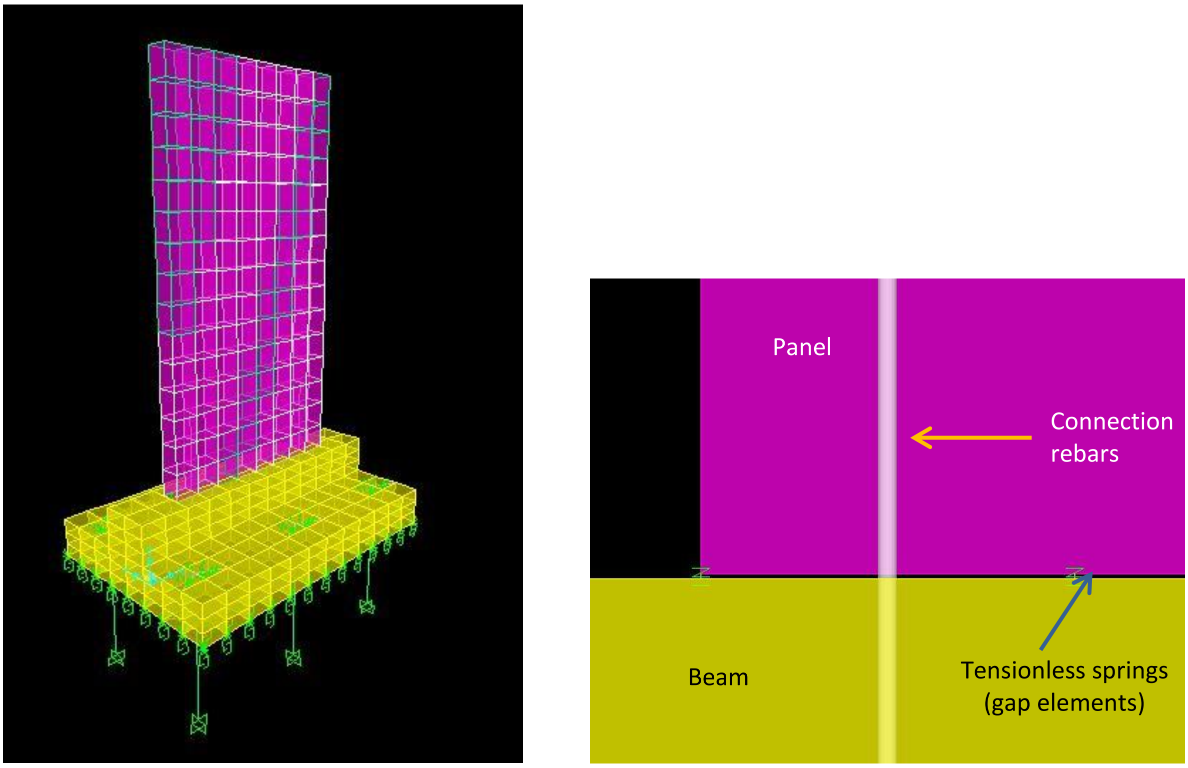

(a) (b)

Figure 8.4. (a) F.E. numerical model of the specimens; (b) detail of the connections.

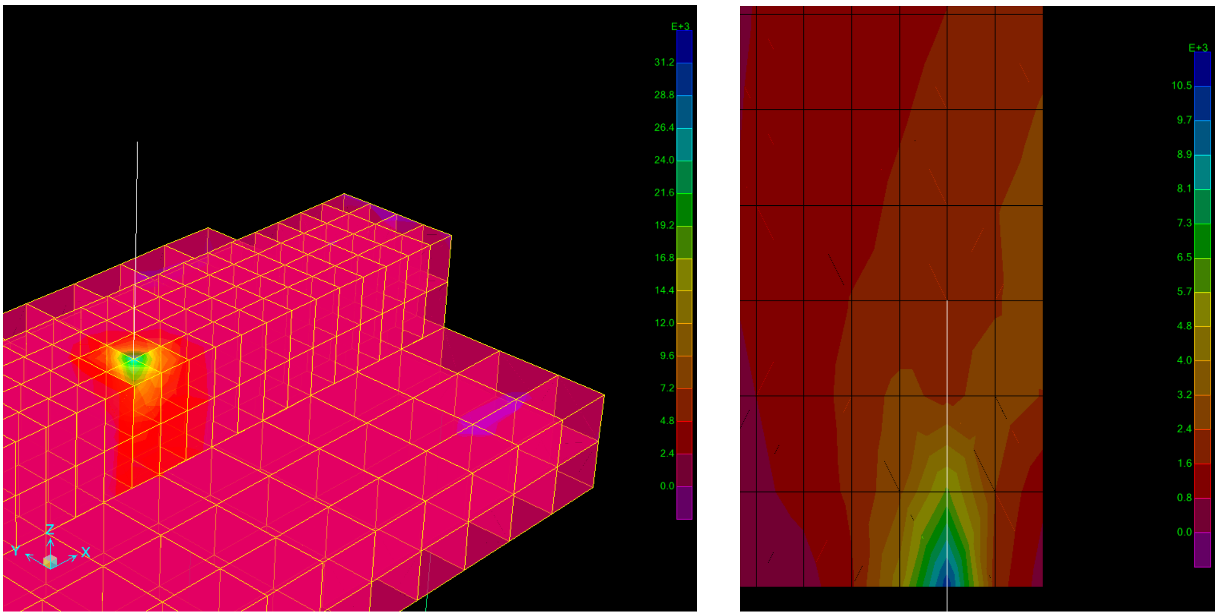

(a) (b)

Figure 8.5. (a) Tensile stress that develop in the concrete: (a) beam; (b) panel.

8.3.3 Reinforcement Drawings

Based on the results of the numerical analysis, the required reinforcement of the panel and the beam were calculated. Photos of the specimens after placement of the reinforcement and after concreting are shown in Fig. 8.6 and 8.7. The corresponding reinforcement drawings are shown in Fig. 8.8 to 8.10.

Figure 8.6. Photos of the specimens after placement of the reinforcement.

Figure 8.7. Photos of the specimens after concreting.

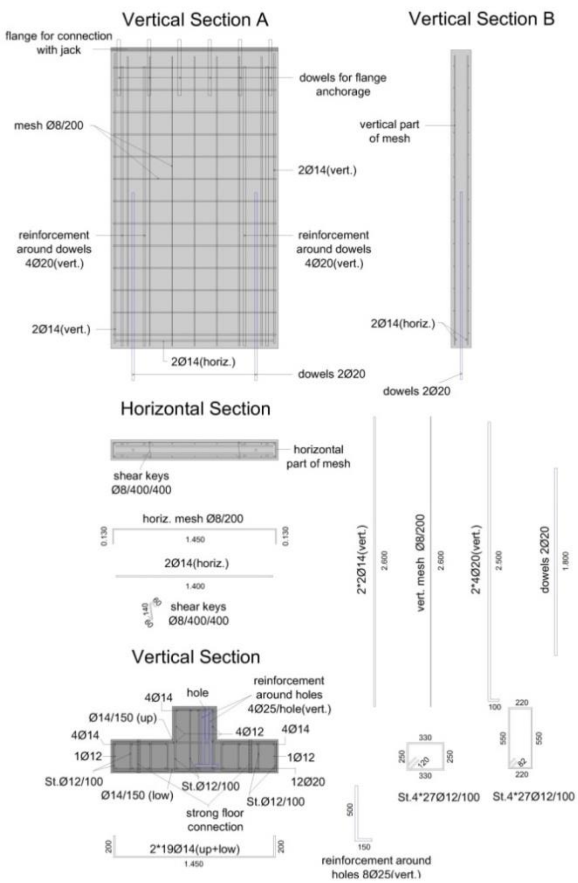

Figure 8.8. Reinforcement details of specimens 1D20M-R1 and 1D20C-R1.

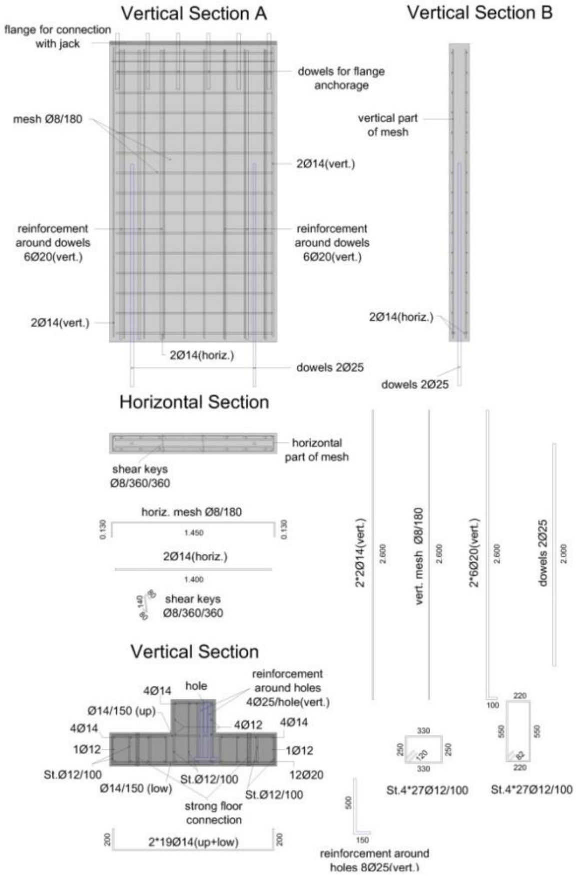

Figure 8.9. Reinforcement details of specimen 1D25M-R2.

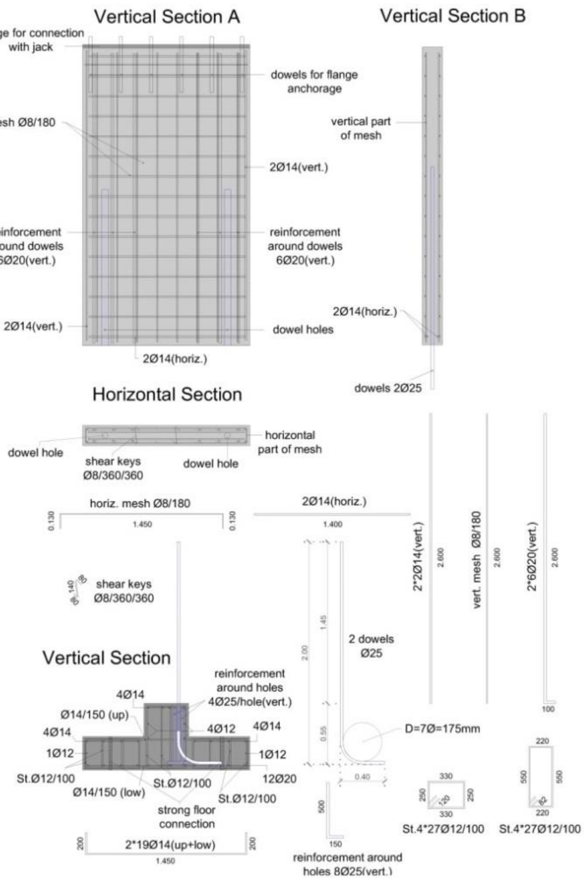

Figure 8.10. Reinforcement details of specimen 1D25M-G.

8.4 Description of the experiments

8.4.1 Experimental setup

The experimental setup is shown in Fig. 8.11 and 8.12(a). As mentioned above, the specimens consisted of a half-height panel and a beam. The horizontal loading was applied at the top of the panel using a hydraulic jack fastened to the reaction wall. The panel was placed vertically, inside the front face of the beam. For the proper fastening of the beam to the strong floor, the beam had a reversed T cross section.

The application of the force at the top of the panel was made through a specially designed steel mechanism which was fastened to the panel through six bolts (Fig. 8.12(b)) in order to obtain a uniform distribution of the load. For further security, this mechanism was restricted against sliding by side "ears".

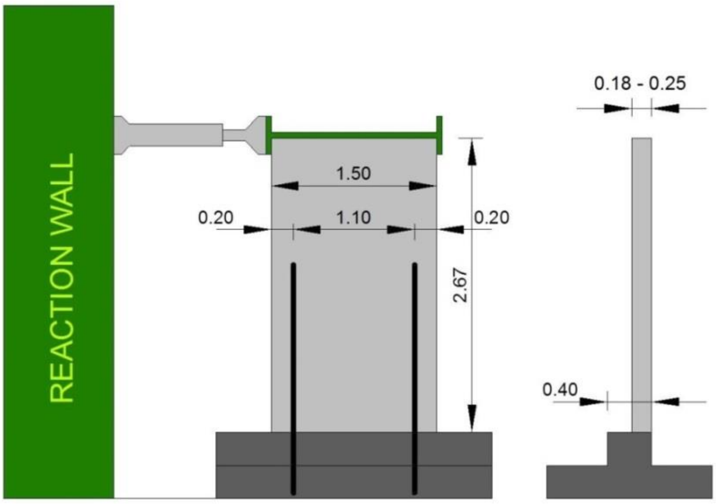

Figure 8.11. Experimental setup.

(a)

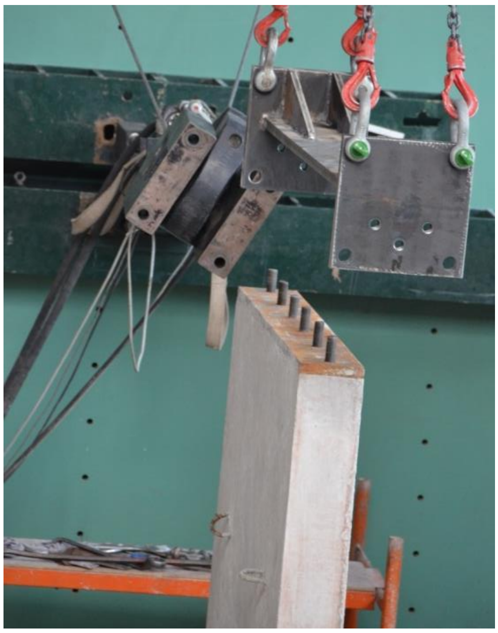

(b)

Figure 8.12. (a) Photo of the experimental configuration; (b) Mechanism for the connection of the hydraulic jack with the panel.

8.4.2 Loading

For all types of connections examined, monotonic and cyclic tests were performed. In both cases, the loading was applied up to the point that failure of the connections occurred.

In monotonic loading, reverse loading was applied after failure of the connection in tension. However, it was not always possible to break the second connection, too, because full contact with the beam in the compression zone could not be re-established, due to the permanent plastic deformation of the broken rebar. This issue is further discussed later, during the presentation of the experimental results.

For cyclic loading, the protocol applied is based on FEMA 461 report: "*Interim Testing Protocols for Determining the Seismic Performance Characteristics of Structural and Nonstructural Components*" (2007), which was prepared with the collaboration of the Applied Technology Council (ATC), the Mid-America Earthquake (MAE) Center, the Multidisciplinary Center for Earthquake Engineering Research (MCEER) and the Pacific Earthquake Engineering Research (PEER) Center. According to the applied protocol, the loading history consists of repeated cycles of step-wise increasing deformation amplitudes. The number of steps with different amplitudes is equal to ten, with two cycles included in each step. A conceptual diagram of the loading history is presented in Fig. 8.13.

The amplitude a_{i+1} of the step i+1 (not of each cycle, since each step has two cycles) is given by the following equation:

$$a_{i+1} = 1.4 \cdot a_i \qquad (8.1)$$

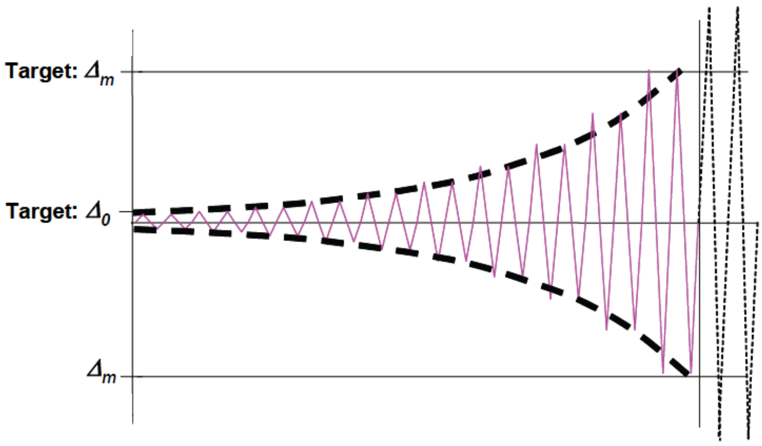

Figure 8.13. Sketch of loading history applied in cyclic tests.

The loading history parameters were defined using the following procedure:

- Final Target Value (Δ_m)
  It is the targeted maximum deformation amplitude of the loading history that corresponds to the imposed deformation at which the most severe damage level is expected to initiate. This value was determined from the displacement that corresponded to connection failure during the monotonic test. In case that failure had not occurred at this displacement level during the cyclic test, the loading history was continued by using further increments of amplitude of $0.3 \cdot \Delta_m$.

- Initial Target Value (Δ_0)
  It is the targeted smallest deformation amplitude of the loading history. It must be safely smaller than the amplitude at which the lowest damage state is first observed. In the tests performed, Δ_0 was determined assuming that the last planned amplitude Δ_m is reached after 10 steps, which leads to the relation:

$$\Delta_o = \Delta_m / 1.4^9 \qquad (8.2)$$

8.4.3 Instrumentation

The displacements at critical positions and the deformation of the connecting mechanism and the concrete at the joint faces were measured during the experiments. Specifically, horizontal and vertical displacements were measured at 10 points using displacement transducers (Fig. 8.14(a)), while 16 strain gauges were used to measure the deformation of the connection rebars and concrete (Fig. 8.14(b) and 8.15). In most cases, displacements and strains were measured at both sides of the panel.

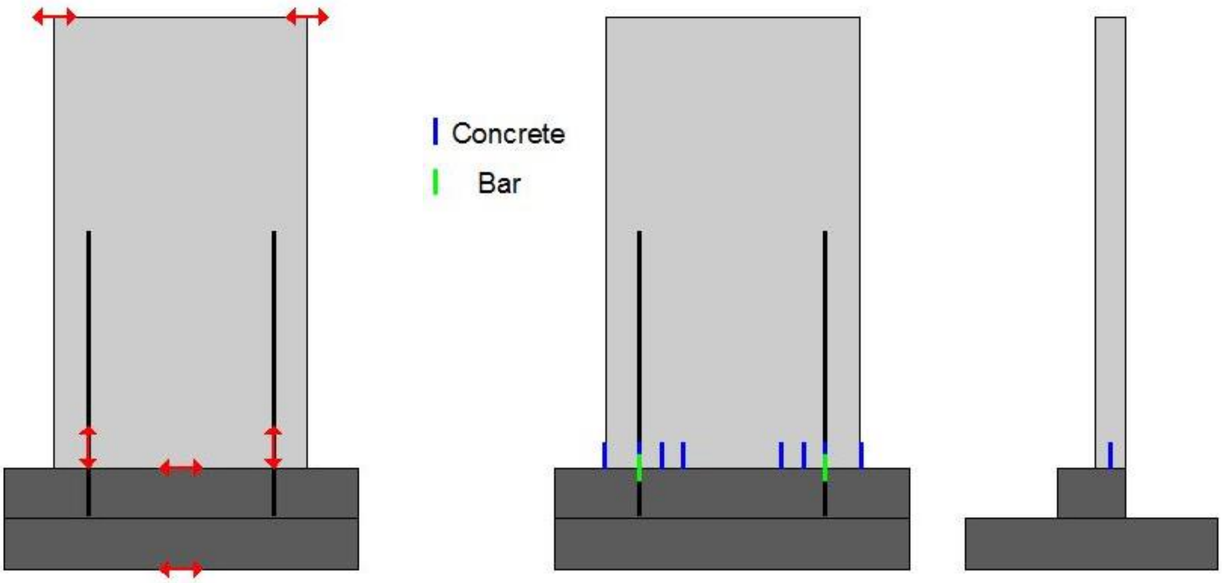

(a) (b)

Figure 8.14. Instrumentation setup: (a) Displacement transducers; (b) strain gauges.

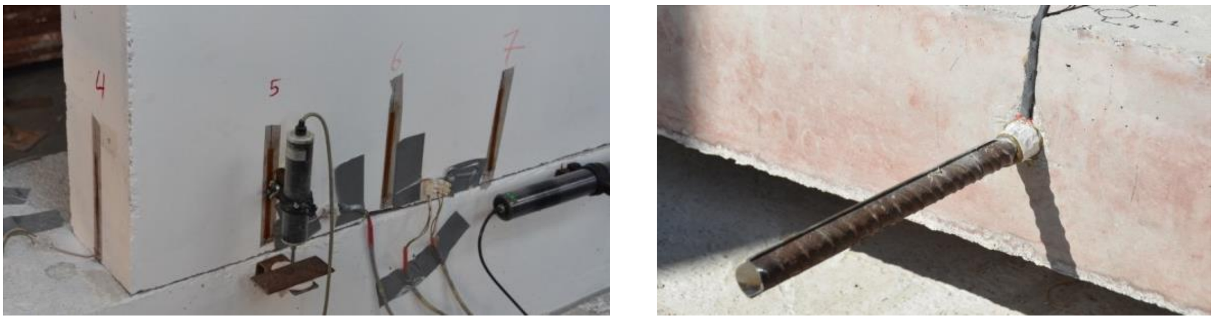

(a) (b)

Figure 8.15. (a) Strain gauges to measure the compression of the concrete and displacement transducers to measure the uplift of the panel; (b) strain gauges to measure the elongation of the rebar around the joint.

8.4.4 Experimental programme

The experimental programme of the tests is tabulated in Table 8.1. For each type of connection, both monotonic and cyclic tests are performed. The test programme includes experiments for all three types of connections ("rebar", "steel plate" and "industrial") and various strengths. The five first tests have been conducted by the completion of this thesis and the rest are planned for the near future. Tests #10 and #11 will be on industrial connections or steel plate connections depending on the results of experiments #6 to #9.

Table 8.1. Experimental Program.

No.	Test	Connection			Nominal strength* (kN)	Loading	Comments
		Type	Rebars/Bolts	Connecting material			
1	A1D20M-R1	Rebars	1∅20	Epoxy resin - 1	137	Monotonic	Completed
2	A1D20C-R1	Rebars	1∅20	Epoxy resin - 1	137	Cyclic	Completed
3	A1D25M-R2	Rebars	1∅25	Epoxy resin - 2	213	Monotonic	Completed
4	A1D25M-G	Rebars	1∅25	Grout	213	Monotonic	Completed
5	A1D25C-G	Rebars	1∅25	Grout	213	Cyclic	Completed
6	A-Ind1M	Industrial	wall shoe	-	400	Monotonic	Pending
7	A-Ind1C	Industrial	wall shoe	-	400	Cyclic	Pending
8	S2M20M	Steel plate	2M20	Steel plate	241	Monotonic	Pending
9	S2M20C	Steel plate	2M20	Steel plate	241	Cyclic	Pending
10		Industrial or steel plate (to be decided)				Monotonic	Pending
11		Industrial or steel plate (to be decided)				Cyclic	Pending

* For "rebar connections", the nominal strength corresponds to the axial resistance of B500C rebars for $\gamma_s = 1.15$.
For "steel plate connections", the nominal strength corresponds to the shear resistance of bolts of class 8.8.

9 Experimental Results

In this section, the results of the experiments that have been performed are presented. Details of the experimental results can be found in the card files that are given in Appendix A.

9.1 Test A1D20M-R1

This test concerned the behaviour of "rebar connections" made with 1∅20 rebar under monotonic loading. The rebars were protruding, about 0.30 m, from the panel into the beam and the bond with the concrete was achieved using epoxy resins.

The horizontal force versus top displacement diagram is shown in Fig. 9.1 with a red line. In the same diagram (for comparison reasons) they are also shown: the strains of the rebar under tension (green line) and the strain of the concrete under compression, around the rebar (blue line).

It is interesting to note that the compressive strains of the concrete around the rebar under compression increase initially, as expected. However, for $d_{top} \approx 20$ mm they start decreasing due to the opening of the joint and the reduction of the length of the compression zone. For $d_{top} \approx 40$ mm the strain become zero and, for larger displacements, the second connection starts been also under tension. This can be better viewed in Fig. 9.2 in which the opening of the joint at the two connections is shown.

In Fig. 9.3, the horizontal displacement at the base of the panel is plotted versus the top displacement. It is seen that there an obvious slip of the panel with respect to the beam, which increases almost linearly with the top displacement up to $d_{top} \approx 25$ mm. For larger displacements, however, this slip stops, probably due to the increased friction on the compression side caused by the reduction of the length of the compression zone.

Concerning the observed damage, only minor cracks at the front face of the panel on the compression side (Fig. 9.4(a)) were observed after the end of the test (breaking of the rebar at the connection on the tension side – Fig. 9.4(b)). On the tension side, no damage was observed.

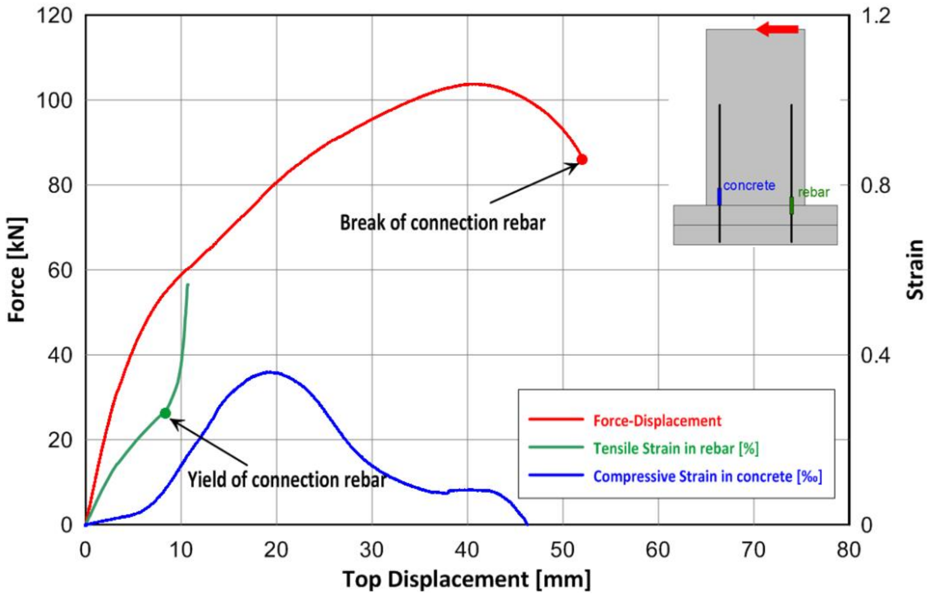

Figure 9.1. Test A1D20M-R1: Horizontal force and strains of rebar and concrete versus top displacement under monotonic loading.

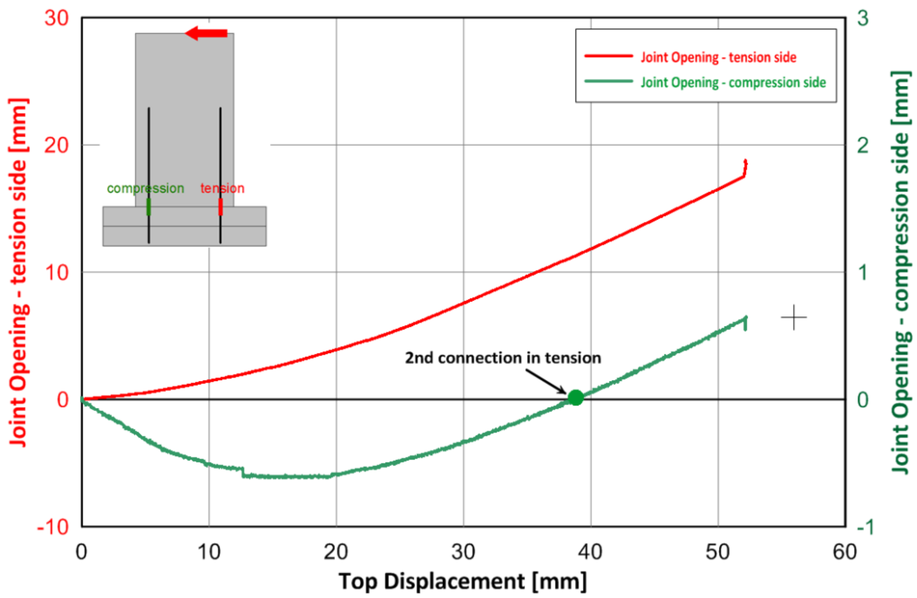

Figure 9.2. Test A1D20M-R1: Joint opening at the place of the connections versus top displacement.

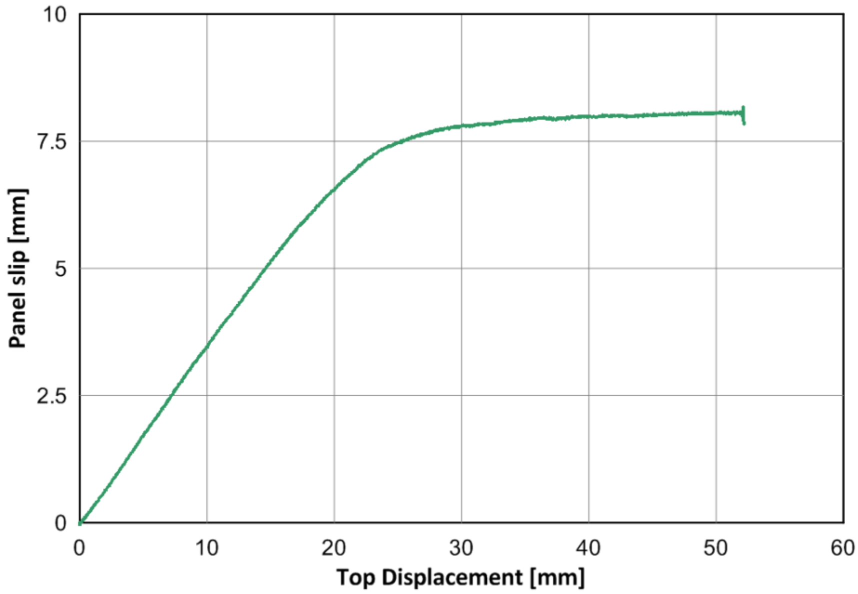

Figure 9.3. Test A1D20M-R1: Base horizontal slip of the panel versus top displacement.

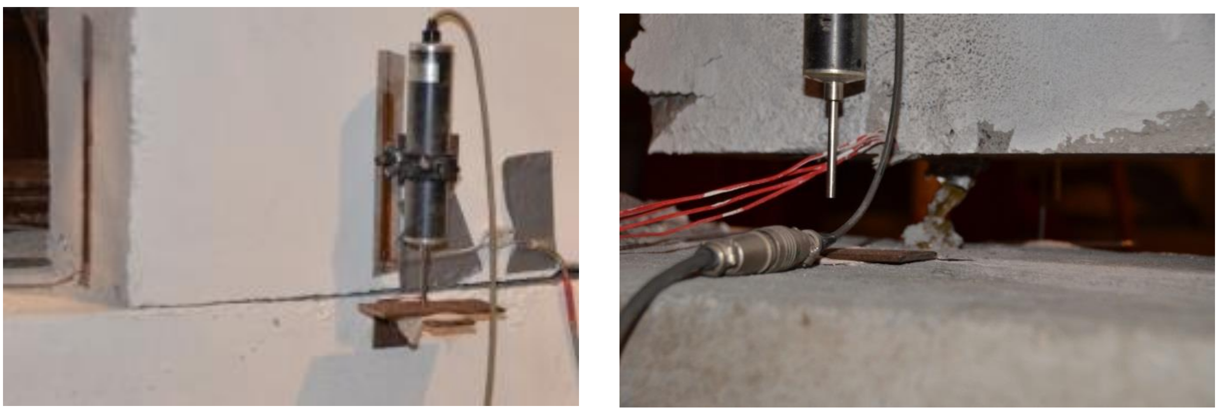

(a) (b)

Figure 9.4. Test A1D20M-R1: Damage observed at the end of the monotonic loading: (a) minor cracks at the panel's front face on the compression side; (b) broken rebar of the connection on the tension side.

After the completion of the test, the loading direction was reversed and the test was repeated with the undamaged connection, which was previously in compression, being now in tension. In this case, the connection rebar slipped due to insufficient bonding (Fig. 9.5(b)). It is interesting to note that significant damage occurred to the panel on the tension side, due to the large tensile stresses that developed around the rebar (Fig. 9.5). Since similar damage was not observed during the first test, it should be attributed to the cracking that must had happened to the concrete due to the compression of this part of the panel during the first test.

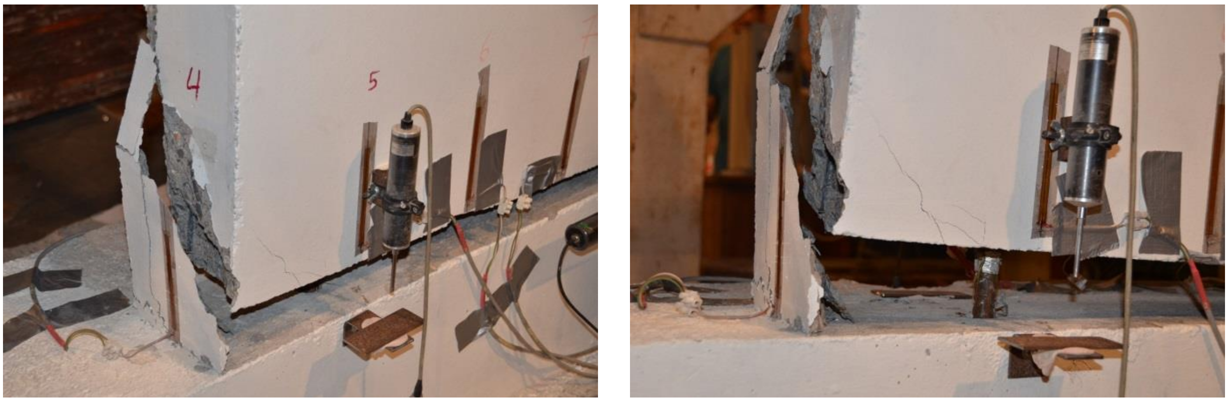

(a) (b)

Figure 9.5. Test A1D20M-R1: Damage observed at the end of the reversed monotonic loading: (a) severe damage at the panel's front face on the tension side; (b) slip of the rebar of the connection due to insufficient bonding.

9.2 Test A1D20C-R1

This test concerned the behaviour of "rebar connections" made with 1∅20 rebar under cyclic loading. As in the corresponding monotonic test, the rebars were protruding, about 0.30 m, from the panel into the beam and the bond with the concrete was achieved using epoxy resins.

The horizontal force versus the top displacement is shown in Fig. 9.6. In the same diagram, the response for monotonic loading (test A1D20M-R1) is also shown for comparison. It is seen that, although the envelope of the cyclic response follows, in general, the monotonic one, it shows larger elastic stiffness.

The cyclic response is non-symmetric due to bond failure that happened to the rebar of one of the connections (the one that is under tension for negative displacements, see Fig. 9.6). Due to the slippage of the rebar, which started at about d_{top} = –7 mm, the response was characterized by:

(a) A softening behaviour for negative displacements (bottom left quarter of diagram in Fig. 9.6) due to the slippage of the rebar of the connection under tension;
(b) A sudden loss of strength for positive displacements (top right quarter of diagram in Fig. 9.6) due to the slippage of the rebar, which was now under compression, to its initial position (the corresponding closure of the joint is evident in Fig. 9.8(a)). However, when all the slippage that had occurred during the reverse motion was absorbed, the strength was regained and the force started increasing again.

Apart of the afore-mentioned bond failure of one of the connections, the cyclic response is characterized by significant pinching, which is attributed to the elongation of the rebars of the connections during their plastic deformation. This is shown in Fig. 9.7, in which the axial strain of the rebars of the two connections is plotted versus the top displacement. As a result, there was an increasing permanent opening of the joint between panel and beam, as shown in Fig. 9.8. Thus, for small top displacements (almost vertical panel) there was not any friction to resist the horizontal force, which was undertaken solely by the dowel action of the rebars. For large top displacements, contact between panel and beam was re-established due to the rotation of the panel and the resistance started increasing again.

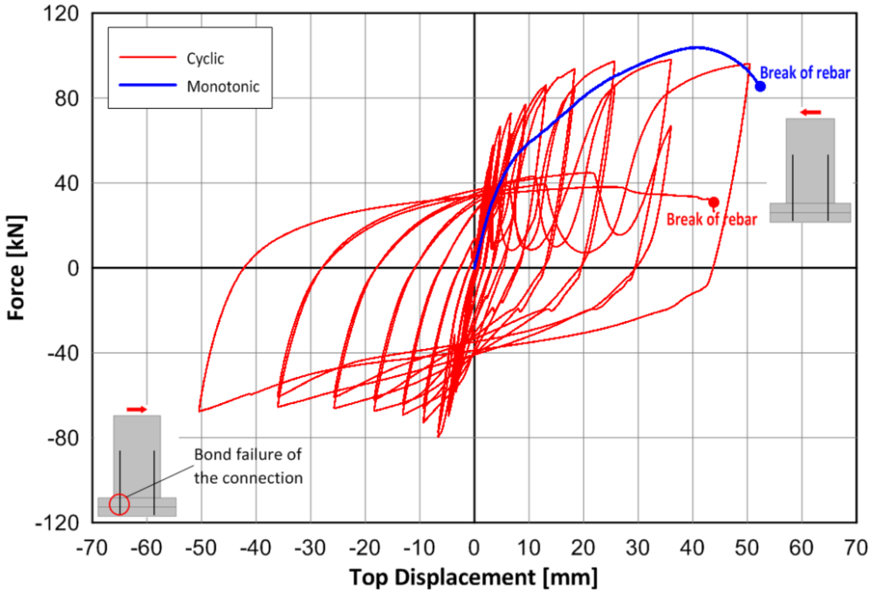

Figure 9.6. Test A1D20C-R1: Horizontal force versus top displacement under cyclic and monotonic loading.

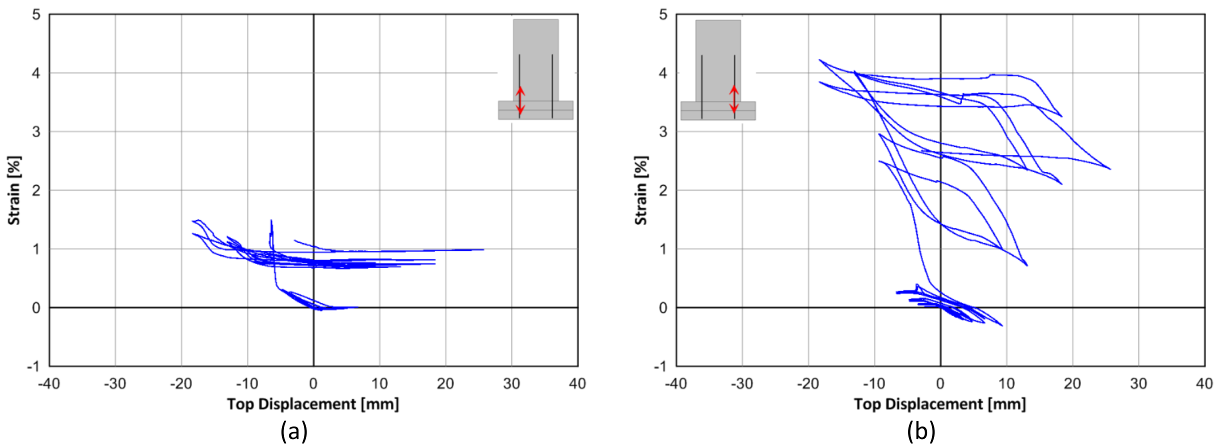

Figure 9.7. Test A1D20C-R1: Strain in the rebars of the connections versus top displacement under cyclic loading: (a) left connection; (b) right connection. The strains in the left rebar are small due to bond failure.

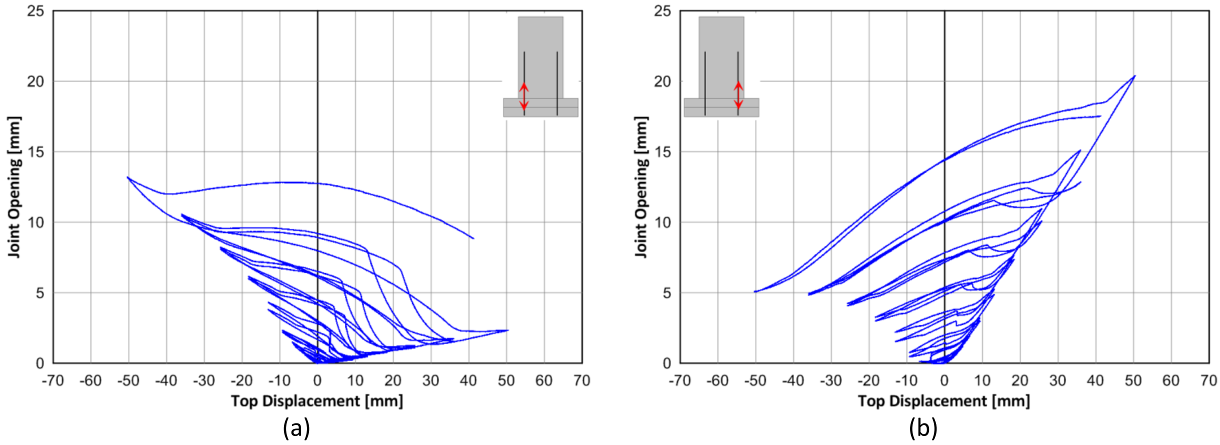

Figure 9.8. Test A1D20C-R1: Joint opening at the place of the connections versus top displacement: (a) left connection; (b) right connection. Positive displacements correspond to motion of the panel to the left. The permanent opening of the joint after few cycles is evident.

The loss of contact between panel and beam after the few first cycles caused significant horizontal displacements at the bottom of the panel relative to the beam (panel slip). This is shown in Fig. 9.9.

At the end of the cyclic test, spalling of concrete was observed at the front of the left side of the panel only (Fig. 9.10(a)). On the other edge of the panel no obvious was observed (Fig. 9.10(b)). No damage was observed in the beam.

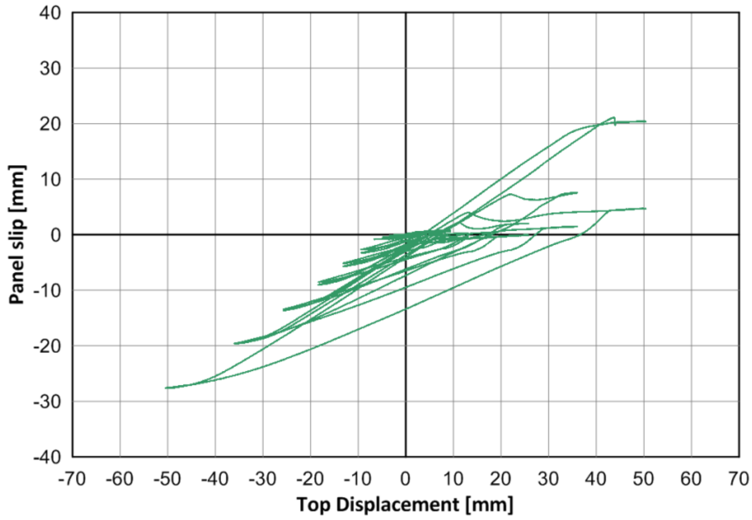

Figure 9.9. Test A1D20C-R1: Base horizontal slip of the panel versus top displacement.

(a) (b)

Figure 9.10. Test A1D20C-R1: Damage observed at the end of the test: (a) spalling of the concrete on the left side; (b) no evident damage on the right connection.

9.3 Test A1D25M-R2

This test concerned the behaviour of “rebar connections” made with 1∅25 rebar under monotonic loading. The rebars were protruding, about 0.30 m, from the panel into the beam and the bond with the concrete was achieved using epoxy resins. Due to the problems with insufficient bonding observed in the afore-mentioned tests of connections with 1∅20 rebar, a different type of resin was used in this test.

Despite the change of the type of resin, bond failure occurred to the rebar of the connection under tension for $d_{top} \approx 10$ mm and $F = 80$ kN, as obvious from the loss of resistance at this point shown in Fig. 9.11(a) and the strain diagram of the rebar shown in Fig. 9.11(b) (red line). The test was stopped at $d_{top} \approx 22$ mm.

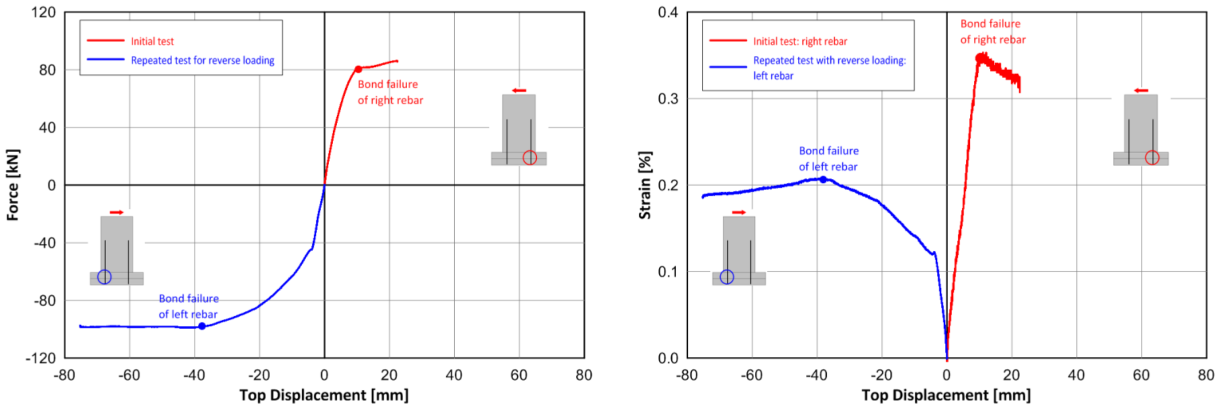

(a) (b)

Figure 9.11. Test A1D25M-R2: (a) Horizontal force and (b) strains of rebars versus top displacement under monotonic loading.

After that, the loading direction was reversed and the test was repeated but bond failure occurred to the rebar of the second connection as well. As shown in Figs 9.11(a) and 9.11(b) (blue line), the slippage of the rebar started at $d_{top} \approx 40$ mm.

Due to the slippage that occurred to the rebars of the connections, significant opening of the joint was observed at the end of the test (Fig. 9.12).

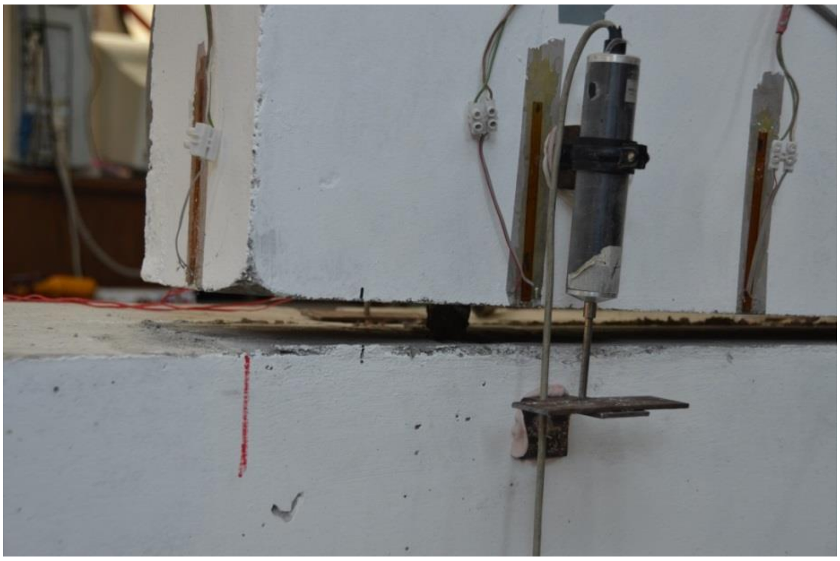

Figure 9.12. Slippage of the rebars observed at the end of test A1D25M-R2.

9.4 Test A1D25M-G

This test also concerned the behaviour of “rebar connections” made with 1∅25 rebar under monotonic loading. However, since the bonding offered by epoxy resins was proven insufficient from the previous tests, it was decided to use high strength, non-shrinking grout instead of resins. As the required anchorage length was much larger in this case, the rebars were protruding now from the beam into the panel, about 1.30 m. In order to pour the grout into the ducts, holes were drilled along the rebars (Fig. 9.13).

Figure 9.13. Filling the ducts with grout for test A1D25M-G.

The horizontal force versus top displacement diagram is shown in Fig. 9.14 with a red line. In the same diagram the corresponding plot of test A1D25M-R2, in which the bond was achieved with epoxy resins, is shown for comparison. It is seen that the two curves are similar up to the point that bond failure occurred during the test A1D25M-R2.

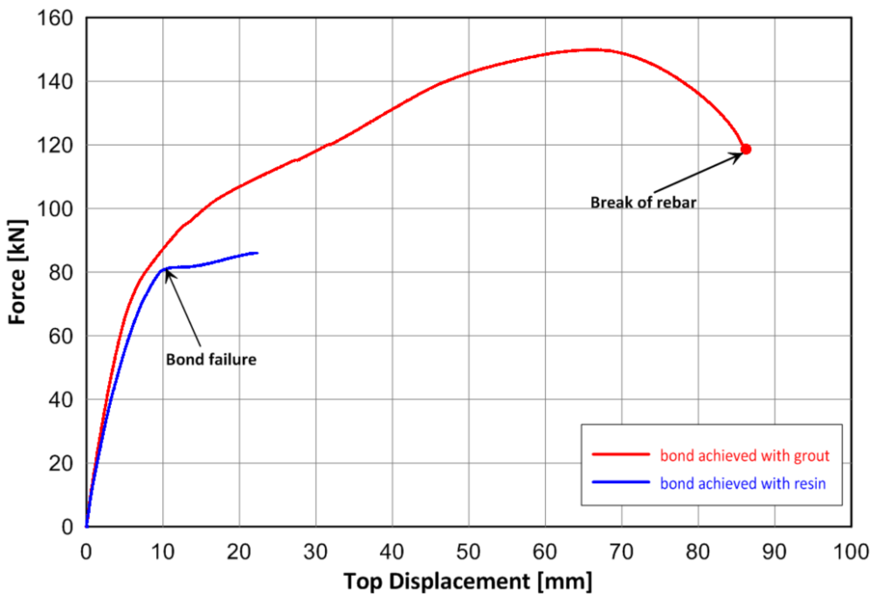

Figure 9.14. Test A1D25M-G: Horizontal force versus top displacement (red line) and comparison with the corresponding curve of test A1D25M-R2 (blue line).

After the completion of the test, the loading direction was reversed and the test was repeated with the undamaged connection, which was previously in compression, being now in tension. The comparison of the response with the one of the initial test is shown in Fig. 9.15. It is noted that, although the maximum attained force was almost the same in both directions of loading, the displacements were much larger during the repeated test. This happened because the broken rebar in the compression zone was preventing the full contact of the panel with the beam, reducing thus the friction. At $d_{top} \approx 110$ mm, however, the contact at the joint was re-established due to the significant rotation of the panel and the stiffness increased again.

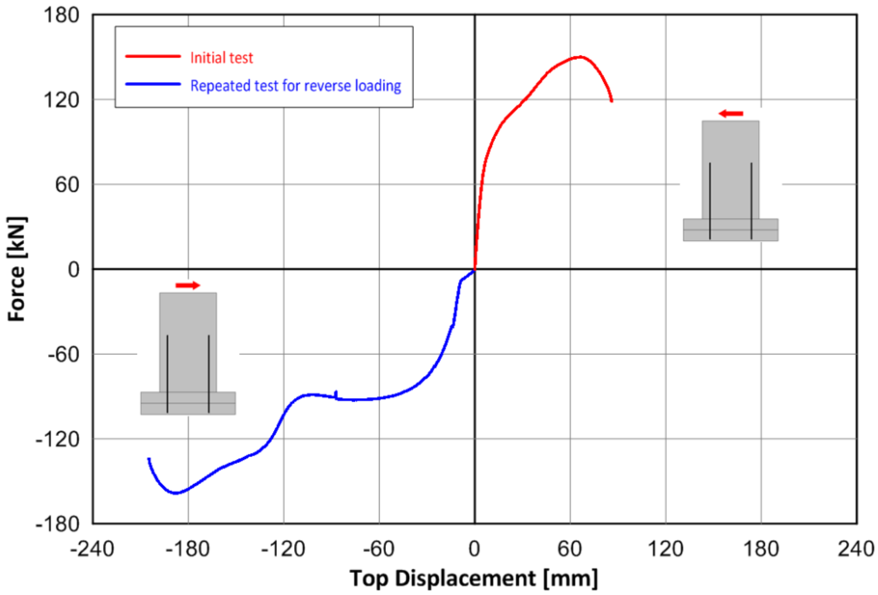

Figure 9.15. Test A1D25M-G: Comparison of the response of the initial test with the one for reverse loading.

In Fig. 9.16, the comparison of the response with the one of test A1D20M-R1, in which the connections were made with 1∅20 rebar, is shown. It is seen that the maximum force attained with rebars ∅25 was almost 50% larger than the one for rebars ∅20, which is close to the increase in the cross section of the rebars of the connections. It seems, therefore, that the role of the cross section of the rebars on the resistance of the connections is essential.

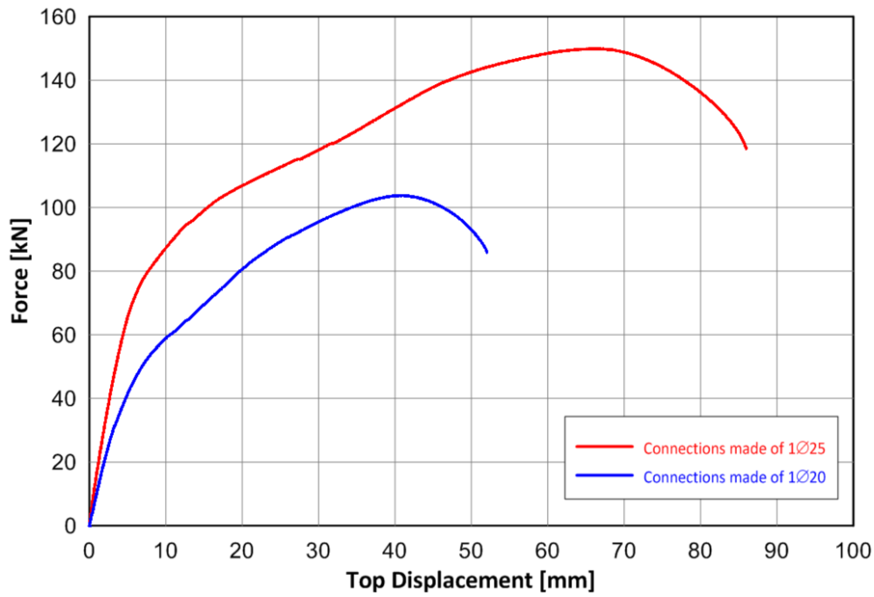

Figure 9.16. Test A1D25M-G: Horizontal force versus top displacement (red line) and comparison with the corresponding curve of test A1D20M-R1 (blue line).

The opening of the joint and the horizontal motion of the bottom of the panel (slip) are shown in Fig 9.17. Notice that the rebar of the connection was elongated 30 mm when it broke. Concerning the slippage, it is seen that it increases almost linearly with the top displacement up to $d_{top} \approx 25$ mm. For larger displacements, however, the slip rate decreases, probably due to the increased friction on the compression side caused by the reduction of the length of the compression zone. A similar behaviour was observed during test A1D20M-R1.

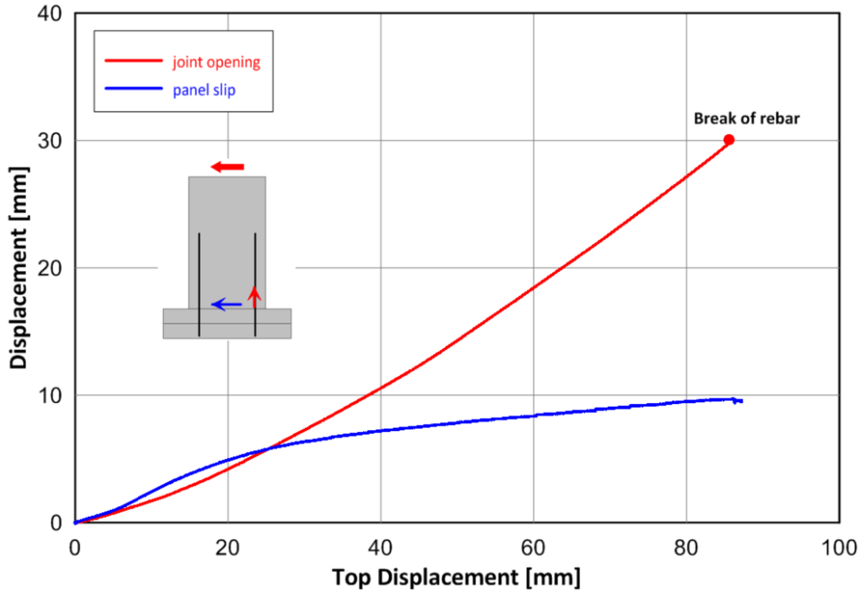

Figure 9.17. Test A1D25M-G: Joint opening at the connection (red line) and slip of the panel (blue line).

Concerning the damage, some spalling of the concrete of the panel and the beam was observed on the compression side after the end of the initial monotonic test (Fig. 9.18). On the tension side, severe damage was observed to the beam around the rebar (Fig. 9.19(a)), but no damage was observed in the panel (Fig. 9.19(b)).

(a) (b)

Figure 9.18. Test A1D25M-G: Spalling of the concrete of the panel and the beam on the compression side at the end of the initial monotonic loading.

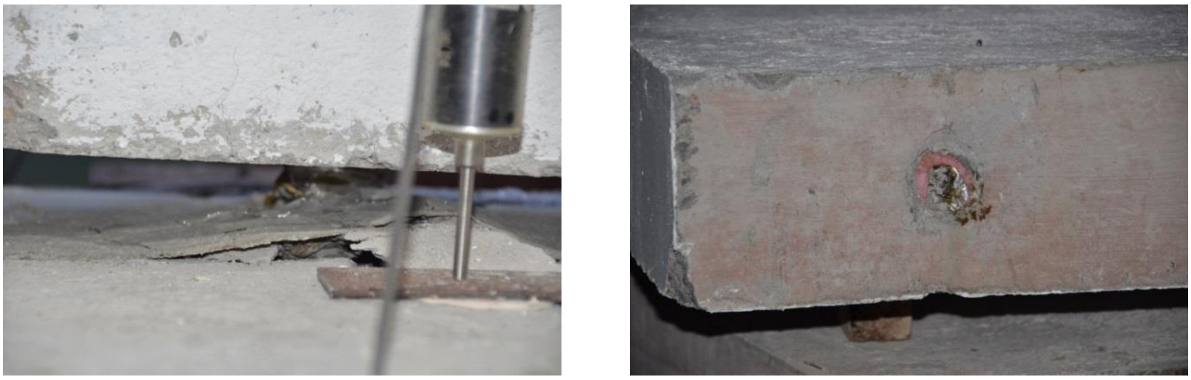

(a) (b)

Figure 9.19. Test A1D25M-G: Damage observed on the tension side at the end of the initial monotonic loading: (a) severe damage to the beam around the rebar; (b) broken rebar but no visible damage to the panel.

As mentioned above, after the completion of the test, the loading direction was reversed and the test was repeated with the undamaged connection being now in tension. In this case, severe damage occurred to the panel and the beam on the tension side, due to the large tensile stresses that developed around the rebar (Fig. 9.20). The damage was much larger than the one observed during the initial test, which is attributed to the fact that the concrete had already cracked (due to compression) during the first test.

(a) (b) (c)

Figure 9.20. Test A1D25M-G: Damage observed at the end of the reversed monotonic loading: (a) & (b) severe damage to the panel on the tension side; (c) severe damage to the beam on the tension side.

9.5 Test A1D25C-G

This test concerned the behaviour of "rebar connections" made with 1∅25 rebar under cyclic loading. As in the corresponding monotonic test, the rebars were protruding, about 1.30 m, from the panel into the beam and the bond with the concrete was achieved using non-shrinking, high-strength grout.

The horizontal force versus the top displacement is shown in Fig. 9.21. In the same diagram, the response for monotonic loading (test A1D25M-G) is also shown for comparison. As in the case of connections with 1∅20 rebar, it is seen that, although the envelope of the cyclic response follows, in general, the monotonic one, it shows larger elastic stiffness. However, the rebar broke in significantly smaller displacement than for monotonic loading.

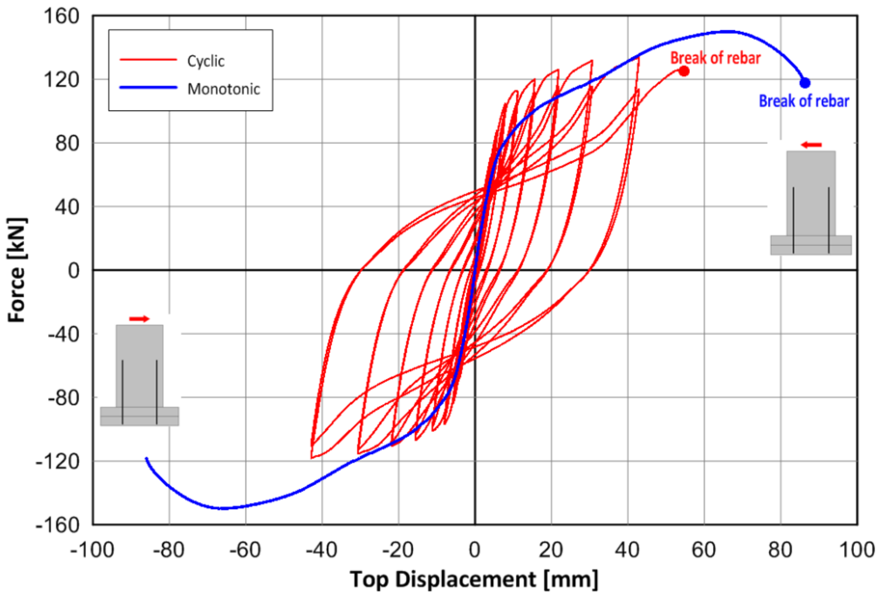

Figure 9.21. Test A1D25C-G: Horizontal force versus top displacement under cyclic and monotonic loading.

Again, the cyclic response shows significant pinching for large displacements, which is attributed to the opening of the joint caused by the plastic elongation of the rebars. As previously explained, the opening of the joints resulted in loss of friction and the consecutive loss of stiffness, which caused the pinching. As the displacement was increasing, however, contact of the panel with the beam was re-established at the panel edge due to its rotation, and the stiffness started increasing again. The opening of the joint with the applied cycles is shown in Fig. 9.22.

The loss of contact between panel and beam after the few first cycles caused significant horizontal displacements at the bottom of the panel relative to the beam (panel slip). This is shown in Fig. 9.23.

Finally, in Fig. 9.24 the comparison of the cyclic response of connections with 1∅25 rebars with the one of connections with 1∅20 rebars is presented. It is interesting to note that the rebar broke at about the same displacement in both tests. This happened because the critical parameter was the strain developed in the rebar, which is independent of its diameter.

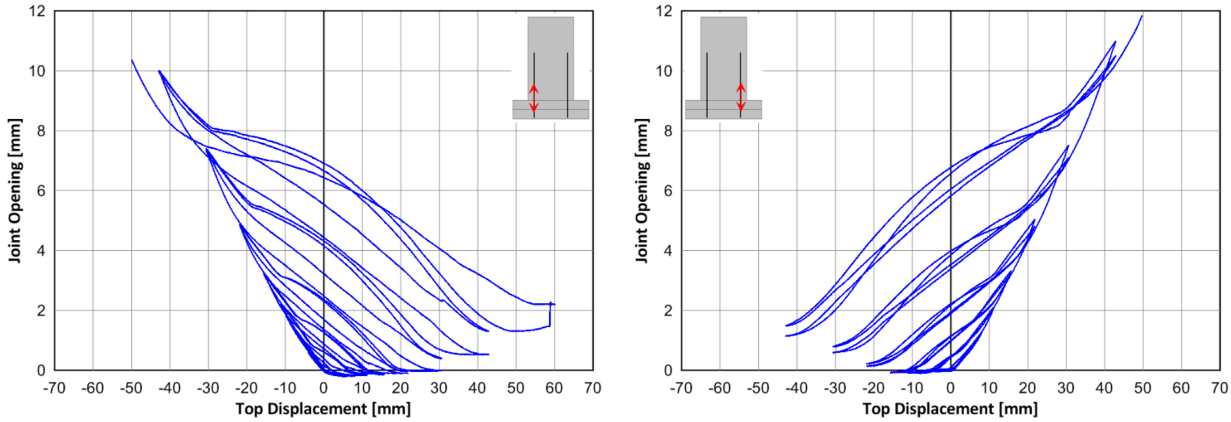

(a) (b)

Figure 9.22. Test A1D25C-G: Joint opening at the place of the connections versus top displacement (a) left connection; (b) right connection. Positive displacements correspond to motion of the panel to the left.

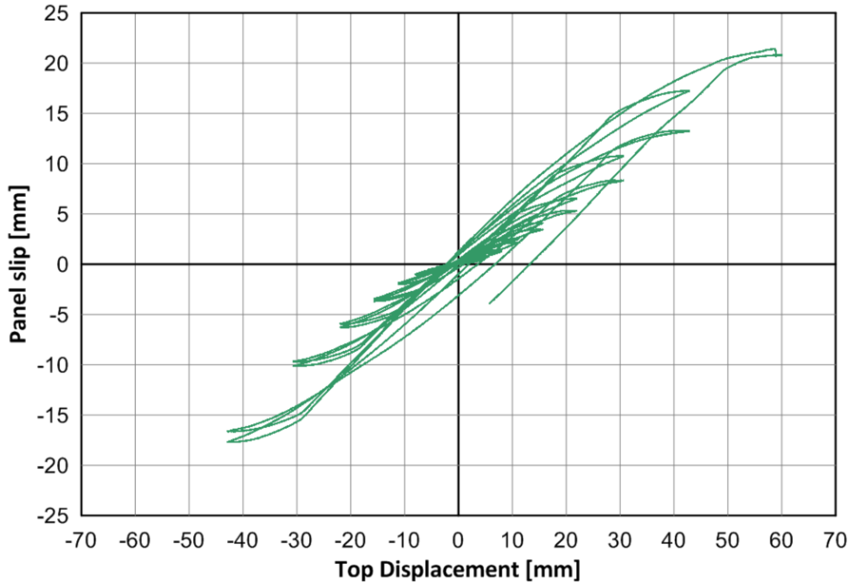

Figure 9.23. Test A1D25C-G: Base horizontal slip of the panel versus top displacement.

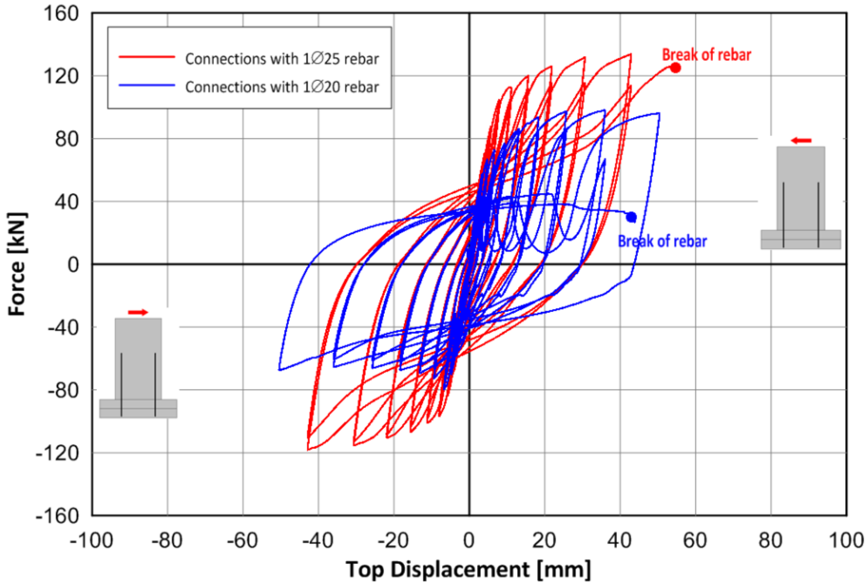

Figure 9.24. Comparison of the cyclic response of connections with 1∅25 and 1∅20 rebars.

At the end of the test, spalling of the concrete was observed at one side of the panel around the rebars in the area of the joint (Fig. 9.25(a)), evidently due to the tensile stresses developed. Significant spalling of the concrete was also observed in the beam (Fig. 9.25(b)).

(a) (b)

Figure 9.25. Test A1D25C-G: Damage observed at the end of the test: (a) spalling of the concrete around the rebars in the area of the joint; (b) spalling of the concrete in the beam.

10 Conclusions

Although the experimental programme experiments for all three types of connections ("rebar", "steel plate" and "industrial"), by the completion of this thesis almost one half of the planned static (monotonic and cyclic) tests have been performed. These tests concerned "rebar connections" and interesting results were obtained, which can be summarized as follows:

- The use of epoxy resins as the bonding material of the connections proved to be insufficient, even for relatively small forces.

- An inherent problem of the "rebar connections" was recognized for large deformations. Specifically, large horizontal displacements cause significant rotations of the panel and consecutive opening of the joint and, as a result, the rebars located on the tension zone suffer large plastic axial strains which lead to their permanent elongation and the permanent opening of the joint. For this reason, full contact of the panel with the beam cannot be re-established during the reverse loading and the friction force at the joint cannot be fully developed. Due to this phenomenon, the horizontal force induced to the panel is sustained mainly by the "dowel action" of the rebars instead of the friction at the joint.

- The envelope of the cyclic response follows, in general, the monotonic response. However, it shows larger elastic stiffness.

- The attained ductility of the connections under cyclic loading was around five. However, because of the afore-mentioned opening of the joint, it might be problematic to design the connections for ductile response. Therefore, it is suggested to design the connections to behave elastically under the design earthquake, as is the common practice for connections in precast structures.

- The maximum force that can be attained is proportional to the cross section of the rebars of the connections.

- The ultimate displacement that corresponds to breaking of the rebars is independent of their cross section and is mainly determined by the strains induced to the rebars.

- In monotonic tests and during the reverse loading, significant damage was observed around the connection on the tension zone, which is attributed to the cracking of the concrete that had occurred during the initial test caused by the high compression stresses. Such damage was not observed on the tension zone during the initial monotonic test.

Appendix A: Card files

A.1 Connections with 1∅20 rebar

A.1.1 General description

“Rebar connections” made with 1∅20 rebar under monotonic and cyclic loading.

The rebars were protruding about 0.30 m from the panel into the beam and the bond with the concrete was achieved using epoxy resin of type 1 (for material properties see Appendix B).

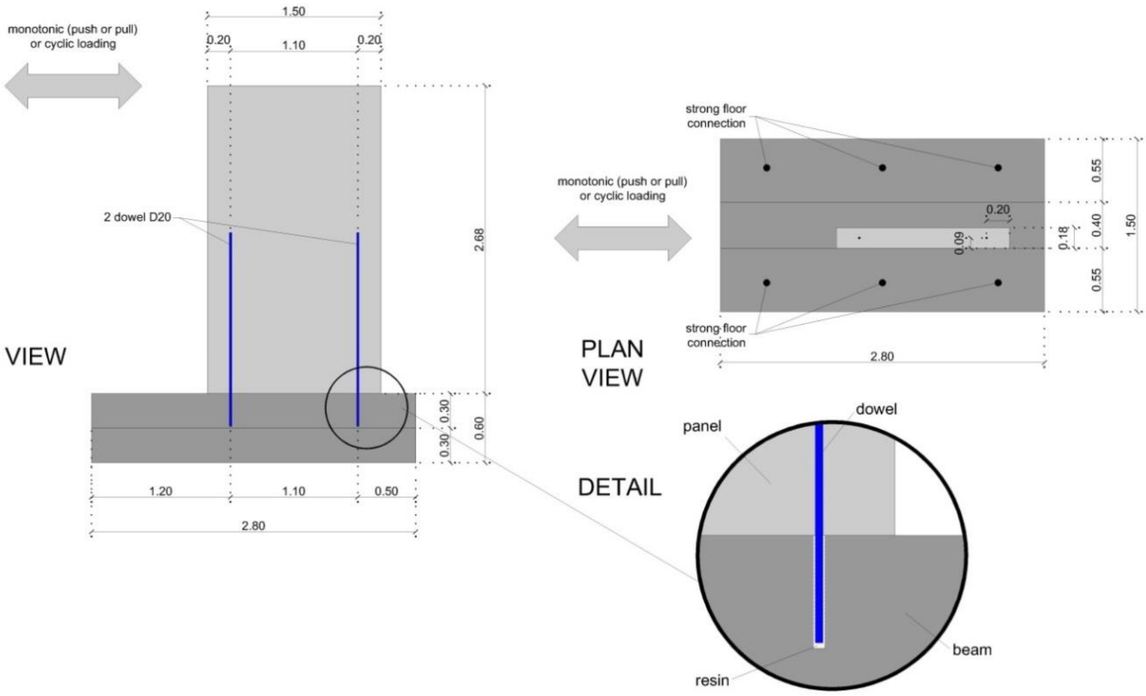

Figure A.1. Sketch of the experimental configuration of specimens 1D20M-R1 and 1D20C-R1.

A.1.2 Main characteristics of the connection

Number and diameter of the rebars	1 ∅20
Panel thickness	18 cm
Distance from panel’s edges to dowel	20 cm

Materials	Concrete class	C30 (1)
	Steel class	B500C
	Bond material (duct infill)	epoxy resin type 1 (2)

(1) The measured strength of the concrete is given in Appendix B.
(2) The properties of the resin are given in Appendix B.

A.1.3 Reinforcement details of the panel and the beam

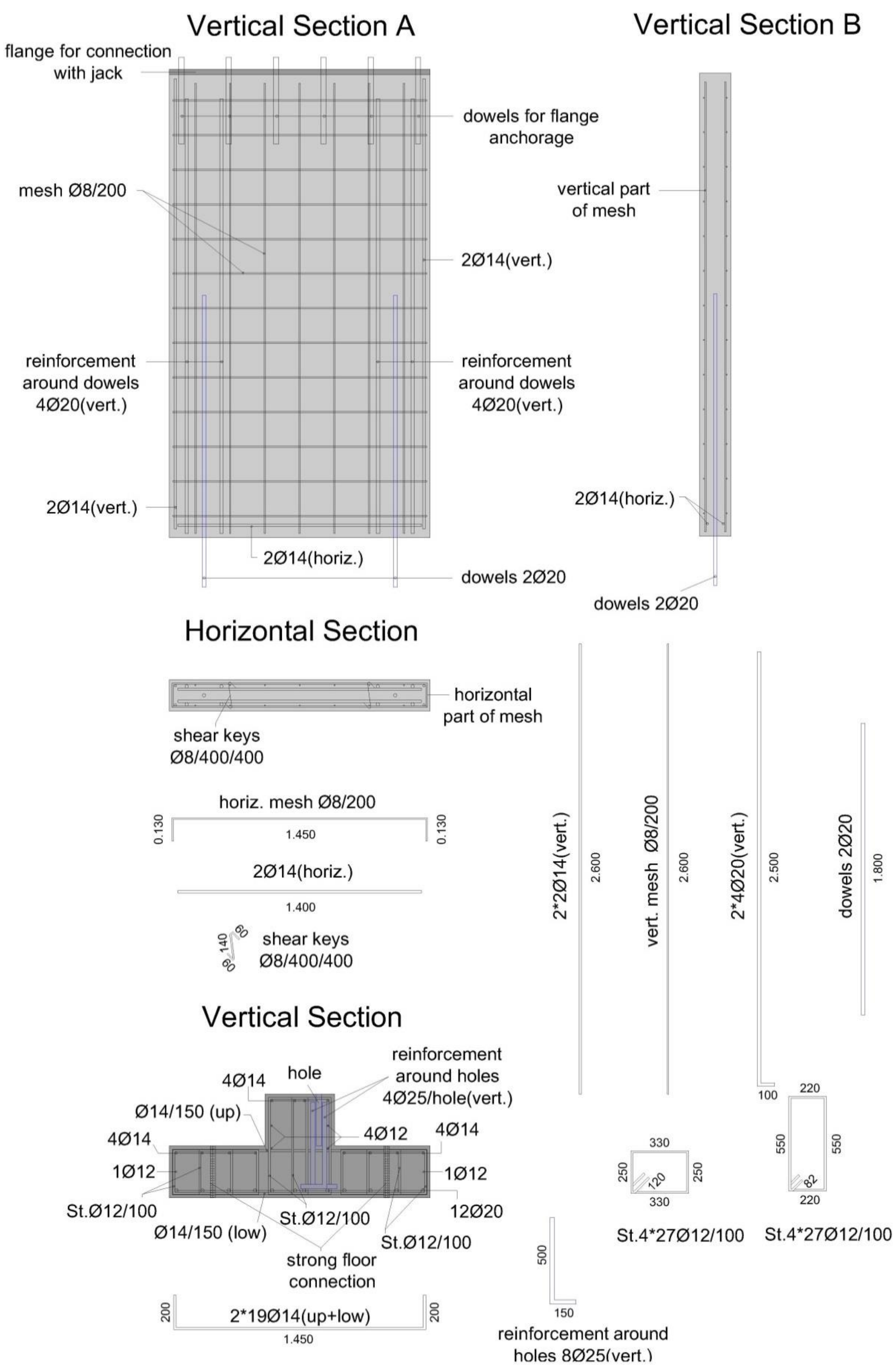

Figure A.2. Reinforcement details of specimens 1D20M-R1 and 1D20C-R1.

A.1.4 Test A1D20M-R1 – Monotonic loading

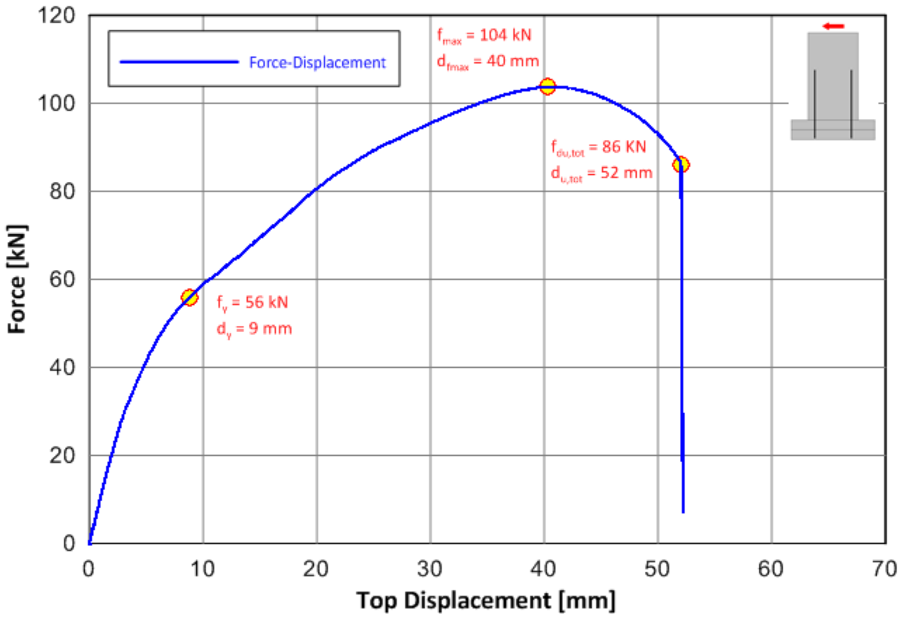

Figure A.3. Test A1D20M-R1: Horzontal force versus top displacement.

Table A.1. Test A1D20M-R1: Response data.

Monotonic loading	
"Yield" strength(1)	56 kN
Maximum strength	104 kN
"Yield" displacement(1) (d_y)	9 mm
Displacement at maximum strength (d_{fmax})	40 mm
Ultimate displacement ($d_{u,20\%}$; 20% reduction of strength)	Not acquired
Ultimate displacement ($d_{u,tot}$; total failure of the connection	52 mm
Ductility	4.4 (calculated as d_{fmax}/d_y)

(1) "Yield" point corresponds to the significant change in stiffness in the curve and doesn't necessarily refer to the yielding of the rebar (it may also be associated with the crushing of the concrete).

Main characteristics of the behaviour

During the initial monotonic loading:
- The rebar under tension broke
- Minor cracks were developed on the compression side

During the reversed monotonic loading:
- The bar under tension slipped due to bond failure
- Severe spalling of the concrete on the tension side occurred

Observed damage

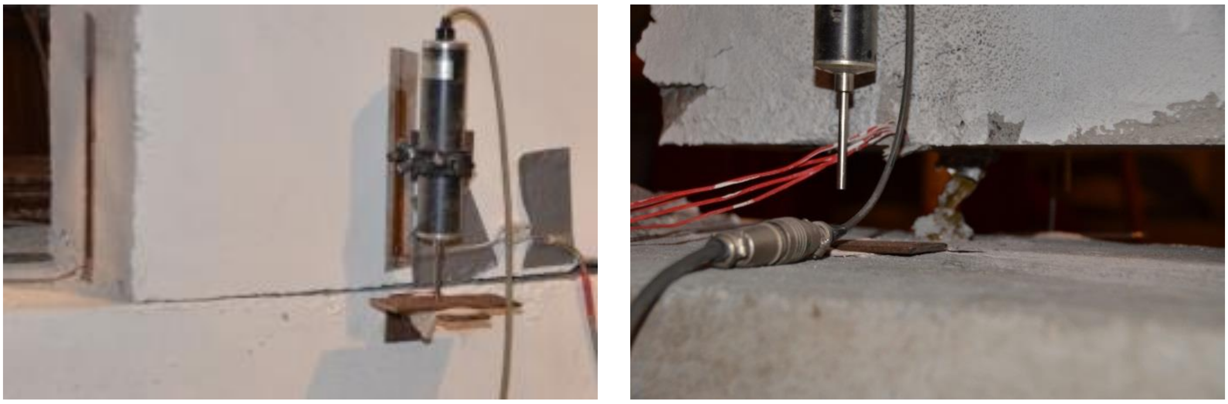

(a) (b)

Figure A.4. Test A1D20M-R1: Damage observed at the end of the initial monotonic loading: (a) minor cracks at the panel's front face on the compression side; (b) broken rebar of the connection on the tension side.

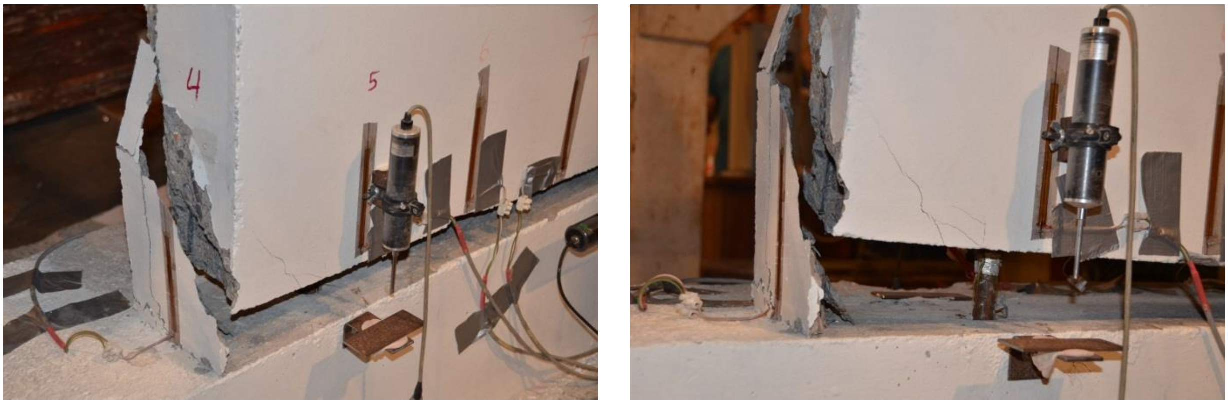

(a) (b)

Figure A.5. Test A1D20M-R1: Damage observed at the end of the reversed monotonic loading: (a) severe damage at the panel's front face on the tension side; (b) slip of the rebar of the connection due to insufficient bonding.

A.1.5 Test A1D20C-R1 – Cyclic loading

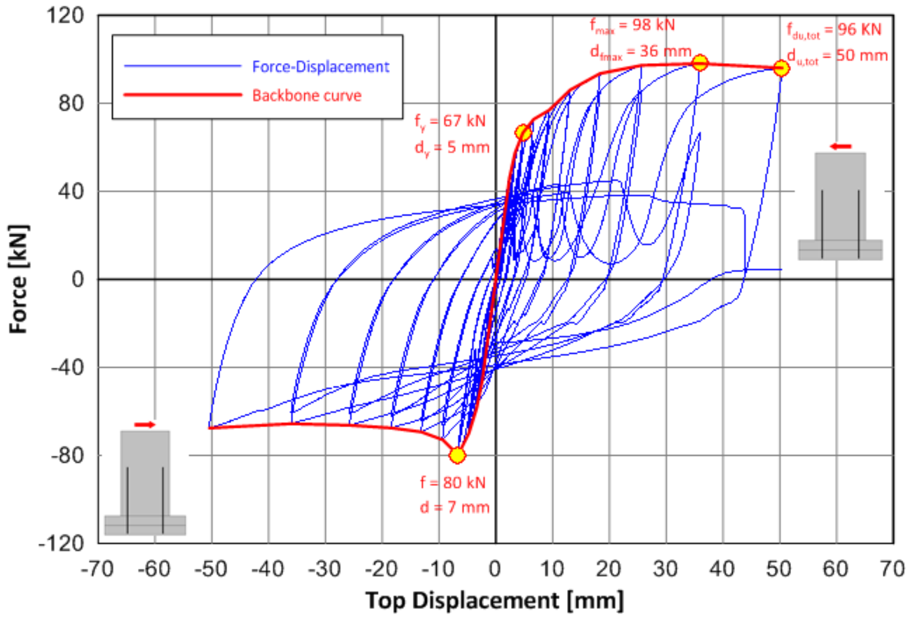

Figure A.6. Test A1D20C-R1: Horzontal force versus top displacement.

Note

Bonding failure occurred to the rebar of the left connection during the test.

Table A.2. Test A1D20C-R1: Response data.

Cyclic loading	
"Yield" strength(1)	67 kN
Maximum strength	98 kN
"Yield" displacement(1) (d_y)	5 mm
Ultimate displacement ($d_{u,tot}$; total failure of the connection	In the last cycle with magnitude 50 mm
Ductility (calculated as d_{fmax}/d_y)	Initial loading: 7.2 Reverse loading: not appropriate backbone curve
Total energy dissipated	28949.27 kNmm
Specific energy (2)	0.07 0.05 0.07 0.06 0.11 0.09 0.17 0.15 0.25 0.23 0.30 0.28 0.34 0.31 0.36 0.34 0.38 0.44 0.39
Force decay(3)	Initial loading: 0.041 / 0.060 / 0.104 / 0.133 / 0.052 / 0.012 / 0.090 / 0.117 / 0.319 Reverse loading: 0.013 / 0.026 / 0.029 / 0.026 / 0.092 / 0.069 / 0.080 / 0.078 / 0.073

(1) "Yield" point corresponds to the significant change in stiffness in the backbone curve and doesn't necessarily refer to the yielding of the rebar (it may also be associated with the crushing of the concrete).

(2) Specific energy was calculated as the area corresponding to the i-th cycle divided by the one corresponding to the perfect plastic cycle. The cycle referring to failure is not included.

(3) The decay is computed between the maximum force of the first cycle (f_{j1}) and of the second cycle (f_{j2}) of any group before the failure: $r_j = (f_{j1}-f_{j2})/f_{j1}$

Main characteristics of the behaviour

During the cyclic test:

- The rebar on the right side broke and the one on the left slipped
- Spalling of concrete **only on the left side** occurred
- Significant horizontal slip occurred when the joint was totally open

Observed damage

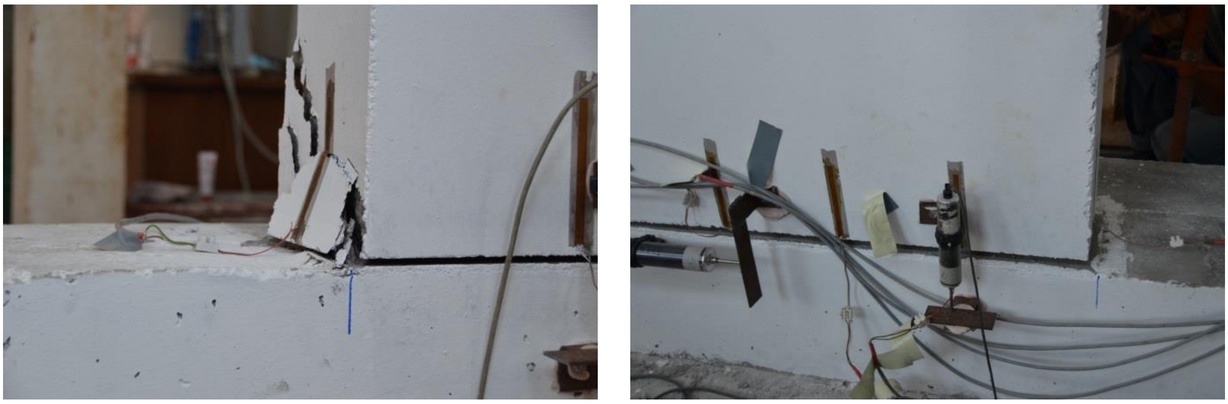

(a) (b)

Figure A.7. Test A1D20C-R1: Damage observed at the end of the test: (a) spalling of the concrete on the left side; (b) no evident damage on the right connection.

A.2 Connections with 1∅25 rebar

A.2.1 General description

"Rebar connections" made with 1∅25 rebar under monotonic and cyclic loading.

In test A1D25M-R2, the rebars were protruding about 0.30 m from the panel into the beam and the bond with the concrete was achieved using epoxy resin of type 2 (for material properties see Appendix B).

In tests A1D25M-G and A1D25C-G, the rebars were protruding about 1.30 m from the beam into the panel and the bond with the concrete was achieved using high strength, non-shrinking grout (for material properties see Appendix B).

<u>Test A1D25M-R2 – Bond: resin type 2</u>

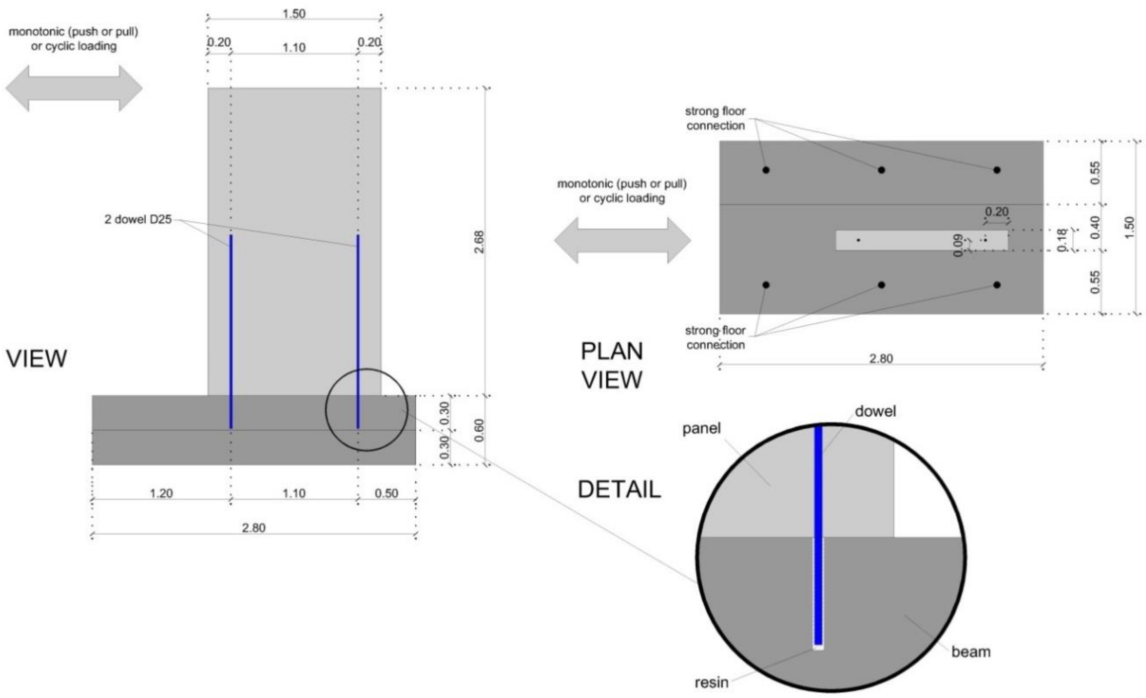

Figure A.8. Sketch of the experimental configuration of specimens 1D25M-R2.

Tests A1D25M-G & A1D25C-G – Bond: grout

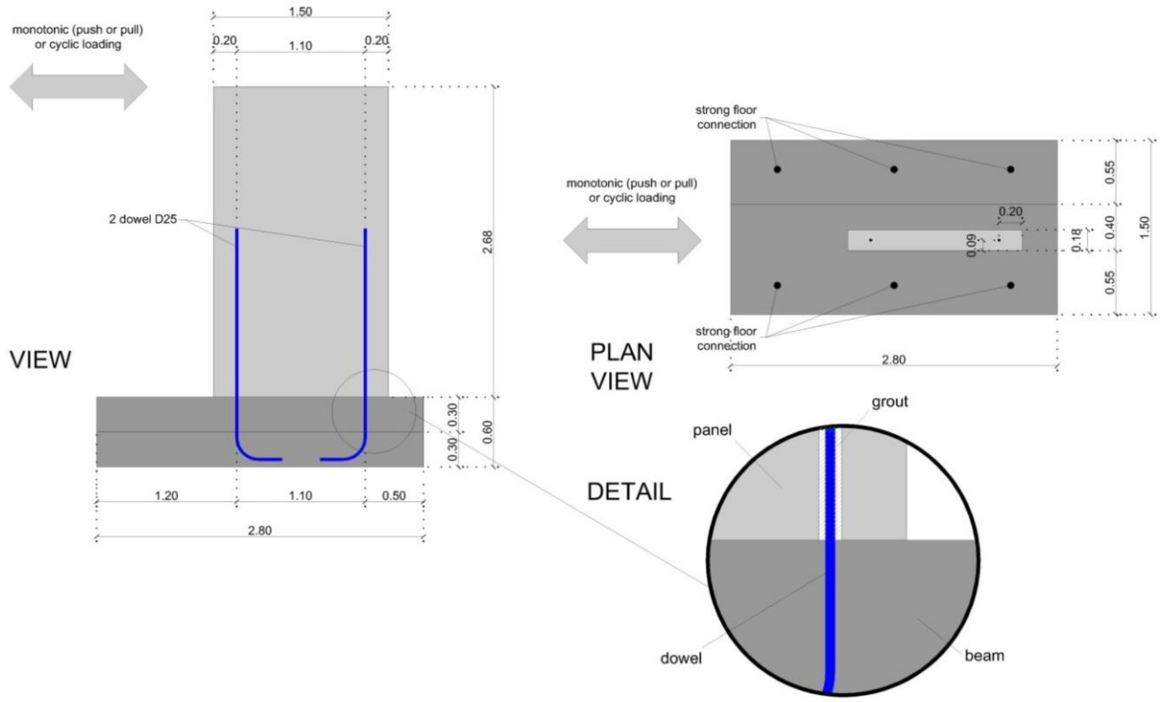

Figure A.9. Sketch of the experimental configuration of specimens 1D25M-G and 1D25C-G.

A.2.2 Main characteristics of the connection

Number and diameter of the rebars	1 ∅25
Panel thickness	18 cm
Distance from panel's edges to dowel	20 cm

Materials	Concrete class	C30(1)
	Steel class	B500C
	Bond material (duct infill)	epoxy resin type 2 / grout(2)

(1) The measured strength of the concrete is given in Appendix B.
(2) The properties of the resin and the grout are given in Appendix B.

A.2.3 Reinforcement details of the panel and the beam

Test A1D25M-R2 – Bond: resin type 2

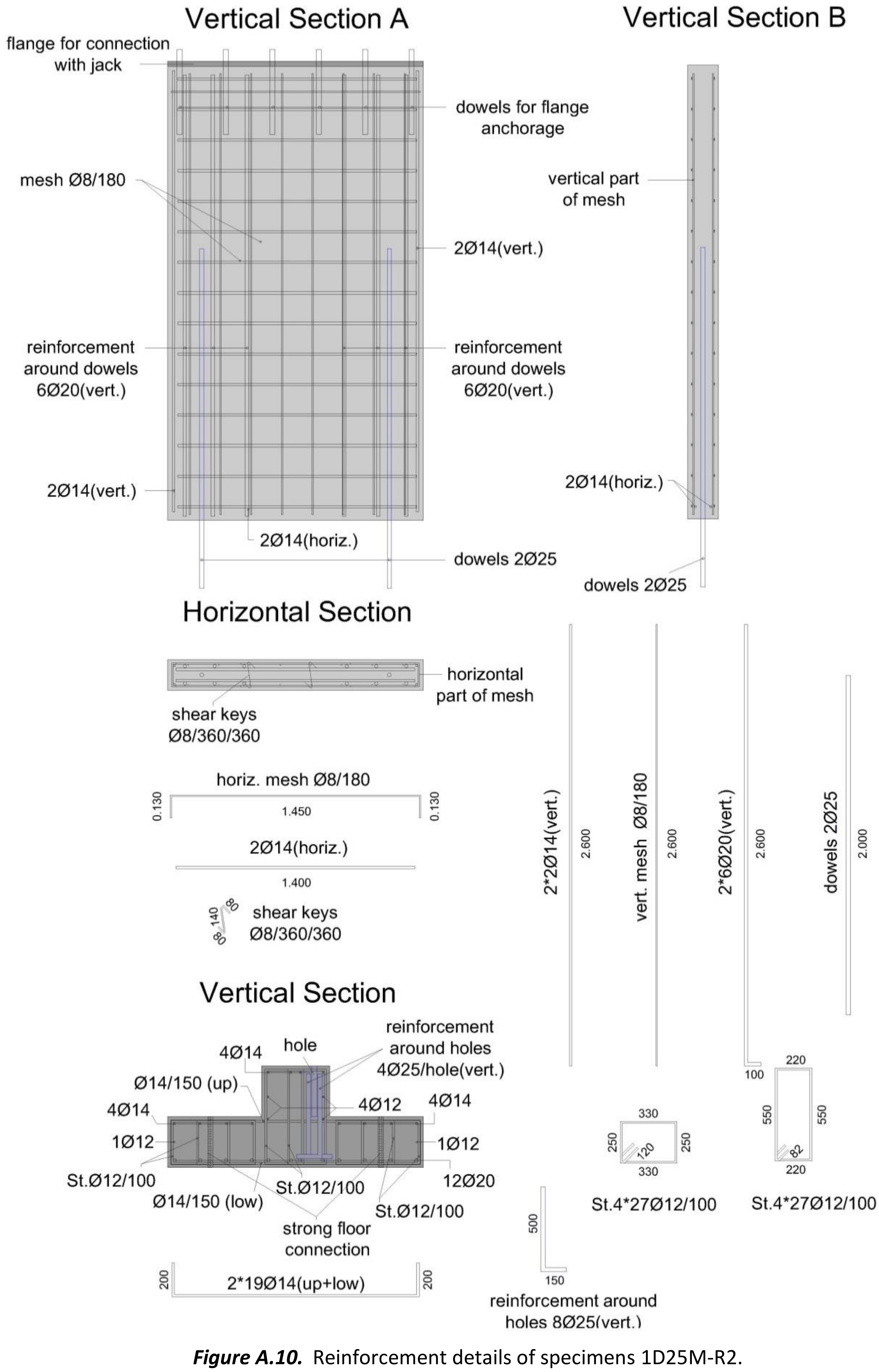

Figure A.10. Reinforcement details of specimens 1D25M-R2.

Tests A1D25M-G & A1D25C-G – Bond: grout

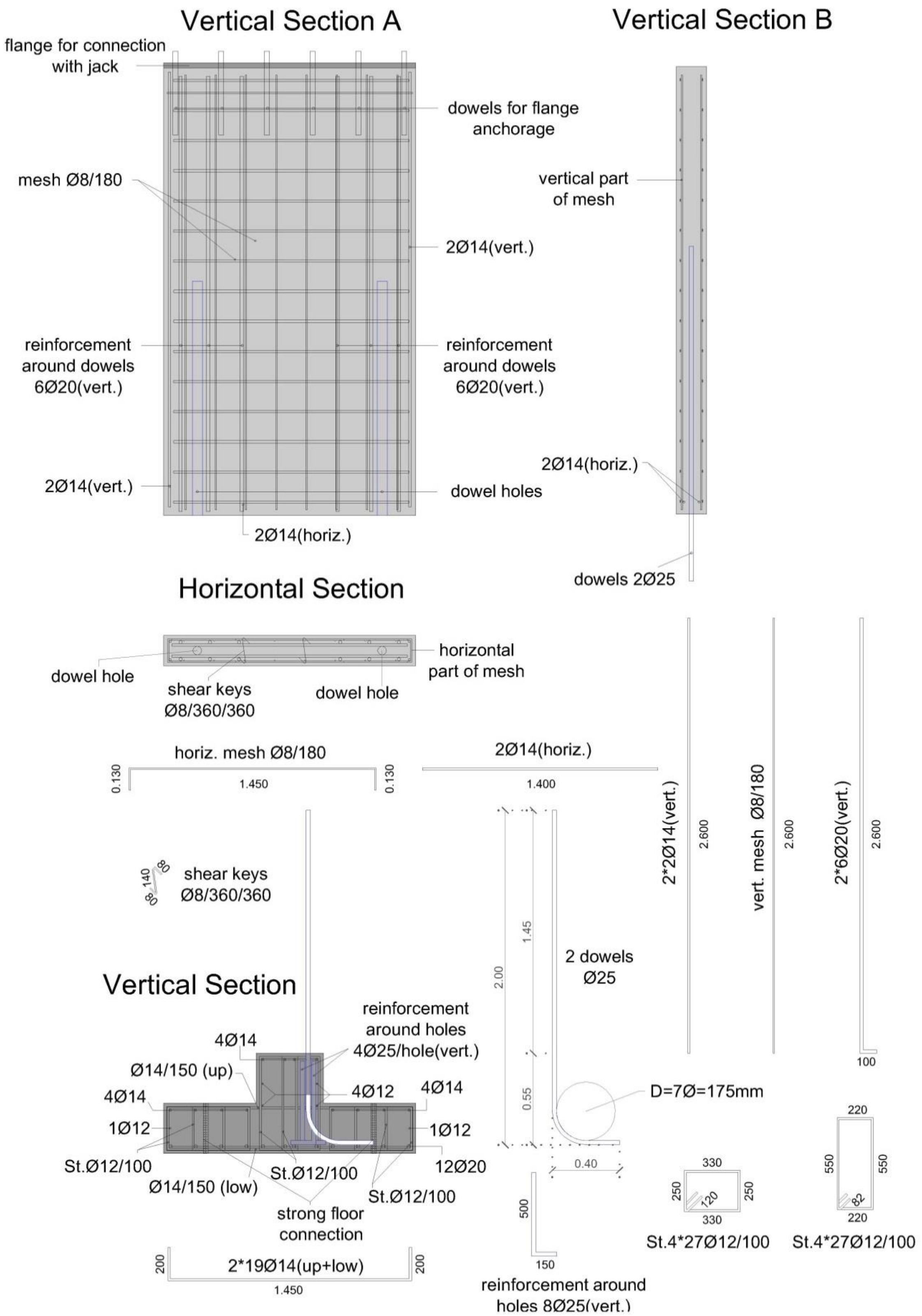

Figure A.11. Reinforcement details of specimens 1D25M-G and 1D25C-G.

A.2.4 Test A1D25M-R2 – Monotonic loading

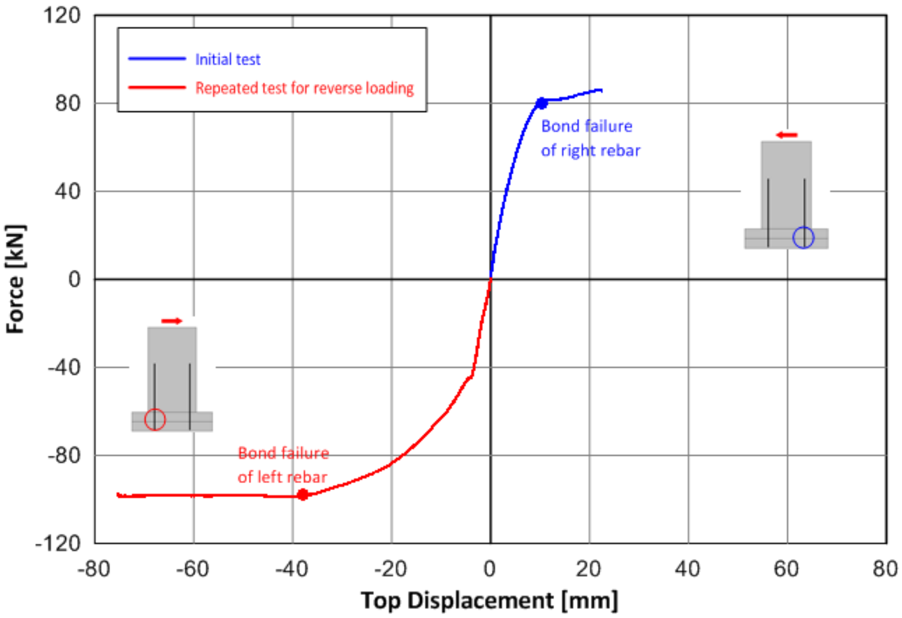

Figure A.12. Test A1D25M-R2: Horzontal force versus top displacement.

Table A.3. Test A1D25M-R2: Response data.

(Initial and Reversed) Monotonic loading	
“Yield” strength[1]	Not acquired
Maximum strength	Not acquired
“Yield” displacement[1] (d_y)	Not acquired
Displacement at maximum strength (d_{fmax})	Not acquired
Ultimate displacement ($d_{u,20\%}$; 20%reduction of strength)	Not acquired
Ultimate displacement ($d_{u,tot}$; total failure of the connection	Not acquired
Ductility	Not acquired

[1] “Yield” point corresponds to the significant change in stiffness in the curve and doesn’t necessarily refer to the yielding of the rebar (it may also be associated with the crushing of the concrete).

Main characteristics of the behaviour

During the monotonic (initial and reversed) loading:
- Slippage of both rebars due to bond failure
- Significant opening of the joint at the end of the test

Observed damage

Figure A.13. Test A1D25M-R2: Slippage of the rebars observed at the end of test.

A.2.5 Test A1D25M-G – Monotonic loading

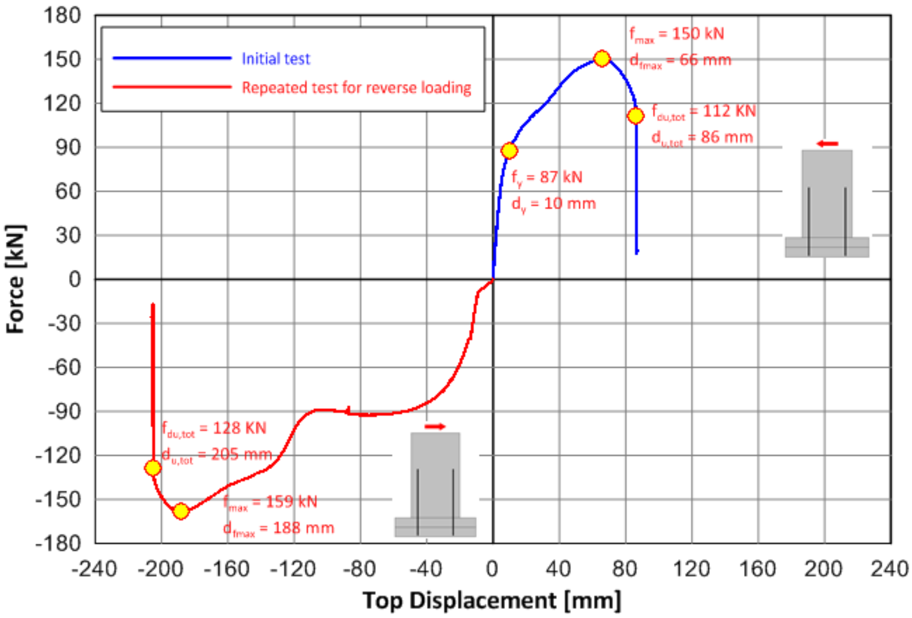

Figure A.14. Test A1D25M-G: Horzontal force versus top displacement.

Table A.4. Test A1D25M-G: Response data.

Initial Monotonic loading	
"Yield" strength(1)	87 kN
Maximum strength	150 kN
"Yield" displacement(1) (d_y)	10 mm
Displacement at maximum strength (d_{fmax})	66 mm
Ultimate displacement ($d_{u,20\%}$; 20% reduction of strength	86 mm
Ultimate displacement ($d_{u,tot}$; total failure of the connection	86 mm
Ductility	6.6 (calculated as d_{fmax}/d_y)

(1) "Yield" point corresponds to the significant change in stiffness in the curve and doesn't necessarily refer to the yielding of the rebar (it may also be associated with the crushing of the concrete).

Main characteristics of the behaviour

During the initial monotonic test:
- The rebar under tension broke
- Spalling of the concrete of the panel and the beam on the compression side occurred
- Severe damage to the beam around the rebar on the tension side was observed

During the reversed monotonic test:
- The rebar under tension broke
- Severe damage to the beam and the panel on the tension side was observed

Observed damage

(a) (b)

Figure A.15. Test A1D25M-G: Spalling of the concrete of the panel and the beam on the compression side at the end of the initial monotonic loading.

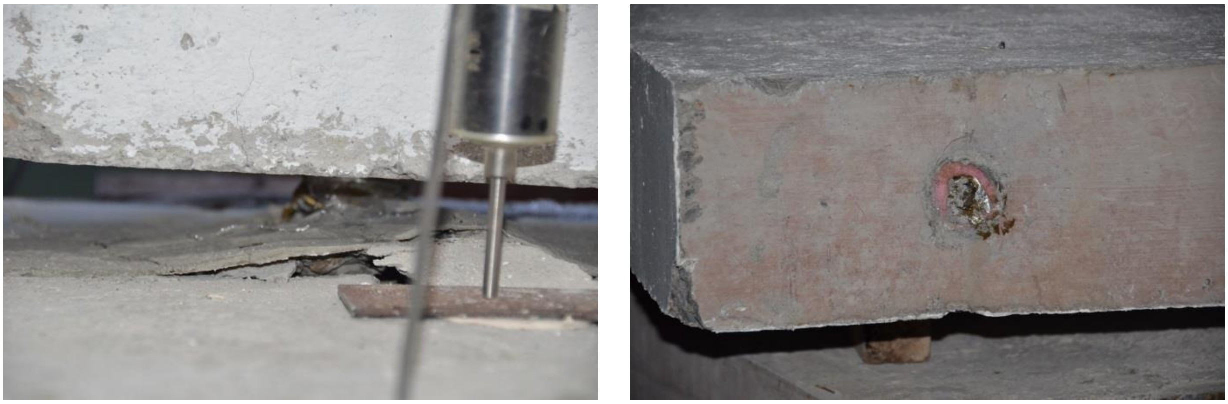

(a) (b)

Figure A.16. Test A1D25M-G: Damage observed on the tension side at the end of the initial monotonic loading: (a) severe damage to the beam around the rebar; (b) broken rebar but no visible damage to the panel.

(a) (b) (c)

Figure A.17. Test A1D25M-G: Damage observed at the end of the reversed monotonic loading: (a) & (b) severe damage to the panel on the tension side; (c) severe damage to the beam on the tension side.

A.2.6 Test A1D25C-G – Cyclic loading

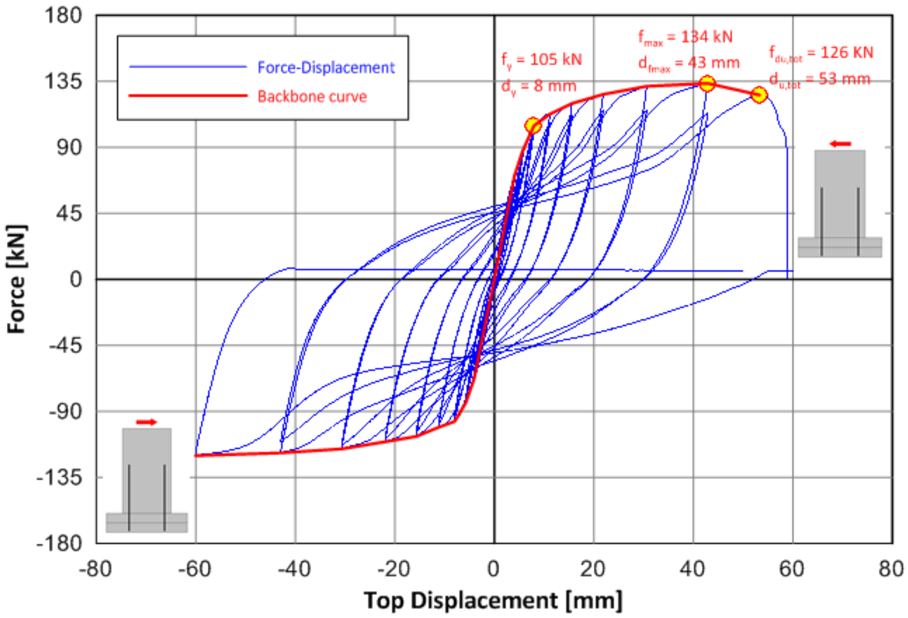

Figure A.18. Test A1D25C-G: Horzontal force versus top displacement.

Table A.5. Test A1D25C-G: Response data.

Cyclic loading	
"Yield" strength(1)	105 kN
Maximum strength	134 kN
"Yield" displacement(1) (d_y)	8 mm
Ultimate displacement ($d_{u,tot}$; total failure of the connection	53 mm (in the cycle with magnitude 61.4 mm)
Ductility (calculated as d_{fmax}/d_y)	Positive loading: 5.4 Negative loading: 7.5
Total energy dissipated	40949.81 kNmm
Specific energy(2)	0.09 0.06 0.08 0.06 0.11 0.08 0.18 0.15 0.23 0.22 0.29 0.28 0.32 0.33 0.35 0.36
Force decay(3)	Positive loading: 0.037 / 0.033 / 0.028 / 0.053 / 0.068 / 0.085 / 0.123 / 0.150 Negative loading: 0.037 / 0.032 / 0.031 / 0.021 / 0.028 / 0.018 / 0.024 / 0.066

(1) "Yield" point corresponds to the significant change in stiffness in the backbone curve and doesn't necessarily refer to the yielding of the rebar (it may also be associated with the crushing of the concrete).

(2) Specific energy was calculated as the area corresponding to the i-th cycle divided by the one corresponding to the perfect plastic cycle. The cycle referring to failure is not included.

(3) The decay is computed between the maximum force of the first cycle (f_{j1}) and of the second cycle (f_{j2}) of any group before the failure: $r_j = (f_{j1}-f_{j2})/f_{j1}$

Main characteristics of the behaviour

During the cyclic test:

- The rebar breakage happened at the same displacement as the previous test
- The elongation of the rebars led to significant joint opening
- Large horizontal slip occurred when the joint was totally open
- Spalling of concrete of the beam and the panel occurred

<u>Observed damage</u>

(a) (b)

Figure A.19. Test A1D25C-G: Damage observed at the end of the test: (a) spalling of the concrete around the rebars in the area of the joint; (b) spalling of the concrete of the beam.

Appendix B: Material properties

B.1 Concrete

Results of uniaxial compression of cylindrical concrete samples (D = 150 mm, H = 300 mm) for the estimation of the compressive concrete strength are given in the following.

B.1.1 Tests A1D20M-R1 & A1D20C-R1

Table B.1. Test A1D20M-R1 and A1D20C-R1: Concrete uniaxial compression results.

No.	Failure load (kN)	Compressive strength (MPa)
1	797	45.1
2	814	46.0
3	790	44.7
4	796	45.0
5	787	44.6
6	903	51.1
7	929	52.6
8	826	46.8
9	910	51.5
10	794	44.9
11	764	43.2
12	780	44.1
	Average compressive strength of 12 cores, X_{12m}	**46.6**
	Standard deviation, s	**3.2**

B.1.2 Test A1D25M-R2

Table B.2. Test A1D25M-R2: Concrete uniaxial compression results.

No.	Failure load (kN)	Compressive strength (MPa)
1	793	44.9
2	819	46.4
3	823	46.6
4	702	39.7
5	785	44.4
6	785	44.4
7	754	42.7
8	747	42.3
9	931	52.7
10	732	41.4
11	752	42.6
12	879	49.8
	Average compressive strength of 12 cores, X_{12m}	**44.8**
	Standard deviation, s	**3.7**

B.1.3 Tests A1D25M-G & A1D25C-G

Table B.3. Test A1D25M-G and A1D25C-G: Concrete uniaxial compression results.

No.	Failure load (kN)	Compressive strength (MPa)
1	605	34.2
2	535	30.3
3	649	36.7
4	565	32.0
5	556	31.5
6	635	35.9
7	690	39.1
8	678	38.4
9	671	38.0
	Average compressive strength of 9 cores, X_{12m}	**35.1**
	Standard deviation, s	**3.3**

B.2 Infill of the ducts (bond material)

The mechanical properties of the infill materials given in the following are according to the manufacturer's data.

Table B.4. Mechanical properties of the infill materials.

Material	**Epoxy Resin type 1**	**Epoxy Resin type 2**	**Grout**
Compressive strength [N/mm^2]	104 (after 1 day, in +23^{o}C)	89.5	12 (after 1 hour) 44 (after 28 days)
Modulus of Elasticity [N/mm^2]	-	2434	29000
Shear strength [N/mm^2]	-	8.5	-
Pull-out test in accordance with EN 1505-6 [mm]	< 0.6	< 0.6	-
Thermal coefficient	-	70×10^{-6} per K	-